Multi-Objective Optimization of the Steam Alternating Solvent (SAS) Process using Pareto-based Multi-Objective Evolutionary Algorithms

by

Israel Mayo Molina

A thesis submitted in partial fulfillment of the requirements for the degree of

Master of Science

in

Petroleum Engineering

Department of Civil and Environmental Engineering
University of Alberta

Abstract

The Steam Alternating Solvent (SAS) process is a relatively new auspicious alternative recovery process to produce heavy oil and bitumen resources. This process consists of injecting steam and solvent (i.e. propane) alternatively using the same well configuration as the widely adopted Steam-Assisted Gravity Drainage (SAGD) process. The SAS and other solvent-based processes have gained popularity as they aim to reduce the environmental footprint by reducing water usage and Greenhouse Gas (GHG) emissions. However, to successfully apply these processes in the field, vast knowledge and a proper design of all controllable parameters that intervene in each process and their operational ranges that might conflict with multiple objectives (especially in reservoirs with heterogeneities such as shale barriers) are needed. This study proposes a robust Multi-Objective Optimization (MOO) workflow based on Pareto optimality to determine the optimal operational ranges to implement the SAS process in homogenous and various heterogeneous reservoirs.

The MOO is carried out by constructing different simulation models under the following steps. First, a 2-D homogeneous reservoir model is built based on the Fort McMurray formation in the Athabasca region in Alberta, Canada. Then, for the heterogeneous case, multiple model sets superimposing shale barriers at different locations and geometries (shale proportions and lengths) are constructed and subjected to simulation to assess the impacts of heterogeneities according to those characteristics. After, a detailed sensitivity analysis is performed on the most impactful models 1) to determine the controllable operational parameter (decision variables) that impact the most in each model and 2) to select the targets (objective functions) to be optimized. Subsequently, three different Multi-Objective Evolutionary Algorithms (MOEAs) such as Multi-Objective Particle Swarm Optimization (MOPSO), Pareto Envelope-Based Selection Algorithm (PESA-II)

and Strength Pareto Evolutionary Algorithm II (SPEA-II) are applied. This is to 1) obtain the Pareto optimal set of decision variables and 2) identify the most suitable algorithm for each problem. Finally, Response Surface Methodology (RSM) to build proxy models is incorporated to estimate each objective function from the chosen decision variables to reduce the computational effort.

For the homogenous case, the results indicate that high propane concentration injected over short cycles, coupled with more extended steam injection, is more optimal for the first period. The bottom-hole pressure in the injector and producer should be kept low to reduce the steam and solvent injection and to allow the fluids to be produced, respectively. In contrast, lower solvent concentration and longer cycles are preferred for the second period, and higher steam injection is more optimal to achieve a higher reservoir temperature.

In heterogeneous reservoirs was observed that the steam-solvent chamber growth and production profiles are highly impacted by the location and geometry of these heterogeneities. This impact, especially in the area near the wells, is more representative. Conversely, in areas away from the wells pair, just longer and thicker shale barriers are relevant; this conclusion is consistent with other processes studies such as SA-SAGD (Al-Gosayir et al., 2012). The controllable parameters in heterogeneous reservoirs such as solvent composition (i.e. $\%Propane, \%Methane$), cycle duration (when either steam or solvent are injected), bottom-hole pressure (BHP) and some production constraints such as steam trap and Bottom-Hole Gas (BHG) have a significant impact on the SAS performance. Since this is a MOO, some trade-offs and relationships among the controllable variables in the process are observed.

The robust and detailed optimization workflow presented in this study accounts for multiple targets (objective functions) involving many controllable operational parameters

(decision variables). Also, by using different MOEAs to optimize the process, the results might be more accurate and reliable. Thus, this study intends to give a more profound analysis of the SAS process to facilitate field-scale decisions, minimizing the risk that this new technology might have.

Preface

This thesis content is an original work by Israel Mayo Molina. Parts of this study have been previously published or are ready for journal submission.

Chapter 1 of this thesis is originally written by Israel Mayo Molina and has not been published before.

Parts of Chapters 2 – 5 are sections of manuscripts that will be submitted to peer-review journals.

Some sections of Chapter 5 were published in a conference paper: Mayo Molina, I., Leung, J.Y. (2021). "Design of optimal operational parameters for steam-alternating-solvent processes in heterogeneous reservoirs – A multi-objective optimization approach". SPE Paper 205120 presented at the SPE Europec featured at 82nd EAGE Conference and Exhibition, virtual meeting, June 14-17.

Dedicated to God for his endless love. To my life partner, Michelle Haro, for her encouragement, enormous love and unlimited support. To my beloved parents, Julio Jorge Mayo Garcia and Flor de Maria Molina Paul, you know how important you are to me; I would not have accomplished this goal without your support and infinite love. Thank you for everything, I love you. Thanks for all the support and love to my sister, Amsi Mayo Molina and her beautiful family, Jose Dominguez and Tessa Dominguez.

This achievement is not only mine, it belongs to all of you. Thank you.

Acknowledgments

I would like to thanks first and foremost to my supervisor Dr. Juliana Y. Leung, for all the support, encouragement and insightful advice during my stay at the University of Alberta. Many thanks for each meeting, class, guidance, and time dedicated to finishing this research work. I genuinely believe my journey at the university and my research work would not have been the same without all her help, inspiring enthusiasm and infinite patience. Thank you!

I am also grateful to my examining committee members, Dr. Japan Trivedi, Dr. Huazhou Li and Dr. Alireza Nouri, for their time reviewing my thesis and all the constructive comments and suggestions to enhance my research work.

I would like to thank all the professors in the department for all the knowledge provided and all the university staff for all the support during this time.

Moreover, special thanks to all of Dr. Leung's research group and the friends I met in this incredible experience for their help, teachings and valuable comments regarding my research.

Table of Contents

List of tables

List of figures

Chapter 1: Introduction

This chapter presents the background of the Steam Alternating Solvent (SAS) process and its implementation, the problem statement, the research objectives, and the thesis outline.

1.1. Background

The total Canadian proven oil reserves are estimated at 171 billion barrels, of which 166.3 billion barrels are found in Alberta's unconventional oil sands (Government of Canada, 2020). Considering the global energy consumption is still increasing, heavy oil resources have drawn much attention, offering the potential to satisfy current and future oil demand (Speight, 2009). The main challenge with this type of oil is its high viscosity. Currently, two widely commercial recovery techniques have been used for extracting bitumen from this type of reservoir. 1) Surface mining for shallow deposits with depths ≤ 75 m and 2) In-situ (thermal) recovery methods for deeper deposits with depths > 75 m; 80% of the resources must be extracted via in-situ (Souraki et al. 2013). These thermal recovery methods entail transferring heat to the fluid by either injecting hot fluids (e.g., hot water, steam, or solvent) or by electric heating (Farouq et al., 2018). As a result, since the oil viscosity is very sensitive to temperature variation, it is reduced, improving oil mobility.

Nowadays, many field-tested thermal processes, such as Steam flooding, Cyclic Steam Stimulation (CSS) (Ali and Blunschi, 1983), and Steam-Assisted Gravity Drainage (SAGD) (Butler et al., 1981), exist. For these processes, the thermal energy added dilutes the oil and allows it to flow into the producer. For example, the CSS method consists of three phases. First, steam is injected at high pressure and high temperature into a horizontal well. Then, the well is shut-in at the surface during the soak phase, and finally, the well is re-opened to produce the bitumen and condensed steam or water; this process is repeated cyclically. Steam-Assisted Gravity Drainage

(SAGD) process, which was pioneered and developed by Butler et al., 1981, is the most widely used Enhance Oil Recovery (EOR) technology for commercial production in Alberta (Ipek et al., 2018). This process involves injecting steam into the reservoir using a horizontal injector well at the top to develop a high-temperature chamber to heat the oil until its viscosity is reduced considerably so it can flow by gravity to the horizontal producer well located 5 m below the injector. In this process, the void space after the oil is drained is occupied by the steam creating a bigger chamber reaching more of the reservoir. Even though SAGD is a very effective recovery method, the trade-off, similar to the CSS process, comes in terms of its high-water consumption and high Greenhouse Gas (GHG) emissions (e.g., burning of natural gas to produce steam). Additionally, this method is less effective in heterogeneous reservoirs where thief zones or shale barriers are found (Souraki et al., 2013).

Therefore, alternative solvent-based recovery techniques have been proposed in the past several years and have gained popularity. Some pilot tests examples of this technic are the "Solvent+" project developed by Suncor Energy Inc. (2020), where a light hydrocarbon solvent (e.g., propane or butane) is injected to mobilize the bitumen. Another pilot project is the Solvent-Aided Process (SAP) by Cenovus (2020), where a mixture of propane and steam is injected using the same SAGD well configuration; an operational demonstration is being prepared for their Foster Creek project. Nevertheless, previous studies have proved that injecting solvent without heat (e.g., Vapor Extraction or VAPEX) is typically inefficient since diffusion or dispersion is much slower than heat transfer (Leung, 2014). Thus, these steam-solvent techniques appear to be most promising that might significantly reduce GHG emissions, so the footprint at the surface will be smaller than the traditional methods. Also, these projects pretend to be more profitable since the solvent is recovered and could be reused (Emission Reduction Alberta, 2020). Some examples of

these recovery oil methodologies are the Expanding Solvent Steam-Assisted Gravity Drainage (ES-SAGD) process developed by Nasr et al. (2001) and the Steam and Gas Push (SAGP) proposed by Jiang et al. (1998). The advantage of these processes is the considerable environmental footprint reduction, but the disadvantage is that the oil production rates are generally lower, and solvent recycling is challenging.

Another variant of these steam-solvent processes is the relatively new Steam Alternating Solvent (SAS) process proposed by Zhao et al. (2005). The SAS process used the same well-configuration as the SAGD process where steam and solvent are injected alternatively instead of injecting pure steam or a mixture of solvent and steam, similar to Suncor and Nsolv projects, the solvent can be recycled. This process pretends to be more energy-efficient and environmentally friendly, reducing water usage, and as a consequence, Greenhouse Gas emissions are minimized. The main challenge of this technique is that many controllable operational parameters that conflict with multiple objectives need to have a proper design to maximize the success of the process; thus, because of that characteristic, it can be treated as a Multi-Objective Optimization Problem (MOOP).

1.2. Problem Statement

The SAS process was proposed as an alternative that combines the SAGD and VAPEX process advantages: minimize the energy input in heavy oil and bitumen recovery processes. Lab results presented in Zhao et al. (2005) revealed that the SAS process energy reduction could be in ranges of 47% lower than the SAGD process recovering the same oil proportion. However, to reach this objective, some challenges arise.

According to Zhao (2005), the first challenge is to find a proper design of the controllable operational parameters to reach the desired profiles. A systematic sensitivity analysis

encompassing a wide range of operational parameters is needed, but such an analysis is not available in the existing literature.

Another challenge is the complexity of the physical processes to be simulated (i.e., coupling heat, mass transfer and multiphase fluid flow equations). In addition, the computational cost associated with repeating multiple optimization scenarios is high. Therefore, alternative proxy modelling techniques such as Response Surface Methodology (RSM) need to be applied to estimate faster and accurately the objective functions.

Moreover, the presence of heterogeneities such as shale barriers renders the multi-objective optimization problem more complex. It should be noted that different heterogeneity scenarios would have significant impacts on the production behaviour, and the optimal operating strategies should be adjusted accordingly.

1.3. Research Objectives

The main objective of this research is to present a Multi-Objective Optimization workflow able to reproduce reliable sets of solutions based on Pareto optimality and at the same time reduce the computational effort that it might take to optimize this process. This entails:

a) Perform an in-depth sensitivity analysis to assess the relations and interactions among different operating parameters for the SAS process in homogeneous and heterogeneous reservoirs.

b) Implement the Response Surface Methodology (RSM) to create non-linear multivariate regression models (proxy models) that estimate the objective functions from the decision variables chosen in the sensitivity analysis to minimize the computational time to optimize the SAS process.

c) Compare the results using three different MOEAs to determine whether one or more of these methods would be more suited for this specific process.

d) Identify and analyze key and feasible insights about the proposed optimal operational sets obtained from the Pareto front solution.

e) Define the optimum operational ranges for each selected decision variable and formulate an optimal operating strategy for each particular scenario.

1.4. Thesis Outline

This thesis consists of 6 chapters. The outline of these chapters is provided as follows:

Chapter 1 presents the background of the SAS process, the problem statement, and the research objectives.

Chapter 2 presents the literature review, including some steam and solvent-bases-assisted thermal processes for heavy oil and the existing studies about the SAS process. Also, the Multi-Objective Optimization and the Response Surface theory are included in this section.

Chapter 3 present the research methodology that includes the base case process modelling and preliminary results. Also, the sensitivity studies implementation and the targets (objective functions) formulation are presented. Moreover, a brief description of all three MOEAs (i.e., MOPSO, SPEA-II and PESA-II), the proxy models construction process and the entire proposed Multi-Objective workflow are shown.

Chapter 4 presents the application of the proposed Multi-Objective workflow in a homogenous reservoir that includes results of the sensitivity and proxy analysis and Pareto front solution sets.

Chapter 5 presents the superimposed methodology used to build different heterogeneous realizations and how the proposed Multi-Objective workflow was applied for each scenario.

Moreover, results of the sensitivity and proxy analysis and Pareto front solution sets accounting for two and three objective functions are presented.

Chapter 6 presented the conclusions, contributions, recommendations and future work.

Chapter 2: Literature Review

This chapter reviews the literature regarding steam and solvent-based Enhanced Oil Recovery (EOR) methods, the fundamentals, and the existing studies on the SAS process. Additionally, the general Multi-Objective Optimization and proxy modelling theory is presented.

2.1. Enhance Oil Recovery (EOR) Methods.

Enhance Oil Recovery methods are widely accepted oil extraction techniques in which a considerable amount of crude in the reservoir can be recovered. These techniques involve changing the reservoir make-up. In essence, properties like density and viscosity of the oil change, making oil displacement easier in the reservoir. EOR methods can be classified as thermal and non-thermal methods (Sarapardeh et al., 2013); this study will be focused on thermal methods. A thermal method uses thermal energy to raise the reservoir temperature, and as a result, oil viscosity is decreased (Naqvi, 2012). These sorts of techniques are considered one of the most advanced EOR processes, and they currently provide a significant amount of oil all around the world. Many different thermal EOR methods include hot fluid injection, such as hot water flooding, steam or solvent injection, and In-situ combustion (ISC), also called fire flooding (Mokheimer et al., 2019).

2.1.1. Steam-based EOR methods.

Different methods that imply water injection and its derivatives have been widely used over the last few decades. Some of the most prominent techniques are the Cyclic Steam Stimulation (CSS), where steam is injected into a production well for several weeks. Then a soaking period is given to the steam to diffuse through the reservoir, and finally, the oil is produced. Other methods in this category are the In-situ Combustion (ISC) process, where gas (i.e. air) is injected into the reservoir, and the Steam-Assisted Gravity Drainage (SAGD) process, where steam is injected in a horizontal

pair well, and the oil is produced by gravity. In Canada, the SAGD process is the most widely EOR used method. However, these methods' main technical challenges are the high cost of heat to produce the steam, water usage, and the environmental footprint generated by the Greenhouse Gas (GHG) emissions.

2.1.2. Solvent-based EOR methods.

Solvent-based methods have been studied for many years in the development of heavy oil or bitumen resources extraction. Compared with the conventional thermal-based methods mentioned in section 2.1.1, solvent injection is more energy-saving, eco-friendly and particularly useful in the majority of the reservoirs. These methodologies take advantage of both the thermal and solvent mechanisms, showing a considerable increase in the oil recovery factor. Some examples of these processes are the Vapor Extraction (VAPEX) technique proposed by Butler and Mokrys (1991), where a vaporized solvent is injected into the reservoir to form a solvent vapour chamber due to the high pressure and oil is produced by gravity. Another method is the Thermal Solvent Reflux (TSR) developed by Frauenfeld et al. (2009). This methodology is a modification of the VAPEX process that includes steam injection and an electrical heater. Basically, the electrical heater is set inside the well to heat the reservoir fluids near the wellbore; steam could be injected to improve the recovery factor. N-Solv® patented by Nenniger and Nenniger (2005), and Warm-VAPEX, developed by James (2009), are similar processes. The main difference between these two methods is that N-Solv® injects the solvent into the reservoir at the dew point, while in Warm-VAPEX, it is superheated before the injection. However, the disadvantage is the poor condensation phenomenon that reduces solvent dissolution with the oil. Another wildly studied method mentioned previously is the Expanding Solvent Steam-Assisted Gravity Drainage (ES-SAGD) process. This process is quite similar to the VAPEX process, but the difference is that the solvent

is co-injected with steam and uses the same configuration as the typical SAGD process. The advantages of this methodology are that Steam-Oil Ratio (SOR) is much lower than the original SAGD, and the production rate is high compared with other solvent-based methods (i.e. VAPEX). Another SAGD process modification similar to the ES-SAGD process is the Steam and Vapour Extraction (SAVEX) process (Gutek et al., 2003). The main difference between ES-SAGD and SAVEX is that SAVEX starts with a SAGD period, and then just solvent is injected. The Solvent Aided Process (SAP), proposed by Gupta (2005), uses light hydrocarbons as a solvent where solvent injection timing is the key factor in this method's success. Some other examples are Cyclic Solvent Process (CSI) and Enhance Cyclic Solvent Process (ECSP) that are very similar to CSS. These processes inject cold solvents such as hydrocarbons and carbon dioxide. The main difference between them is that in ECSP, different solvents are injected in a particular sequence, while in CSP, the solvents are injected at once (Yadali and Ben, 2013). Another CSS modification is the Liquid Addition to Steam for Enhancing Recovery (LASER) process (Leaute and Carey, 2007), where liquid hydrocarbons (i.e. C5+) are injected into the reservoir that leads to a SOR reduction in comparison with the CSS process. For fractured reservoirs, Steam Over Solvent injection in Fractured Reservoirs (SOS-FR) was first proposed by Babadagli and Al-Bahlani. (2008). In this process, the main objective is to create thermal and chemical turbulence by injecting steam, solvent, steam cycles to make the reservoir readjust, and the oil will be pushed out from the matrix to the fractures (Al-Bahlani and Babadagli, 2011). Another variant is the Steam Alternating Solvent (SAS) Process.

2.1.2.1. Steam Alternating Solvent (SAS) Process.

As mentioned in section 1.1, the SAS process was proposed by Zhao (2005) and uses the same typical SAGD configuration, and instead of injecting steam alone, steam is alternated with solvent

injection. The core concept of alternate steam/solvent injection is that the solvent might prevent the steam from going into the formation too fast. Also, the steam could re-heat the solvent and heavy oil to reduce further the viscosity, which might help speed up the solvent diffusion and dispersion.

This process can be divided into three main phases:

1. Pre-heating phase: in this phase, pure steam is injected through the wells to establish vertical communication between them.

2. SAGD phase: this is a short phase where pure steam is injected to establish a steam chamber into the reservoir. The SAGD phase may finish when the pay zone is reached and/or the heat lost to overburden becomes significant.

3. Cycling phase: this phase starts with solvent alone injection, and it stops when the steam-solvent chamber temperature is reduced significantly. At that point, steam begins to be injected to increase the chamber temperature; the steam cycles are shorter than the solvent cycles to keep this process eco-friendly. This phase is repeated until it is no longer economically profitable. The production is continuous in the entire SAS operation, and soaking or shut-in periods are not needed.

Previous SAS studies by Coimbra et al. (2019) propose an optimization strategy considering three operational parameters: solvent composition and solvent duration cycles (early- and late-times). They recommend that when injecting a mixture of methane and propane, propane concentration should be maximized. Also, the duration for solvent injection within each cycle, particularly in the early cycles, should be prolonged. However, the major limitation of their work is that only a few conflicting targets (i.e. $cSOR$ and $Propane_{retention}$) and few operational parameters that involve the SAS process were considered. Another study by Lima et al. (2016)

incorporates heptane (C_7H_{16}) as a solvent, and they proposed to inject this solvent in periods of 8 years to increase the RF. The drawbacks of this study are 1) C_7H_{16} is an expensive solvent; hence, the economics of the project could considerably be affected negatively. 2) Just one objective function (i.e. RF) and two decision variables (i.e. % solvent and solvent injection duration) were considered. 3) Any MOO technique was incorporated in the study.

Many conflicting targets (objective functions) such as maximizing oil production, reducing solvent consumption, and minimizing steam injection should be considered to optimize the SAS process. To improve these targets, several controllable operational parameters (decision variables) can be adjusted. For example, according to Zhao et al. (2005), solvent retention is strongly affected by the solvent and temperature distribution within the chamber. This phenomenon could be considered a function of operating parameters such as bottom-hole pressures of the injector and producer (BHP), steam trap and bottom-hole gas rate (BHG) in the producer, cycle duration, or injected solvent compositions. Therefore, since multiple conflicting objectives or criteria should be considered, this can be formulated as a Multi-Objective Optimization Problem (MOOP) (Deb, 2014).

2.2. Optimization techniques theory.

Optimization techniques are considered as robust and helpful tools that efficiently compare and manage various potential solutions till an optimum or a satisfactory solution is found of a well-defined problem. Furthermore, these techniques aim to maximize or minimize some objectives (Alonso et al., 2020). There are two widely primary categories to optimize engineering problems: 1) Gradient-based and 2) Non-gradient-based (stochastic) methods. Gradient-based methods have been developed since the 1950s to solve nonlinear optimization problems. These techniques focus only on local information (solutions at a certain point) in the optimum solution search process;

thus, they converge only in a local minimum threshold for the objective function (Arora, 2012); the adjoint method (Zandvliet et al., 2008) is an example of these techniques.

On the other hand, Non-gradient-based, also known as stochastic methods, involve searching solutions in the entire domain via various stochastic approaches and are, in principle, more suitable for seeking the optimal global solutions (Adams et al., 2015). Nonetheless, the primary drawback of these methods is the slow rate of convergence. An example of this technique are the many existing genetic algorithms (GA).

Additionally, a variation of these two categories is some hybrid stochastic gradient-based methods, such as Ensemble-based Optimizer (EnOpt), that aim to integrate some gradient calculations in the stochastic framework. However, depending on the techniques, computational costs can remain high. Thus, non-gradient multi-objective methods are used in this study to ensure the global minimal are identified.

2.2.1. Multi-Objective Optimization (MOO) Theory.

In the Multi-objective optimization framework (also known as multi-objective programming, vector optimization, multicriteria optimization or multi-attribute optimization) exist two important concepts of optimality, 1) Pareto: this analysis framework considers the trade-offs between two or more conflicting objectives giving equal weights (importance) to all the targets (Pareto, 1896) and implements multiple-criteria decision-making (Deb, 2014). Conversely, in 2) Lexicographic optimality: the objective functions are ordered according to their importance. So, the problem is solved hierarchically and treated as a series of single-objective problems (Arora, 2012). In this study, the Pareto approach is selected.

In a non-trivial Multi-Objective Optimization Problem (MOOP) using the Pareto MOO framework, multiple, often conflicting, objective functions are optimized simultaneously. Thus,

there is no single solution that simultaneously optimizes each objective. Instead, there are several Pareto optimal solutions (Miettinen, 1999), meaning none of the objectives can be improved without affecting others. Therefore, a MOO model solution could be expressed as a Pareto optimal set, also known as a non-dominated solution set (Mirjalili and Lewis, 2015).

2.2.1.1.   Multi-Objective Optimization techniques.

Multi-Objective Optimization techniques have been widely applied in designing and optimizing various EOR processes (Gunantara, 2018). There are four common MOO approaches 1) Vector Evaluated Genetic Algorithm (VEGA): this technique splits the population into sub-populations and each sub-population towards a different part of the vector (or another vector). In this approach, the fitness function returns a vector, and additional comparisons are produced to get the best result (Schaffer, 1985). 2) Niched Pareto Genetic Algorithm (NPGA): this approach includes a tournament selection scheme based on Pareto dominance principles where only two individuals are randomly selected for the tournament, and to find the winner solution, a comparison set is randomly selected that contains some other individuals in the population. Then, the dominance of both candidates is tested concerning the comparison set. If one candidate only dominates the comparison set, it is selected as the winner. Otherwise, a sharing procedure is implemented to specify the winner (Horn et al., 1994). 3) Multi-Objective Genetic Algorithm (MOGA): this technique was introduced by Fonseca and Fleming, 1993 and uses the non-dominated classification of the Genetic Algorithms (GA) population. MOGA explicitly emphasizes non-dominated solutions and simultaneously maintains diversity in them; this approach differs from a standard tripartite GA in how fitness is assigned to each solution in the population (Fonseca and Fleming, 2011). 4) Multi-Objective Evolutionary Algorithms (MOEAs): these sorts of algorithms have attracted a lot of research effort during the last 20 years since these

algorithms can approximate the Pareto optimal set in a single run. All the developed algorithms belonged to this category are based on conventional aggregation approaches in which a MOOP is decomposed into a number of Scalar objective Optimization Problems (SOPs), and the objective of each SOP (subproblem) is a linearly or non-linearly weighted aggregation of the individual objective; neighbourhood relations among these SOPs are defined based on the distance between their aggregation weight vector (Zhou et al., 2011). Some examples of the uses of this MOEA are Huanyinbo et al. (2020). They employed the Non-dominated Sorting Genetic Algorithm-II (NSGA-II) developed by Deb et al. (2002) to optimize the Warm Vaporized Solvent Injection (WSI) process having two objective functions, Solvent Retained-Oil Ratio ($SolOR$) and Recovery Factor (RF). Similarly, Ma and Leung (2019) used the same algorithm to optimize the same process in a heterogeneous reservoir targeting cumulative Steam-Oil Ratio ($cSOR$) and Recovery Factor. Coimbra et al. (2019) also used NSGA-II to optimize the SAS process having as targets two objective functions (i.e., oil recovery and solvent usage).

2.2.1.2.   Multi-Objective Evolutionary Algorithms (MOEAs)

An MOEA is one of many engineering optimization techniques to solve MOOP and is considered a guided random search method capable of exploring the diverse regions of the solutions space to search a diverse set of solutions (Zolpakar et al., 2019). These techniques lie in the natural selection mechanisms simulation to find the non-dominates solutions of the problem, also known as the Pareto optimal set. (Coello, 2018). In a MOOP solved by an MOEA, two kinds of solutions exist: dominated and non-dominated solutions. A solution is called a dominated solution if it satisfies the conditions in statements (1) and (2):

I.   The solution in vector x_1 is no worse than vector x_2 in all objective functions.

$$\forall_i \in \{f_1(\vec{x}), f_2(\vec{x}), \dots, f_o(\vec{x})\} : \ f_i(x_1) \leq, f_i(x_2) \tag{1}$$

II. The solution in vector x_1 is strictly better than x_2 at least in one of the objective functions.

$$\exists_j \in \{f_1(\vec{x}), f_2(\vec{x}), \dots, f_o(\vec{x})\} : f_j(x_1) \leq, f_j(x_2) \tag{2}$$

hence x_1 dominates x_2 if both conditions are true. If either of these conditions is breached x_1 does not dominate x_2; thus x_1 is non-dominated by x_2.

The basic steps for an Evolutionary Algorithm (EA) can be described as follows: 1) A set of possible potential solutions (population) is randomly generated; each solution or individual of the population consists of the decision variables. 2) The fitness (objective function) of each individual is calculated. 3) A selection mechanism is applied to pick a set of parents from which new offspring, called children, are generated. 4) Finally, a mutation probability is incorporated to maintain diversity among the population. This process is repeated until a particular stop condition (usually the maximum number of generations defined by the user) is reached (Eiben and Smith, 2003).

There are many MOEAs proposed, such as Pareto Archived Evolutionary Strategy (PAES) (Knowles and Corne, 1999), Multi-Objective Differential Evolution Algorithm (MODEA) (Ali et al., 2012), etc. However, for this study, three widely used algorithms were chosen: 1) Multi-Objective Particle Swarm Optimization (MOPSO) (Coello and Lechuga, 2002), 2) Pareto Envelope-Based Selection Algorithm (PESA-II) (Corne et al., 2001) and 3) Strength Pareto Evolutionary Algorithm II (SPEA-II) (Zitzler et al., 2001). A brief description of each scheme is presented in Chapter 3.

2.3. Response Surface Methodology (RSM) – Proxy Modelling.

RSM was introduced by Box and Wilson (1951) and is a useful mathematical and statistical tool for the approximation and optimization of stochastic models that include high-degree polynomial equations that give more flexibility to fit a curve along highly complex responses. In

this study, this methodology is used to create non-linear multivariate regression models (Proxy models) relating the targets (objective functions) with the decision variables (controllable operational parameters). It should be noted that many other techniques, such as Polynomic, Kriging, Splines, and Neural Networks Models, can be used for proxy modelling.

Historically, proxy models have been uni-variate or multi-variate quadratic polynomials that fit discrete input and resulting output parameters predictions (Nnamdi, 2020), providing benefits in terms of simplicity and reductions in computational effort. For example, regarding the SAS process, Coimbra et al. (2019) applied RSM using 144 experiments to train the proxy model to calculate $cSOR$ and $Propane_{retention}$ reducing the expensive computational effort from 97 days to 1 minute on average.

CMOST, an optimization tool of the Computing Modelling Group (CMG, 2019), is incorporated in this study to build the proxy models. This software program uses a full quadratic polynomial model (Zubarev, 2009; CMOST, 2019), as is shown in equation (3):

$$F(\vec{x}) = \beta_0 + \sum_{i=1}^{l} \beta_i x_i + \sum_{i>j}^{l} \sum_{j=2}^{l} \beta_{ij} x_i x_j + \sum_{i=1}^{l} \beta_{ii} x_i^2 + \varepsilon \tag{3}$$

where x_i and x_j are independent input factors (decision variables), l is the length of the decision variable vector, $F(\vec{x})$ is the response (objective function), $\beta_0, \beta_i, \beta_{ij}$ and β_j represents the unknown regression coefficients and the error term $\boldsymbol{\varepsilon}$ is adjusted during the calibration process; the β_s' terms are estimated by the least-square method.

Chapter 3: Research Methodology Implementation

This chapter presents the base-case modelling process, the preliminary simulation results, a description of the Multi-Objective Evolutionary Algorithms methods, and the detailed sensitivity analysis using Response Surface Methodology. Additionally, the entire proposed optimization workflow for the SAS process is shown.

3.1. Base Case Process Modelling.

A base 2-D homogeneous SAS reservoir model is constructed based on reservoir properties extracted from the Fort McMurray formation in the Athabasca region in Alberta, Canada. In particular, the data is extracted from Suncor's Firebag project (Zheng et al., 2017) and the Surmont project (Li, 2006). The base model is 50 m deep along the I-axis with a pay zone of 25 m in thickness (z-axis). The wells are located parallel to the J-axis and are separated 5 m apart from each other near the bottom of the pay zone. Regarding the grid size, $\Delta x = \Delta z = 0.5\ m$ and $\Delta y = 1\ m$. The set-up of the domain is illustrated in Figure 1. The initial input condition, grid, rock and fluid properties are listed in Table 1. These parameters were taken from SAGD field studies done by Ma et al. (2015) and are consistent with the work reported by Coimbra et al. (2019). The results were compared with the simulated SAS studies done by Coimbra et al. (2019).

Table 1. SAS process Model properties for the base-homogenous reservoir.

Description	Parameters	Values
Grid Properties	Number of grid blocks in X-direction	100
	Number of grid blocks in Y-direction	1
	Number of grid blocks in Z-direction	50
	Size of grid block (Δx)(m)	0.5
	Size of grid block (Δy)(m)	1
	Size of grid block (Δz)(m)	0.5
	Permeability in I-direction (mD)	2,500
	Permeability in J-direction (mD)	2,500
	Permeability in K-direction (mD)	1,500

17

	Porosity (fraction)	0.33
	Injector depth (m)	20
	Producer depth (m)	25
Initial Conditions	Reference depth (m)	25
	Reservoir Pressure (kPa)	3,100
	Initial oil Saturation	0.85
	Reservoir temperature (°C)	12
Rock/Fluid properties	Bitumen viscosity at 12°C (cP)	47,956
	Bitumen viscosity at 220°C (cP)	4.6
	Initial Gas Oil Ratio (GOR)	3.4
	Relative permeability endpoints	$K_{rw} = 0.79$, $K_{row} = 0.948$ $K_{rg} = 0.2$, $K_{rog} = 0.948$
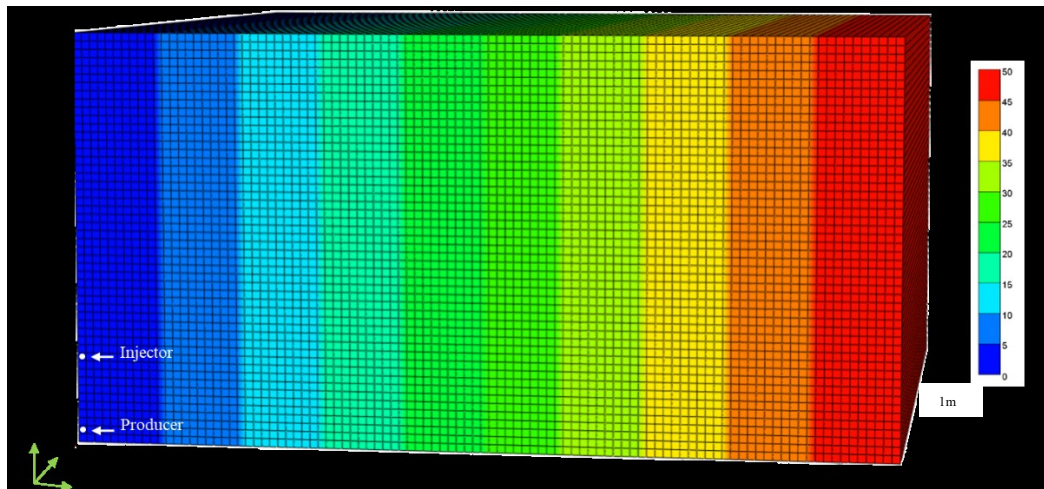
Figure 1. 3-D view of SAS simulation model.

STARS (CMG, 2019), a compositional thermal simulation, is used in this study to carry out the simulation. The simulation is run for seven years (2,555 days) and consists of the three SAS phases described in section 2.1.2.1. First, the pre-heating phase is imposed for the first 60 days. Then, the second phase contemplates 18 months of SAGD operation, where 95% quality steam is injected into the formation at a constant pressure of 3,400 kPa at 237°C until, as mentioned in chapter 2, the steam chamber is fully developed and reaches the top of the pay zone. Finally, the third phase is an alternate injection process between steam and solvent over multiple cycles; this phase is repeated until it is no longer economically profitable. A steam trap of 2°C below the steam

saturation temperature is imposed as a production control during the steam injection to prevent live steam production.

The solvent composition was chosen according to Yadali and Ben (2013), which recommend the injection of propane and methane as a solvent mixture. Additionally, according to Zhao et al. (2005), propane is the primary component responsible for reducing the liquid viscosity during depressurization; meanwhile, methane serves as a carrier gas that helps the solvent remain in the vapour phase at lower temperatures. Thereby, a mixture of 20 mol% methane and 80 mol% propane is selected for the base case. This mixture is heated to a temperature of $237°C$ and injected at a pressure of $3,400\ kPa$. A fixed bottom-hole gas (BHG) constraint is imposed during the solvent injection. A timeline for the SAS base process simulation is shown in Figure 2. The x-axis represents the simulated time span, the diamonds represent the exact moment each event starts, and the y-axis refers to well locations (5 m apart from each other).
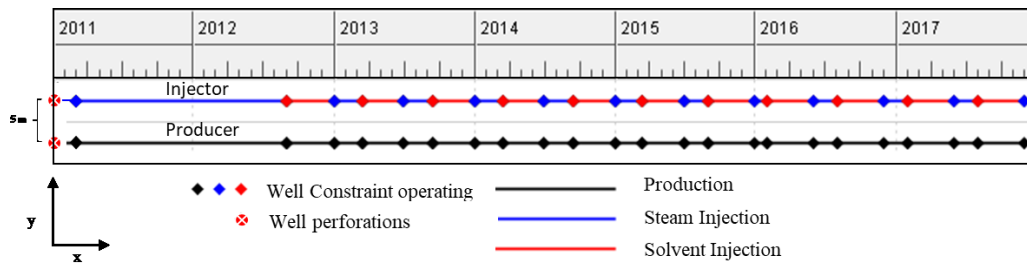
Figure 2. Timeline of the SAS process for the base case.

3.2. Base Case Simulation Results.

The results are analyzed with the oil saturation (S_o), temperature (T), and the global methane and propane mole fraction profiles plotted in Figure 3 at different SAS elapsed times.

Similar to the numerical simulation results presented in Zhao (2007) and Coimbra et al. (2019), it can be seen that at the end of phase 2 (end of SAGD phase), the steam chamber grows upward while steam is injected because the density of steam is lower than that of oil. However, in phase

3, when solvent starts to be injected, the vapour chamber is shifted downward since the solvent mixture's molecular weight (and density) is higher than that of steam, resulting in a noticeable change in the chamber shape in this phase. As a result, the chamber continues to expand horizontally than simply rising upward (when only steam is injected). The most significant chamber growth occurs at the end of phase 2, where only steam is injected since steam is more effective for mobilizing the oil than solvent.
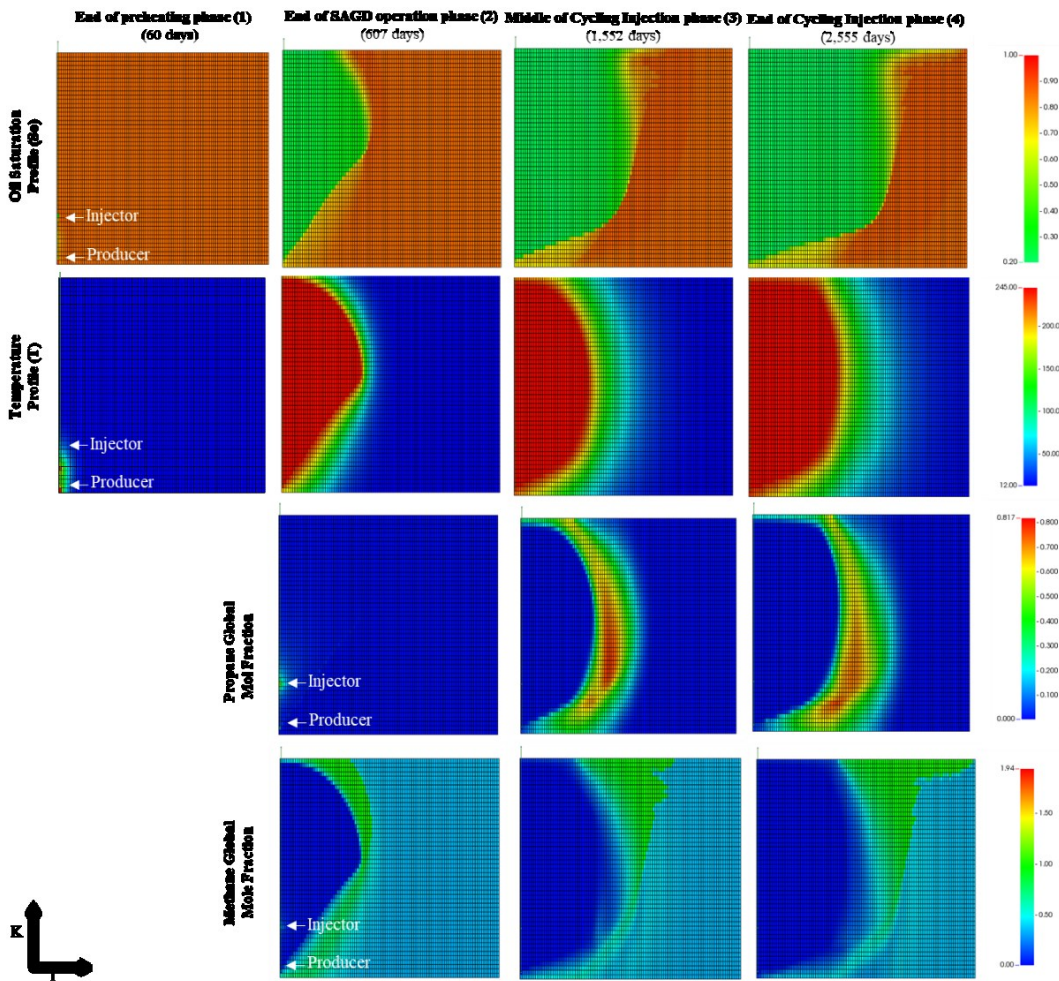
Figure 3. Oil saturation (S_o), temperature (T), and solvent global mole fraction distribution at different SAS times.

Interestingly, high propane concentrations tend to accumulate in the frontage of the chamber, allowing a better dilution with the oil; thus, the viscosity is reduced while methane is accumulated

at the top of the reservoir. It is also evident that the highest temperatures zones correspond to areas where steam tends to accumulate.

3.3. Sensitivity Analysis.

Sensitivity analysis (SA) is a tool used in a wide range of fields (including the oil and gas industry) to analyze how different values of a set of independent variables (decision variables) affect a specific dependent variable (objective function) under certain conditions. The robustness of these studies is evaluated according to the number of included parameters (Pichery, 2014).

In this study, a detailed SA is performed to examine the effects of various operational parameters on the SAS process performance and the objective functions. Also, a mesh sensitivity analysis is performed.

Two different SA methodologies are applied. 1) One Parameter At A Time (OPAAT): this method adopts a local approach where each parameter is varied independently while the others remain fixed. 2) Response Surface Methodology (RSM): uses a global approach to capture the correlation among numerous variables; overall, multiple parameters are adjusted together, and the results are fitted based on a response surface model (Polynomial equation or Neural Network). Figures 4 and 5 show an example of how oil fraction and the temperature profiles behave, respectively, on the base model using OPAAT methodology, changing the solvent composition. As can be seen, the more considerable chamber growth occurs when 80% propane and 20% methane are injected; this due to higher propane concentration in the solvent mixture leads to a better solvent dissolution with the oil, thus, higher viscosity reductions. Although even this methodology is widely used, adjusting more parameters simultaneously (i.e. RSM) allows having a better and deeper understanding of the interaction that the variables might have.
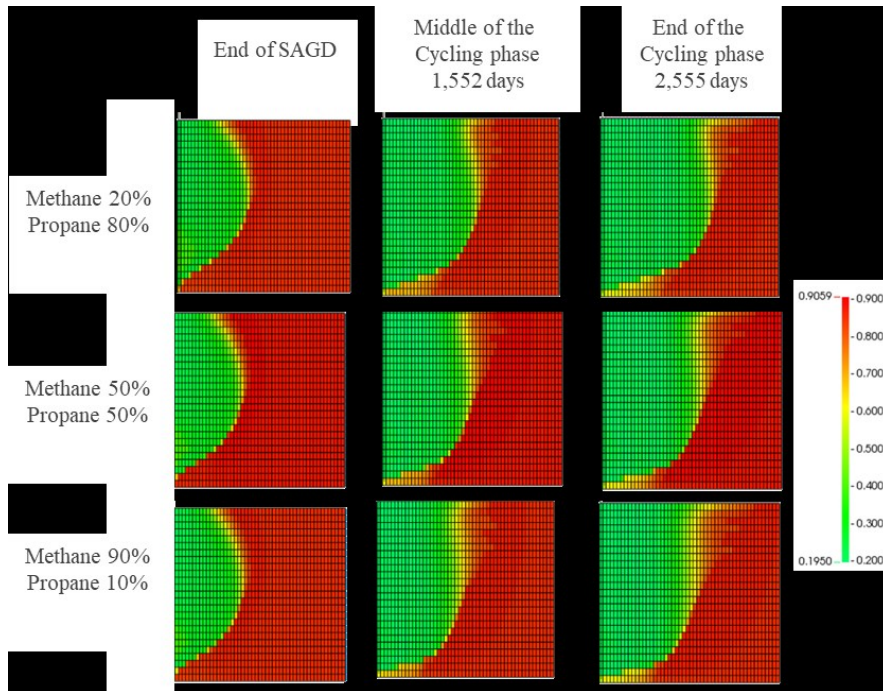
Figure 4. Oil fraction distribution at different SAS times using OPAAT.
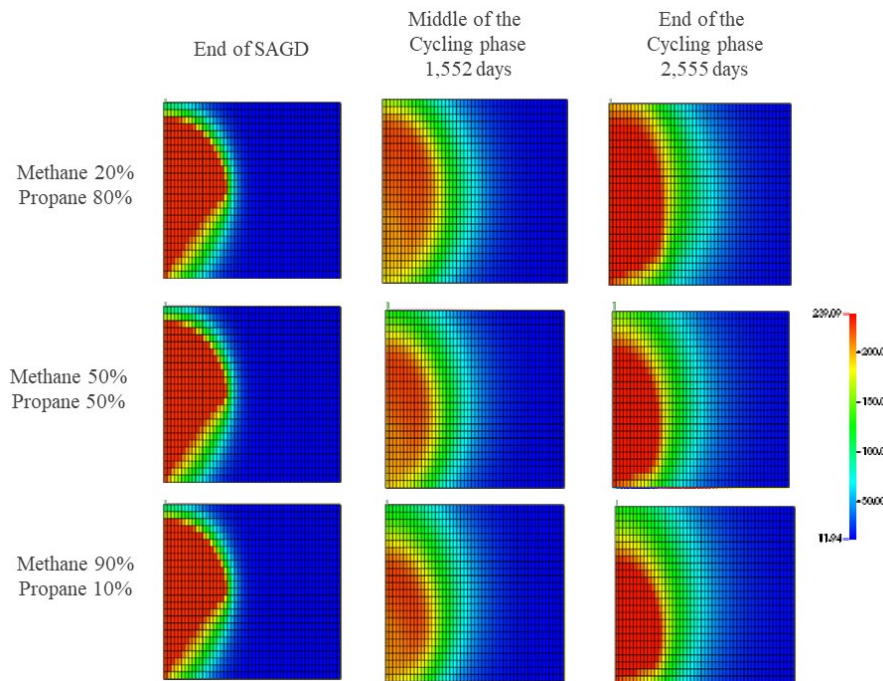
Figure 5. Temperature (T) distribution at different SAS times using OPAAT.

Using RSM, the total number of operational parameters could be quite high. Hence, to formulate a more manageable subset of parameters, the cyclic injection portion (i.e., phase 3) is divided into two periods, where the operational parameters remain constant for a particular period;

there are multiple cycles within each period. Different solvent compositions (i.e., propane mole fraction) and steam and solvent cycles durations in each period are varied. The rationale for dividing phase 3 into two periods is that from the SA results, it was observed that early on in the cycling phase, the steam-solvent chamber is developing, and the injected fluids do not travel far from the wells. In contrast, as more cycles are completed, the injected fluids would have to travel much larger distances to reach the chamber edge. Therefore, different trends regarding optimal operating parameters are observed. Figure 6 shows a timeline of the proposed SAS model for this study, including the pre-heating phase (1), SAGD phase (2), and two periods, part of the cycling phase (3).
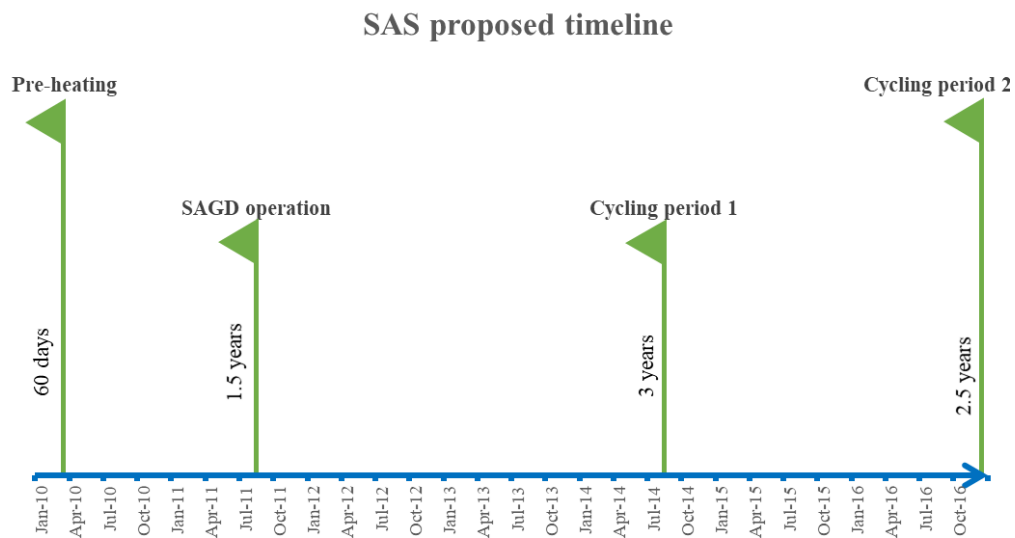
Figure 6. Timeline of the proposed SAS process.

A total of twelve potential decision variables are examined in the sensitivity analysis, such as solvent composition ($Propane_1$ and $Propane_2$), bottom-hole pressure in the injector when steam (BHP_{steam1} and BHP_{steam2}) and solvent (BHP_{solv1} and BHP_{solv2}) are injected, steam ($Cycle_{steam1}$ and $Cycle_{steam2}$) and solvent ($Cycle_{solv1}$ and $Cycle_{solv2}$) cycle duration time for each period within the cycling phase and steam quality. Also, the minimum operational bottom-hole pressure in the producer (BHP_{prod}), steam trap, and bottom-hole gas (BHG) production

23

constraints are incorporated; this is shown in Figure 7a. The subscript 1 and 2 refers to the first and second period of the cycling phase, respectively. The parameters without any subscripts are constant for the entire simulation.
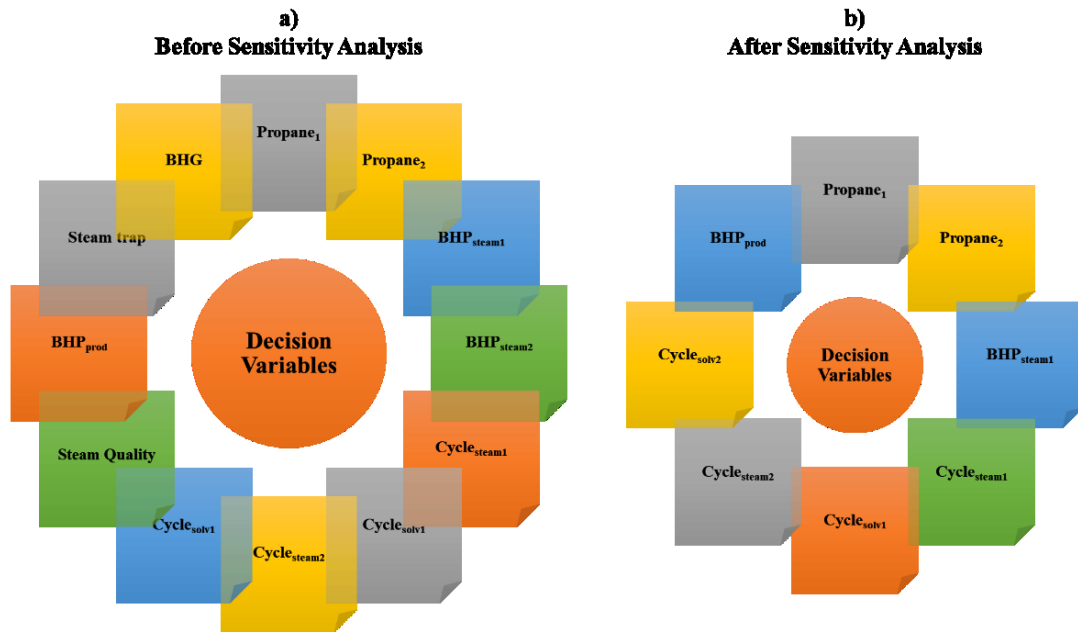
Figure 7. Initial and final decision variables for the optimization process.

Results of the sensitivity analysis (Figure 7b) are used to identify the eight most impactful decision variables, and their respective chosen ranges are presented in Table 2:

- Solvent composition – concentration of propane in the solvent mixture for each period ($Propane_1$ and $Propane_2$).

- Cycle duration – the duration of the steam and solvent injection for the first and second periods ($Cycle_{steam1}$, $Cycle_{solv1}$, $Cycle_{steam2}$ and $Cycle_{solv2}$)

- Maximum injector bottom-hole pressure when steam is injected – it must be greater than the initial reservoir pressure, and it is kept constant through both periods (i.e., the entire cycling phase).

- Maximum bottom-hole pressure of solvent injector – the difference in operating pressures during steam and solvent injection is less than 200 kPa, and it is also kept constant at 96% of BHP_{steam} during the simulation.

- Minimum bottom-hole pressure in the producer (BHP_{prod}) – the ranges are based on Ma and Leung (2019).

Table 2. Ranges of the decision variables in the SAS process.

Decision Variable	Min	Max
$Propane_1$ (%)	50	70
$Propane_2$ (%)	50	90
$Cycle_{Steam1}$ (days)	45	60
$Cycle_{Solv1}$ (days)	60	120
$Cycle_{Steam2}$ (days)	50	70
$Cycle_{Solv2}$ (days)	70	160
BHP_{Steam} (kPa)	3,300	4,000
BHP_{Prod} (kPa)	2,500	2,900

A mesh SA is performed varying the size of each grid block. Table 3 shows the cumulative Oil Production (cOP) for the SAS process using different grid block sizes; 0.5 m in the x and z-axis by 1 m in the y-axis is chosen since the cOP is the lowest (more realistic).

Table 3. Grid block size vs Cumulative Oil Production.

Grid block size (m)			cOP (m³)
x-axis	y-axis	z-axis	
0.5	1	0.5	4,350
0.6	1	0.6	4,856
0.7	1	0.7	5,010
0.8	1	0.8	5,490
0.9	1	0.9	5,553
1	1	1	5,653

3.4. Objective functions.

In this study, to account for the trade-off between oil production, steam injection and solvent usage, three objective functions are chosen: 1) Recovery Factor (RF), 2) cumulative Steam-Oil

Ratio ($cSOR$), and 3) cumulative Solvent consumption ($cSolv$) and can be formulated as follows in equation (4):

$$F(\vec{x}) = \{f_1(\vec{x}), f_2(\vec{x}), \dots, f_i(\vec{x})\} = \left\{\frac{1}{RF}, cSOR, cSolv\right\} \tag{4}$$

where F is the objective function and $\vec{x}$ denotes the decision variable vector. The RF is calculated according to equation (5):

$$RF = \frac{Vol_{oil}}{OOIP} \tag{5}$$

where Vol_{oil} is the produced oil at surface conditions, and $OOIP$ is the Original Oil In Place. Since the problem is framed as a minimization optimization, the Recovery Factor could be expressed as $1/RF$. Cumulative Steam-Oil-Ratio ($cSOR$) is calculated, according to Butler (1987), which is the volume of condensed steam (water) required to produce one barrel of oil.

It is important to mention that an alternative for assessing multiple objectives (i.e. $RF, cSOR$ and $cSolv$) is by combing them into one single target; for example, the net present value (NPV) can be used as an economic measure integrating all costs and price. However, the purpose of this research study is to gain additional insights into the interactions or trade-offs between these different key process measures. Furthermore, understanding these behaviours is needed to identify the optimal operating scenarios under different constraints. Thus, optimizing the SAS process using a single NPV objective function would not reveal such details. Hence, the MOO framework is adopted in this study.

3.5. Multi-Objective Optimization (MOO).

As explained in chapter 2, the purpose of MOO is to minimize or maximize a certain number of objective functions in terms of the decision variables ensuring that the optimal solution set satisfies

different constraints. Therefore, a general Multi-Objective Optimization Problem (MOOP) can be formulated as follows:

$$
\begin{bmatrix}
Minimize\colon F(\vec{x}) = \left(f_1(\vec{x}), f_2(\vec{x}), \dots, f_i(\vec{x})\right) \quad i = 1,2,\dots,c \\
Subject\ to\colon g_i(\vec{x}) \geq 0, \quad i = 1,2,\dots,m \\
h_i(\vec{x}) = 0 \quad i = 1,2,\dots,n \\
L_i \leq x_i \leq U_i \quad i = 1,2,\dots,l
\end{bmatrix} \tag{6}
$$

where f_i represent one of the objective functions, c is the total number of objectives, $\vec{x} = [x_1, x_2, \dots, x_l]^T$ is the vector of decision variables, l is the number of decision variables, m is the number of inequality constraints $g(\vec{x})$, n is the number of equality constraints $h(\vec{x})$, and L_i and U_i are the lower and upper bounds for each decision variable, respectively.

There are many different ways to formulate a MOO, and many commonly adopted methods are based on evolutionary optimization algorithms (Coello, 2018). Thus, three different MOEA are incorporated and are described in the following sections.

3.5.1. Strength Pareto Evolutionary Algorithm 2 (SPEA-II)

This algorithm is an enhancement of the Strength Pareto Evolutionary Algorithm (SPEA) and was developed by Zitzler et al. (2001). This approach incorporates a count and rank-based fine-grained fitness assignment strategy that includes density information to drive solutions toward the Pareto optimal front. Also, it has fast converging speed, good strength and orderly distributed solutions sets. The steps of SPEA-II are outlined below, and a flowchart is shown in Figure 8.

1. Population size (N), repository archive size ($\overline{N}$) and the maximum number of generations (T) are specified.

2. The initial population P_o is generated randomly; an empty archive P'_o is set, with $t = 0$.

3. The fitness or $G(\vec{x})$ for each individual $\vec{x}$ in both P_o and P_o' are calculated as the sum of the raw fitness $R(\vec{x})$ and the density $D(\vec{x})$:

$$G(\vec{x}) = R(\vec{x}) + D(\vec{x}) \tag{7}$$

The strength value of an individual, $S(\vec{x})$, represents the number of solutions that a particular $\vec{x}$ dominates and is calculated as follows:

$$S(\vec{x}) = |\{\vec{x}' \mid \vec{x}' \in P_o + P_o' \land \vec{x} \succ \vec{x}'\}| \tag{8}$$

where $|\cdot|$ represents the cardinality of a set; $\vec{x}'|\vec{x}' \in P_o + P_o'$ denotes a set of individuals $\vec{x}'$ that satisfice $(P_o + P_o')$, where $+$ stands for multi-set union, and $\vec{x} \succ \vec{x}'$ denotes that $\vec{x}$ dominates $\vec{x}'$. $R(\vec{x})$ is calculated by summing the strengths of all its dominators in $(P_o + P_o')$. For example, if an individual $\vec{x}_0$ is dominated by individuals $\vec{x}_1, \vec{x}_2$ and $\vec{x}_3$, the raw fitness $R(\vec{x}_0)$ is the sum of the strength values of $\vec{x}_1, \vec{x}_2$ and $\vec{x}_3$. If $R(\vec{x}) = 0$, $\vec{x}$ is a non-dominated individual.

$$R(\vec{x}) = \sum_{\vec{x}' \in P_o + P_o', \ \vec{x}' \succ \vec{x}} S(\vec{x}'), \tag{9}$$

Although the raw fitness assignment provides a sort of niching mechanism based on the Pareto dominance concept, it may fail when the majority of individuals do not dominate each other. Therefore, the density information $D(\vec{x})$ is used to discriminate between individuals with the same $R(\vec{x})$ values based on the K-nearest neighbour method:

$$D(\vec{x}) = \frac{1}{\sigma_{\vec{x}}^k + 2} \tag{10}$$

$$k = \sqrt{N + \bar{N}} \tag{11}$$

where $\sigma_{\vec{x}}^k$ is the Euclidean distance between the individual $\vec{x}$ and its kth-nearest neighbour. In the denominator, a constant of 2 is added to ensure that its value is always greater than

zero and $D(\vec{x}) < 1$. The solutions with a large k^{th}-nearest neighbour would have a small density score.

The non-dominated individuals in both P_o and P_o' with a fitness value below a certain threshold (y) are copied into the archive of the next generation (P_{o+1}') according to equation (12):

$$P_{o+1}' = \{\vec{x} \mid \vec{x} \in P_o + P_o' \wedge G(\vec{x}) < y\} \tag{12}$$

If the non-dominated solution front fits exactly into the new archive: $P_{o+1}' = \overline{N}$, this step is completed. If $P_{o+1}' < \overline{N}$, the best $\overline{N} - P_{o+1}'$ dominated individuals in $P_o + P_o'$ are copied to P_{o+1}'; this can be implemented by sorting the multi-set $(P_o + P_o')$ according to their G values and copy first $\overline{N} - P_{o+1}'$ individuals with $G(\vec{x}) \geq y$ from the resulting ordered list to P_{o+1}'. If $P_{o+1}' > \overline{N}$, some individuals in P_{o+1}' are removed through an archive truncation procedure shown in equation (12). This procedure eliminates individuals iteratively from P_{o+1}' until $P_{o+1}' = \overline{N}$. At each iteration, two individuals (e.g., $\vec{x}_a$ and $\vec{x}_b$) are randomly chosen from P_{o+1}', and $\vec{x}_a$ is removed for which $\vec{x}_a \leq \vec{x}_b$ if the minimum distance between $\vec{x}_a$ and another individual is less than the minimum distance between $\vec{x}_b$ and another individual; if there are too many individuals satisfying that condition, then a tie-breaker is employed by considering the next closest neighbour, p, and so on:

$$\vec{x}_a \leq \vec{x}_b :\Leftrightarrow \forall 0 < k < |P_{o+1}'|:$$
$$\left[\left(\forall 0 < p < k: \sigma_{\vec{x}_a}^p = \sigma_{\vec{x}_b}^p\right) \wedge \sigma_{\vec{x}_a}^k < \sigma_{\vec{x}_b}^k\right] \tag{13}$$

where $\sigma_{\vec{x}}^k$ denotes the distance of $\vec{x}$ to its kth-nearest neighbour in P_{o+1}'.

4. If the loop number $t \geq T$, P_{o+1}' is the Pareto-optimal set; otherwise, proceeds to step 5.

5. P_{o+1}' is subjected to the crossover and mutation operations to create a new population. The new population would replace the individuals in P_o. t is increased by one.

6. Repeat steps 3-5.

More details about the fitness calculation and the external maintenance of this process can be found in Zitzler et al. (2001).
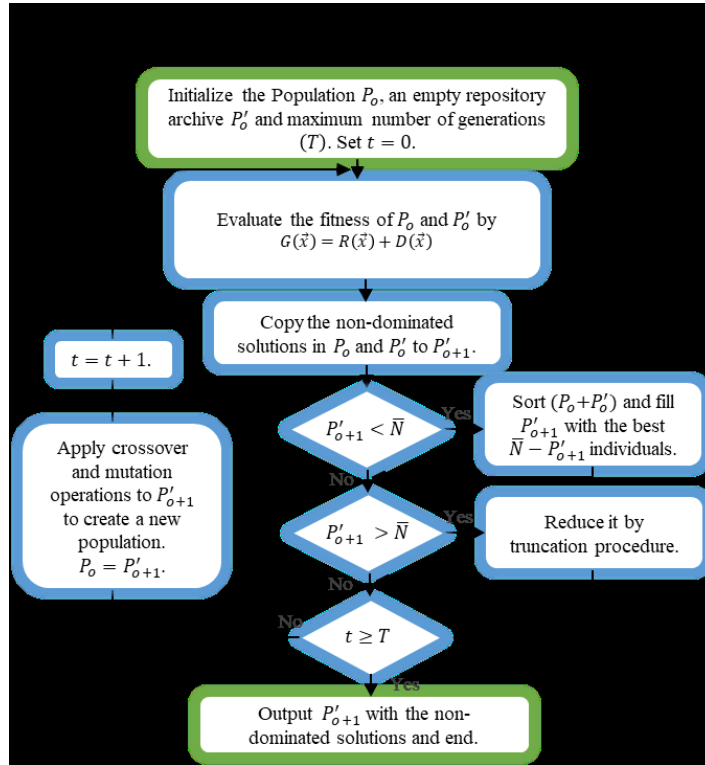
Figure 8. Flowcharts of SPEA-II algorithm.

3.5.2. Multi-Objective Particle Swarm Optimization (MOPSO).

This algorithm is an extended Particle Swarm Optimization (PSO) to MOOPs. This MOEA incorporates elitism and involves two closely related processes. 1) The archiving of good solutions and 2) How the best global for each individual is selected. According to Coello and Lechuga (2002), each individual's behaviour is affected by either the best local individuals within a specific neighbourhood or the best global individuals (the entire swarm population). MOPSO allows individuals to benefit from their experience and uses neighbourhood structures to regulate the algorithm's behaviour. The steps of MOPSO are outlined below, and a flowchart is shown in Figure 9:

30

1. Population size (N), repository archive size ($\overline{N}$) and the maximum number of generations (T) are specified.

2. The initial population P_o is generated randomly; an empty archive P_o' is set, with $t = 0$. The speed of each individual $\vec{x}$ is initialized as $V(\vec{x}) = 0$.

3. The fitness value $F(\vec{x})$ for each individual $\vec{x}$ in P_o is calculated according to equation (6), and the non-dominated solutions are stored in the archive P_o'. All individuals in P_o are distributed spatially in the search space following the hypercube method: First, the entire multi-dimensional search space, where each axis corresponds to one of the objective functions, is sub-divided into many smaller regions. Second, each individual $\vec{x}$ is assigned to one of the regions according to its objective function values. Finally, for each individual, $\vec{x}_{best}$ is initialized according to equation (14); it represents an individual that has the lowest objective functions and is stored in P_o.

$$\vec{x}_{best} = \vec{x}, F(\vec{x}) \tag{14}$$

The speed is the rate of change of each individual $\vec{x}$ in P_o in each dimension (Saka et al., 2013), and is computed using equation (15). For the first iteration ($t = 1$), $V(\vec{x})$ is set equal to 0 and for the subsequent iterations ($t = t + 1$), the velocity is updated with $V(\vec{x})_t = V(\vec{x})_{t-1}$:

$$V(\vec{x}) = W \times V(\vec{x}) + R_1 \times (\vec{x}_{best} - \vec{x}) + R_2 \times (\vec{x}' - \vec{x}) \tag{15}$$

where W is the inertia weight used to control the velocity of the individuals; typically, it is in the range of $0.4 - 0.5$. R_1 and R_2 are random numbers between 0 to 1. $\vec{x}'$ is an individual taken from the repository archive according to the following criteria: those hypercubes containing more than one individual are assigned a fitness value equal to a random number $R > 1$ divided by the number of individuals in that hypercube, as a form of fitness sharing.

Then, the roulette-wheel selection method is applied using the fitness values of all individuals in P_o' to select the hypercube from which $\vec{x}'$ is selected. This step incorporates the concepts of leader and deletion: the leader refers to the probability of a non-dominated solution to be chosen to guide the search; the individuals with a more significant crowding distance would have a higher probability of being selected to maintain spread along the Pareto front; deletion refers to the probability of an individual being deleted when the archive is oversized. To calculate these probabilities (*Prob*), equation (16) is used. These leader and deletion parameters are generally assigned a value of 2 (Motameni, 2016).

$$Prob = e^{-leader\ or\ delation*N} \tag{16}$$

After the fitness sharing and leader/deletion steps are implemented, a hypercube is selected, and a random individual $\vec{x}'$ is sampled from P_o'. The individuals in P_o are updated according to equation (17), adding the speed computed in equation (15):

$$\vec{x} = \vec{x} + V(\vec{x}) \tag{17}$$

Next, the repository archive P_o' is updated by copying the current non-dominated solutions stored in P_o; any dominated solutions in the repository archive are eliminated in the process. If $P_o' = \bar{N}$, this step is completed. If $P_o' < \bar{N}$, the best $\bar{N} - P_o'$ dominated individuals in P_o are copied to P_o' by sorting all these individuals in P_o according to their objective function calculations. If $P_o' > \bar{N}$, individuals in less populated areas of the objective space are given priority over those in populated regions. $\vec{x}_{best}$ is updated with $\vec{x}$ if $\vec{x} \succ \vec{x}_{best}$. The non-dominated solutions in P_o' are copied into an archive of the next generation P_{o+1}'.

4. If the loop number $t \geq T$, P_{o+1}' is the Pareto-optimal set; otherwise, proceeds to step 5.

5. P_{o+1}' is subjected to the crossover and mutation operations to create a new population. The new population would replace the individuals in P_o. t is increased by one.

6. Repeat from step 3.

More details can be found in Coello and Lechuga (2002).
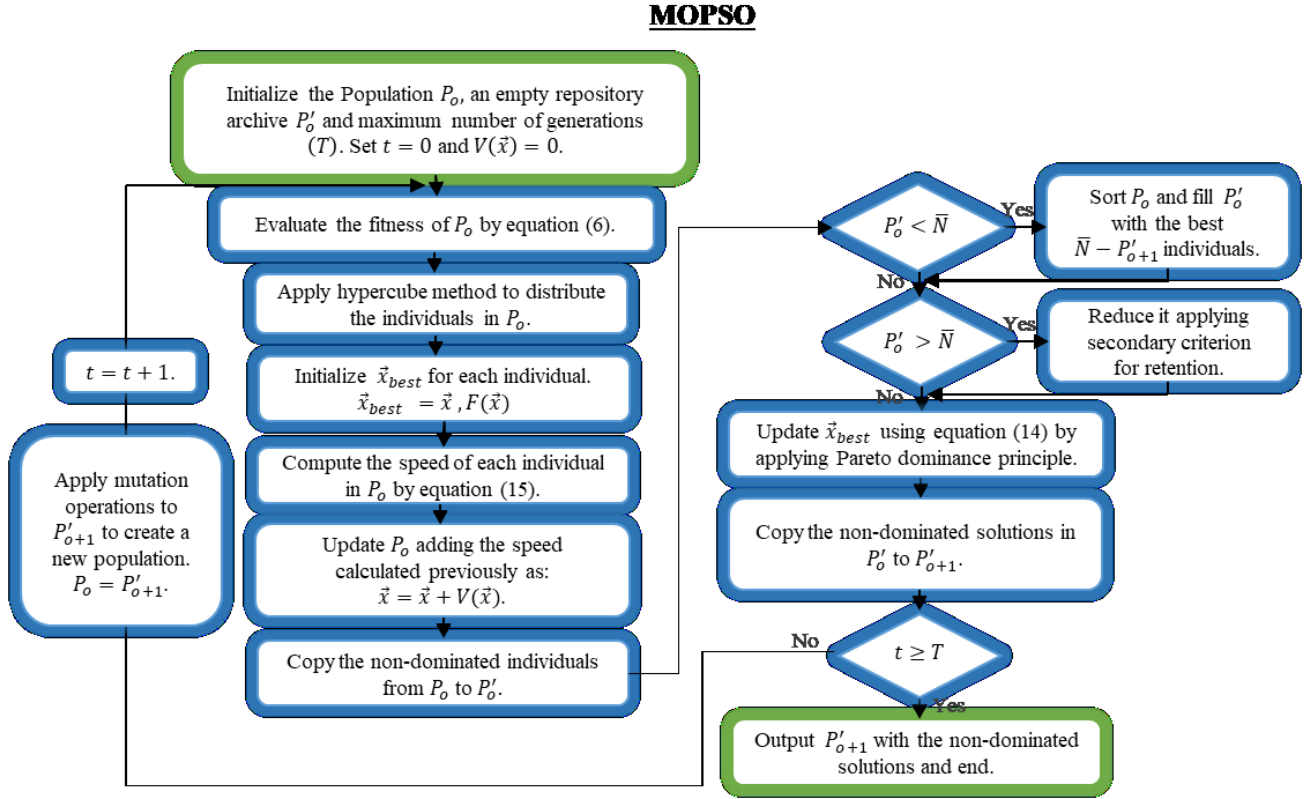
MOPSO

Figure 9. Flowcharts of MOPSO algorithm.

3.5.3. Pareto Envelope-Based Selection Algorithm (PESA-II).

PESA-II developed by Corne et al. (2001) enhances the multi-objective Pareto Envelope-Based Selection Algorithm (PESA, Corne et al., 2000). In this algorithm, the unit of selection is a region-based selection (hypercube method, Goldberg and Keb, 1991) in the objective space. Basically, instead of assessing a selective fitness to each individual, the selective fitness is assigned to the hypercubes in the objective area, which at least one individual occupies in the current approximation to the Pareto front. This selection method is shown to be more sensitive to ensuring a better spread of development along the Pareto front than individual-based selection (such as in

PESA) and aims to reduce the computational cost associated with traditional MOEAs (Coello, 2018). The steps of PESA-II are outlined below, and a flowchart is shown in Figure 10:

1. Population size (N), repository archive size ($\overline{N}$) and the maximum number of generations (T) are set.

2. The initial population P_o is generated randomly; an empty archive P_o' is set, with $t = 0$.

3. The fitness value $F(\vec{x})$ for each individual $\vec{x}$ in P_o is calculated according to equation (6), and the non-dominated solutions are stored in the archive P_o'. All individuals in P_o are distributed spatially in the search space following the hypercube method (same as MOPSO).

   Next, the repository archive P_o' is updated by copying the current non-dominated solutions stored in P_o; any dominated solutions in the repository archive are eliminated in the process. The rest is the same as in MOPSO, except that if $P_o' > \overline{N}$, some individuals in P_o' are removed through a maximum squeeze factor procedure (Schoenauer et al., 2000). The squeeze factor reflects how many other individuals in the archive are inhabiting the same hypercube; it is a selective fitness scheme that aims to select individuals from less-populated hypercubes. The non-dominated solutions in P_o' are copied into an archive of the next generation P_{o+1}'.

4. If the loop number $t \geq T$, P_{o+1}' is the Pareto-optimal set; otherwise, proceeds to step 5.

5. P_{o+1}' is subjected to the crossover and mutation operations to create a new population. The new population would replace the individuals in P_o. t is increased by one.

6. Repeat from step 3.

More details can be found in Corne et al. (2001) and Kaven et al. (2019).

PESA-II

Initialize the Population P_o, an empty repository archive P'_o and maximum number of generations (T). Set $t = 0$.

Evaluate the fitness of P_o by equation (1).

Apply hypercube method to distribute the individuals in P_o.

Copy the non-dominated individuals from P_o to P'_o.

$t = t + 1$.

Apply crossover and mutation operations to P'_{o+1} to create a new population. $P_o = P'_{o+1}$.

$P'_o < \bar{N}$ Yes → Sort P_o and fill P'_o with the best $\bar{N} - P'_{o+1}$ individuals.

No

$P'_o > \bar{N}$ Yes → Reduce it applying the squeeze factor method.

Copy the non-dominated solutions in P'_o to P'_{o+1}.

$t \geq T$

No

Yes

Output P'_{o+1} with the non-dominated solutions and end.

Figure 10. Flowcharts of PESA-II algorithm.

3.5.4. Multi-Objective Evolutionary Algorithm settings.

The specific setting and key futures implemented for the three algorithms are shown in Table 4. It should be noted that MOPSO and PESA-II incorporate a more robust solution model that might lead to improved computational efficiency and accuracy (Alvarez-Benitez et al., 2005; Rakhshani, 2020).

Table 4. configuration settings of the three MOEAs.

Parameters	Algorithm		
	SPEA-II	MOPSO	PESA-II
Number of generations (T)	150	150	150
Population size (N)	50	50	50
Repository size $(\bar{N})$	100	100	100
Number of grids per dimension	N/A	5	5
Inertia weight (R_1)	N/A	0.5	N/A

35

Inertia weight damping rate (R_2)	N/A	0.99	N/A
Personal learning coefficient (C_1)	N/A	1	N/A
Global learning coefficient (C_2)	N/A	2	N/A
Inflation rate	N/A	0.1	0.1
Leader selection pressure	N/A	2	2
Deletion selection pressure	N/A	2	1
Mutation probability	0.3	0.3	0.3
Crossover probability	0.7	N/A	0.7
Crossover gamma	0.15	N/A	0.15

3.6. Proxy Model construction.

As detailed in section 2.3, CMOST (CMG, 2019) is used for proxy modelling. Some experimental design is needed to build these proxy models. CMOST, considering the number of decision variables, determines how many experiments need to be created to obtain a representative sample data set that reproduces the objective function behaviour. A proxy model with a standard deviation lower than 0.6 or with a coefficient of determination (R^2) higher than 0.80, is typically considered to be acceptable (Bevillon and Mohagerani, 2015).

The input variables to construct these proxies are previously listed in Table 2. The training dataset is built by randomly choosing different sets of input variables according to the ranges listed in Table 2 for each decision variable. Then, numerical simulations are performed for each set of inputs to obtain the true output. After, the RSM is applied to build a proxy model for each output variable (objective function). The mismatch between the prediction and target value is minimized using the least-squares method

In this study, two proxy model sets are trained using a different number of training experiments: 50 vs. 90 to compare their accuracy when calculating the objective function and the training time needed to build each one.

3.7. Proposed Multi-Objective Optimization Workflow.

The entire proposed workflow to optimize the SAS process is shown in Figure 11 and consists of four main steps:

1. A base simulation model is built using Builder, a CMG (2019) tool.

2. As detailed in section 3.3, a sensitivity analysis is performed to identify the most impactful decision variables; the simulation results performed in STARS (CMG, 2019) of this sensitivity analysis are also included in the training data for constructing the proxy model (section 3.6).

3. A total of 50 cases for the proxy model are generated (50 training + 7 testing) using RSM.

4. The proxy model is then integrated into each of the three chosen MOEA methods (section 3.5) to search for a set of Pareto-Optimal solutions. The MOEAs implementation is adapted from various MATLAB open code sources developed by Mostapha (2015).
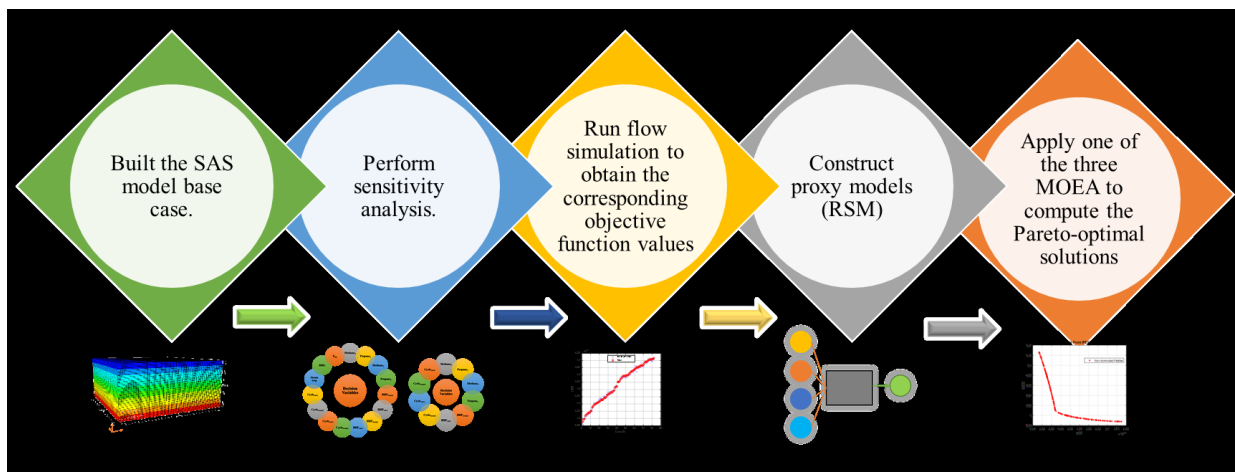
Figure 11. Proposed workflow of the Steam Alternating Solvent (SAS) optimization process.

Chapter 4: Homogeneous case – Result and discussion

This chapter presents the results from the sensitivity and proxy analysis of the homogenous case. Moreover, the solutions Pareto front and the optimal operational parameters for the same base model are shown.

4.1. Sensitivity Analysis - OPAAT methodology

The OPAAT approach, as mentioned in section 3.3, is used to assess the impact of individual parameters in each SAS period. For the first cycling period, here are some important observations:

- Propane concentration ($Propane_1$) in the solvent composition strongly influences the ultimate oil recovery: a reduction in $Propane_1$ leads to a reduction in RF and $cSolv$; less propane also implies that $Cycle_{steam1}$ must be extended thus, $cSOR$ increases; this can be seen in Figure 12a.

- RF and $cSOR$ are not impacted by $Cycle_{steam1}$, while $cSolv$ seems to be exhibit a slightly inverse relationship with $Cycle_{steam1}$ (Figure 12b)

- Figure 12c shows that $Cycle_{solv1}$ does not impact RF and $cSOR$, while $cSolv$ is inversely related to $Cycle_{solv1}$.

For the second cycling period, $Propane_2$ does not significantly impact the objective functions (Figure 13a), while $Cycle_{steam2}$ (Figure 13b) and $Cycle_{solv2}$ (Figure 13c) would affect the objective functions in similar ways to $Cycle_{steam1}$ (Figure 12b) and $Cycle_{solv1}$ (Figure 12c), respectively. Also, the objective functions are not overly sensitive to the ranges of BHP_{prod} (Figure 13d) examined here.
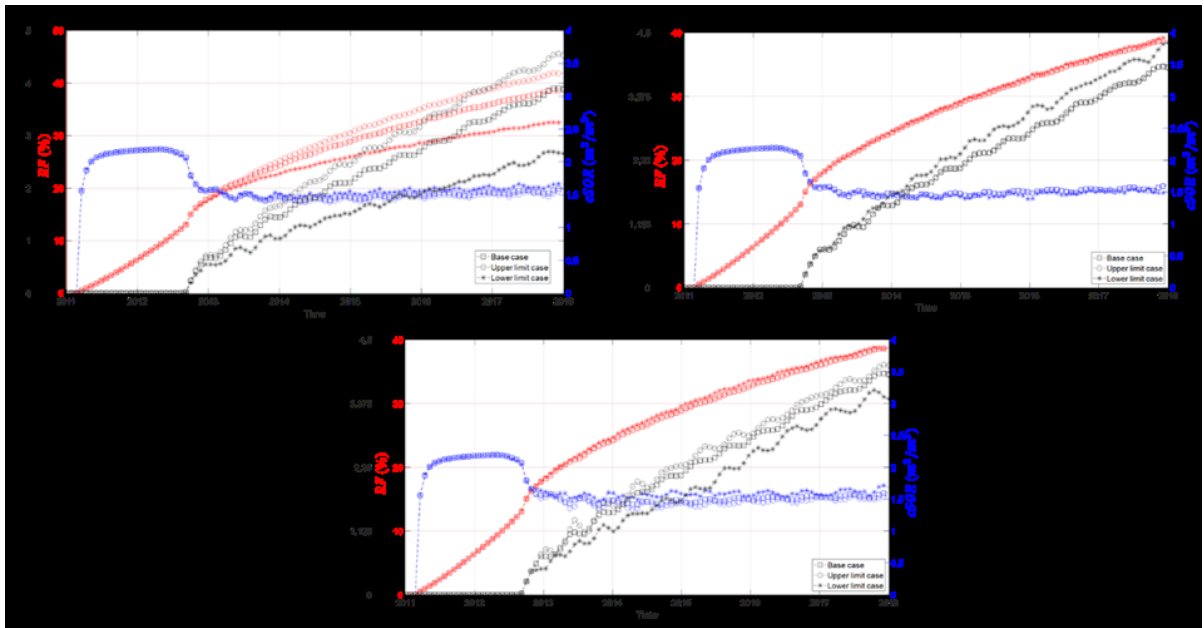
Figure 12. Results of the OPAAT analysis for the first period.
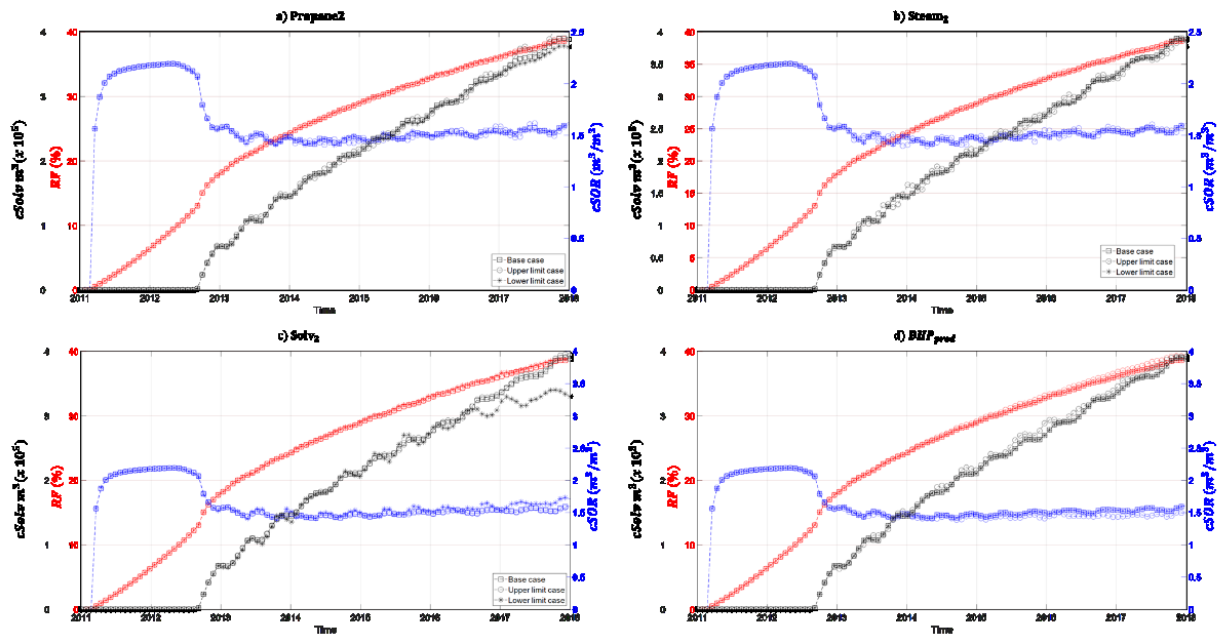
Figure 13. Results of the OPAAT analysis for the second period.

4.2. Response Surface Methodology - Proxy model analysis

Two proxy model sets are trained using 50 and 90 different training experiments. The corresponding training results (prediction accuracy or R^2) and the training time for the RF are

presented in Table 5; similar levels of prediction accuracy and training time are observed for the

other decision variables ($cSOR, cSolv$).

Table 5. Accuracy and training time comparison for RF proxy.

Training Data (experiments)	R^2	Training time (min)
50	0.95	1,680.56
90	0.965	3,025.00

Considering that the R^2 value for the proxy trained with 50 experiments is sufficiently high,

and the corresponding training time is low, results for this set of proxy models (trained with 50

experiments) are used subsequently for all MOEA calculations. Table 6 compares the raw and

adjusted R^2 for each objective function. The RSM coefficients necessary for the mathematical

equation to calculate the $RF, cSOR$, and $cSolv$, respectively is shown in Table 7.

Table 6. Coefficient of determination (R^2) and ($R^2_{adjusted}$) of the RSM proxy model.

Objective Function	R^2	$R^2_{adjusted}$
RF	0.95	0.949
$cSOR$	0.95	0.947
$cSolv$	0.943	0.938

Table 7. RSM coefficients.

Term	RSM Coefficient RF	Term	RSM Coefficient $cSOR$	Term	RSM Coefficient $cSolv$
Interception (β_0)	44.26	Interception (β_0)	3.4759	Interception (β_0)	1,512,900
Propane$_1$ (β_1)	-92.43	Propane$_1$ (β_1)	0.1629	Propane$_1$ (β_1)	-2,375,300
Propane$_2$ (β_2)	11.23	Propane$_2$ (β_2)	0	Propane$_2$ (β_2)	238,867
Cycle$_{solv1}$ (β_3)	-0.0804	Cycle$_{solv1}$ (β_3)	0.0010	Cycle$_{solv1}$ (β_3)	-1,706.02
Cycle$_{steam1}$ (β_4)	0	Cycle$_{steam1}$ (β_4)	0.0021	Cycle$_{steam1}$ (β_4)	-19,461.80
Cycle$_{steam2}$ (β_5)	0.3669	Cycle$_{steam2}$ (β_5)	0.0012	Cycle$_{steam2}$ (β_5)	5,724.81
Cycle$_{solv2}$ (β_6)	0.0208	Cycle$_{solv2}$ (β_6)	-0.0012	Cycle$_{solv2}$ (β_6)	1,168.80
BHP$_{steam1}$ (β_7)	0.0013	BHP$_{steam1}$ (β_7)	-0.0008	BHP$_{steam1}$ (β_7)	2.44
BHP$_{prod}$ (β_8)	-0.0043	BHP$_{prod}$ (β_8)	-0.0007	BHP$_{prod}$ (β_8)	-400.49
(β_1)^2	55.9839	(β_1)*(β_3)	-0.0037	(β_1)^2	1,242,600.00

$(\beta_1)*(\beta_3)$	0.10	$(\beta_7)^2$	1.0741E-07	$(\beta_1)*(\beta_3)$	2,873.72
$(\beta_1)*(\beta_7)$	0.0039	$(\beta_8)^2$	1.3875E-07	$(\beta_1)*(\beta_7)$	228.91
$(\beta_1)*(\beta_8)$	0.0058			$(\beta_2)*(\beta_3)$	-1,830.97
$(\beta_2)*(\beta_3)$	-0.0485			$(\beta_3)*(\beta_5)$	31.02
$(\beta_2)*(\beta_5)$	-0.0871			$(\beta_4)*(\beta_8)$	6.79
$(\beta_3)*(\beta_5)$	0.0006			$(\beta_5)^2$	-68.11
$(\beta_5)^2$	-0.0026			$(\beta_5)*(\beta_6)$	-8.26
$(\beta_5)*(\beta_6)$	-0.0004				

The proxy model predictions vs the actual simulation results comparison for the 50 training cases is shown in Figure 14. As can be observed, the proxy model predictions are in good agreement with the simulated ones since R^2 for each objective function is close to 1 and the Mean Square Error (MSE) is close to zero.
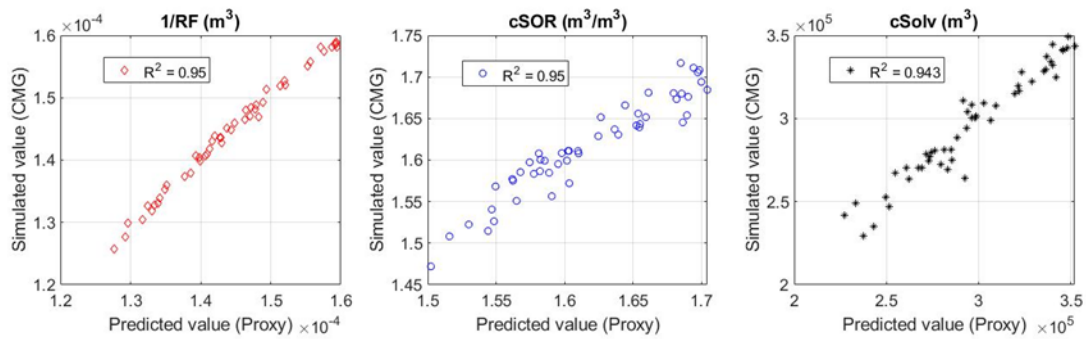
Figure 14. Comparison between the simulated (target) values versus the RSM proxy model predictions for the 50 training cases.

4.3. MOO Analysis – Pareto Front Solutions

The initial population and the 3-D Pareto fronts obtained using the three MOEA algorithms are shown in Figure 15. As can be seen, the shapes of the Pareto fronts are similar, but interestingly, more even and smooth solutions distributions are obtained using the SPEA-II method.

To better visualize the trade-off between the different objective functions, the 3-D Pareto front is divided into three quadrants: blue, green, and magenta sections, and it could be visualized in a series of 2-D plots as shown in Figure 16.
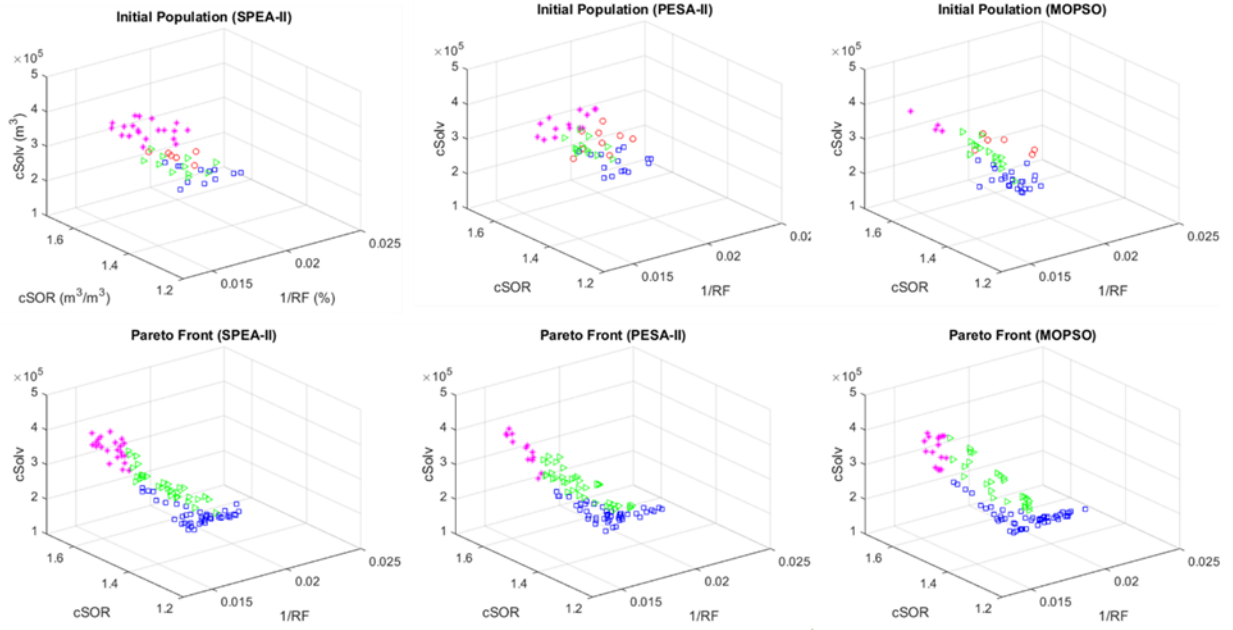
Figure 15. Pareto-front for different MOEAs.
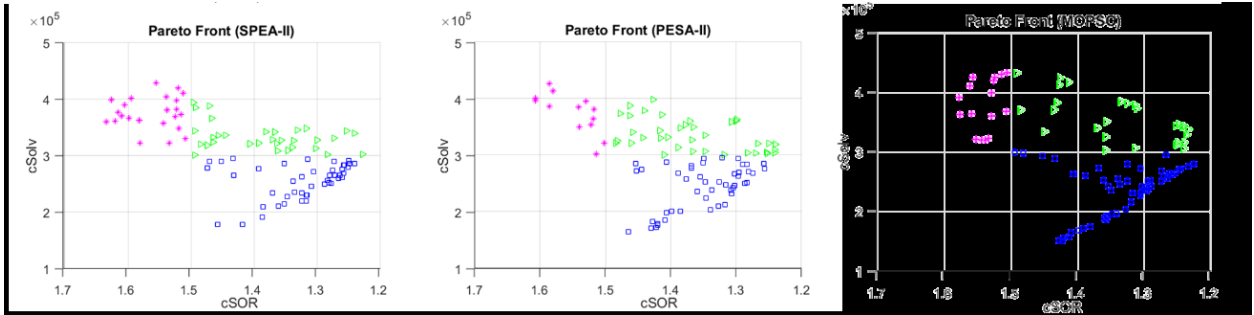
Figure 16. 2-D Pareto-front for different MOEAs.

Table 8 summarizes the computational assessment requirements to perform the SAS optimization with and without using proxy models. One hundred fifty iterations are performed for each optimization, with 50 individuals in each iteration. It is important to mention that after 50 generations on average, the Pareto front is fully developed in all MOEAs. A typical flow simulation run (computation of three objective functions) takes approximately 33.61 minutes. Therefore, significant savings in computational costs can be realized when the proxy models are used for evaluating the objective functions (an average run time for computing all three objectives using the proxy models is approximately 0.0000594 minutes).

Table 8. Comparison of the total computing time with and without proxy models.

Steps	No proxy	Proxy	
		50 experiments	90 experiments
Building time (min)	N/A	1,680.56	3,025
Objective Function Calculation (min)	(33.61 min) × (50 individuals) × (150 iterations) = 252,075	(0.0000594 min) × (50 individuals) × (150 iterations) = 0.4455	(0.0000594 min) × (50 individuals) × (150 iterations) = 0.4455
Rest of MOEA (min)	1.65	1.65	1.65
Total Time (min)	**252,076.65**	**1,682.65**	**3,027.09**

4.4. Optimal Operational Parameters Ranges Analysis

Each Pareto front quadrant represents a distinct optimal operating scenario. In this section, the individual characteristics of each quadrant using SPEA-II are discussed first. Then, general conclusions and insights will be highlighted at the end. The results of the optimal operational ranges using MOPSO and PESA-II are shown in Appendix B.

4.4.1. Low $cSOR$ – Low $cSolv$ (Blue)

Figure 15 illustrates the general characteristic when less steam and solvent are injected. To achieve this, during the first-period short solvent and steam injection durations ($Cycle_{solv1}, Cycle_{steam1}$) at low steam injection pressure (BHP_{steam1}) is recommended, as can be seen in Figure 17. Since the optimum operational strategy aims to reduce solvent and steam injection (two of the objective functions), for the second period (i.e., later stages), slightly lower portions of propane ($Propane_2$) are more optimal; however, longer injection durations ($Cycle_{solv2}$ and $Cycle_{steam2}$) are recommended to maintain reservoir temperature (Figure 18).

Figure 17. Final optimal ranges of the controllable operational parameters obtained using SPEA-II for the first period vs. the objective functions in the blue section.
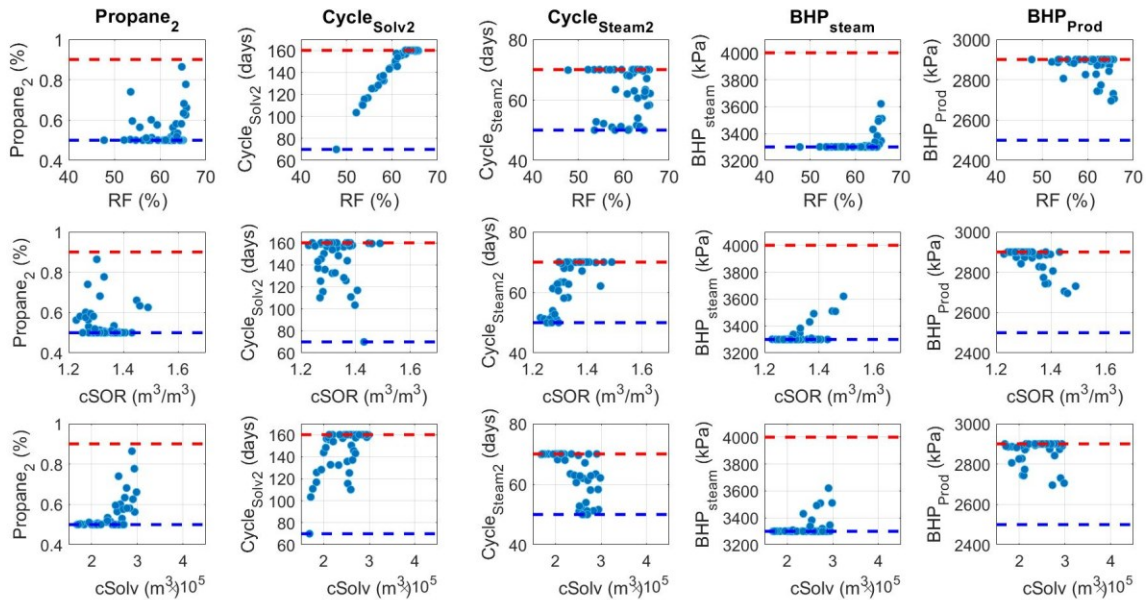
Figure 18. Final optimal ranges of the controllable operational parameters obtained using SPEA-II for the second period vs. the objective functions in the blue section.

The average *RF* for this group is lower than most other sections (e.g., *RF* is in the range of 45-65%, while the green and magenta groups have *RF* > 65%). *RF*, within this group, increases by injecting more solvent and steam, as well as drawing down more aggressively (i.e., increasing

$Propane_1$ and BHP_{steam1}, as well as reducing BHP_{prod}). The drawback, as expected, such strategies would lead to an increase in $cSOR$ and $cSolv$.

The differences between the optimum operational strategy in the first and second periods are related to the distance each fluid needs to travel into the reservoir. For example, during the second period, since the chamber has advanced much further away from the wells pair and the front is more diffused, injecting solvent with high propane content may not be as impactful as increasing the duration of solvent injection.

4.4.2. High $cSOR$ – High $cSolv$ (Magenta)

The solutions in this quadrant represent conditions where most steam and solvent are injected, as illustrated in Figure 15. The ranges of the optimal values for all objective functions are high: RF: 60 to 70%, $cSolv$ 3 to $4.5 \times 10^5 \ m^3$ and $cSOR$: $1.7 \ m^3/m^3$. As can be seen in Figure 19, for the first period, it seems more optimal to have short solvent cycles ($Cycle_{solv1}$) combine with high propane concentration ($Propane_1 \cong 70\%$; long steam cycles ($Cycle_{steam1}$) and high steam injection pressure (BHP_{steam}) are needed.

For the second period (Figure 20), the optimal operational strategy, similar to the blue section, might be injection solvent during long cycles ($Cycle_{solv2}$); however, more flexibility in $Propane_2$ is observed. $Propane_2$, $Cycle_{steam2}$, and BHP_{steam} appear to be correlated: higher propane concentrations should be accompanied by higher BHP_{steam} and reservoir temperature, while $Cycle_{steam2}$ should be reduced accordingly to avoid a dramatic increase in $cSOR$. This flexibility in adjusting the propane concentration might probably be due to the conditions at which the variables were adjusted in the first period and how much of the reservoir has already been reached by the steam-solvent chamber. So, for the second period, it may be more beneficial to inject solvent in fewer quantities (low $Propane_2$) for more time (long $Cycle_{solv2}$) since the solvent need to

travel a longer distance to reach the edge of the chamber. Additionally, it is observed that if less

steam is injected, higher propane concentrations might be needed to maintain a balance among the

objectives.
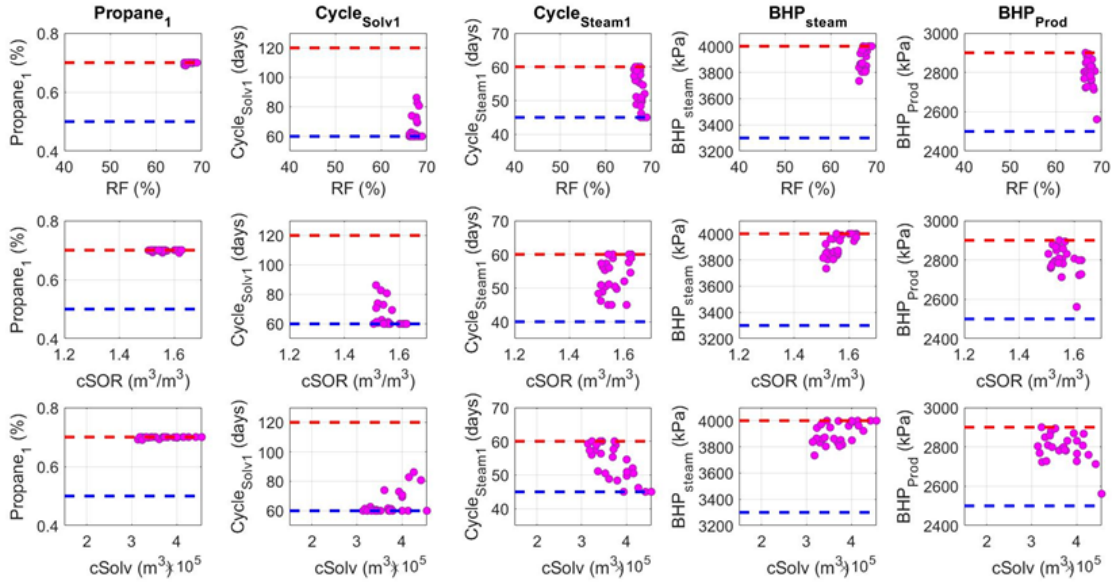
Figure 19. Final optimal ranges of the controllable operational parameters obtained using SPEA-II for the first period vs. the objective functions in the magenta section.
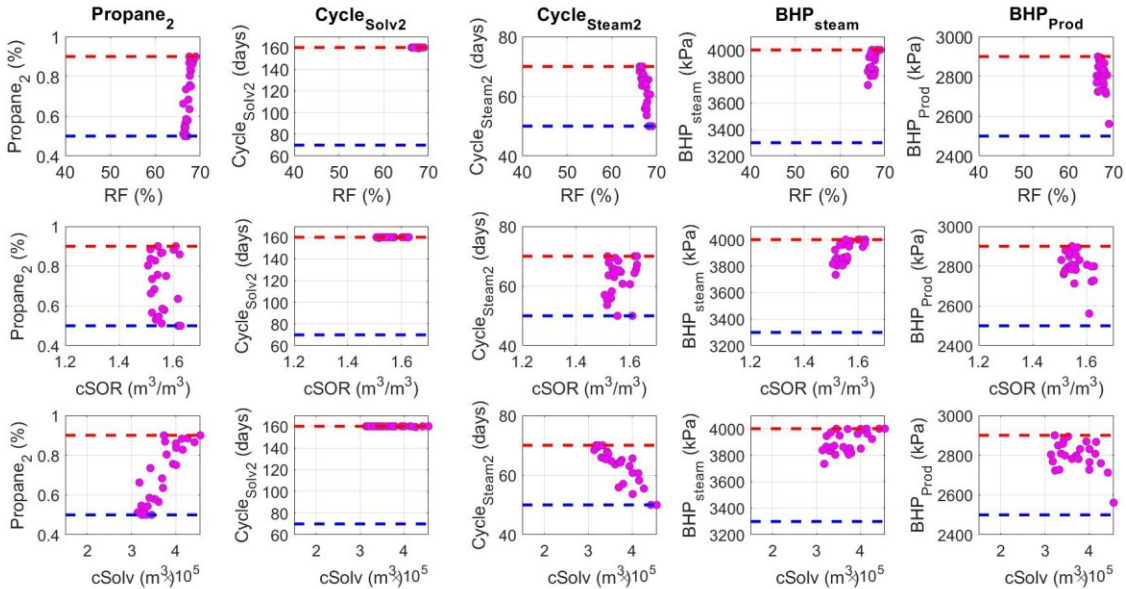
Figure 20. Final optimal ranges of the controllable operational parameters obtained using SPEA-II for the second period vs. the objective function in the magenta section.

4.4.3. Low $cSOR$ – High $cSolv$ (Green)

The solutions in this section represent conditions where less steam and more solvent are injected into the reservoir. The ranges of RF (60 to 70%) and $cSolv$ (3 to $4 \times 10^5 \ m^3$) are the highest, while $cSOR$ is the lowest (1.2 to 1.5 m^3/m^3), among all the other sections (Figure 15). For the first period (Figure 21), similar to the magenta section, it is more optimal to inject propane at a very high concentration ($Propane_1 \cong 70\%$) with short solvent cycles ($Cycle_{solv1}$). However, opposite to the magenta (section 4.4.2) and similar to the blue (section 4.4.1 section) group, BHP_{steam} is generally quite low; although there is potential to inject more steam by increasing BHP_{steam} to keep the temperature high and enabling more solvent to be injected), drawing down more aggressively (reducing BHP_{prod}), would increase RF at the expense of increasing $cSOR$.
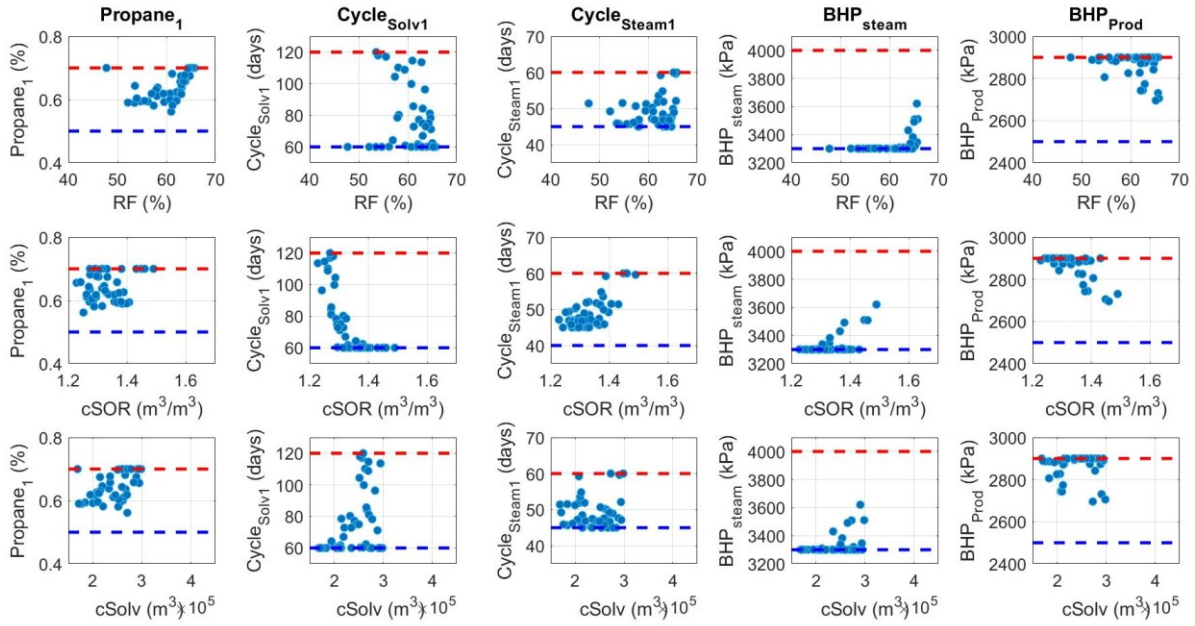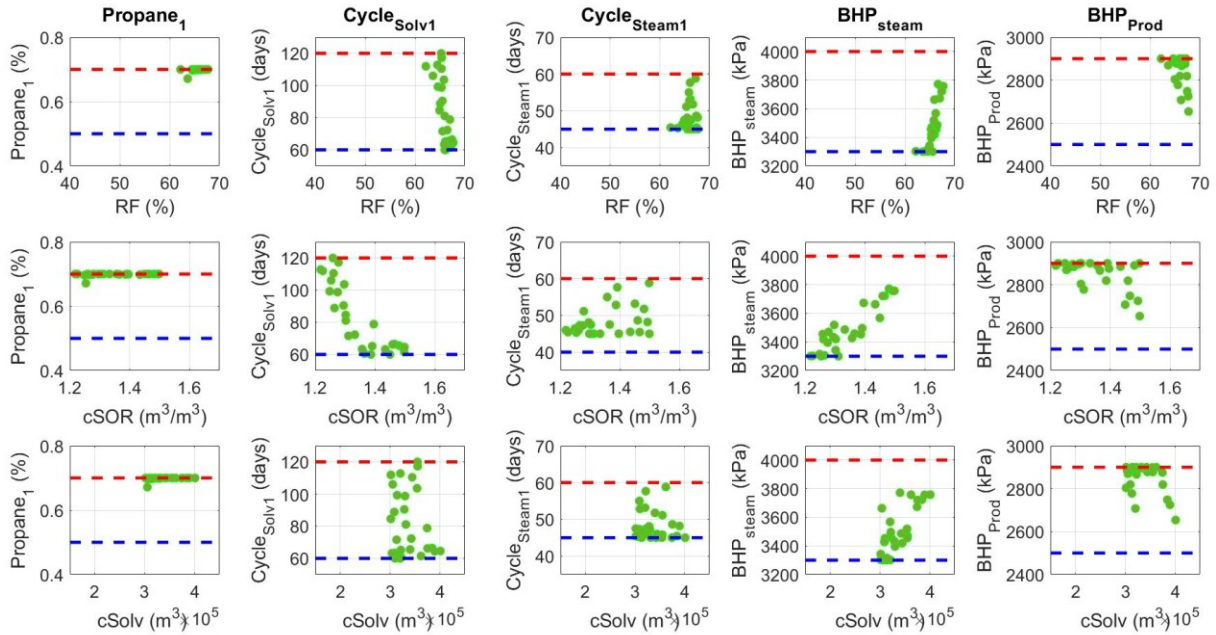

Figure 21. Final optimal ranges of the controllable operational parameters obtained using SPEA-II for the first period vs. the objective functions in the green section.

For the second period (Figure 22), it is possible to implement longer solvent cycles ($Cycle_{solv2} \cong 160\ days$) with more variability in the propane concentration ($Propane_2$). This trend is similar to what is observed for the magenta (section 4.4.2)
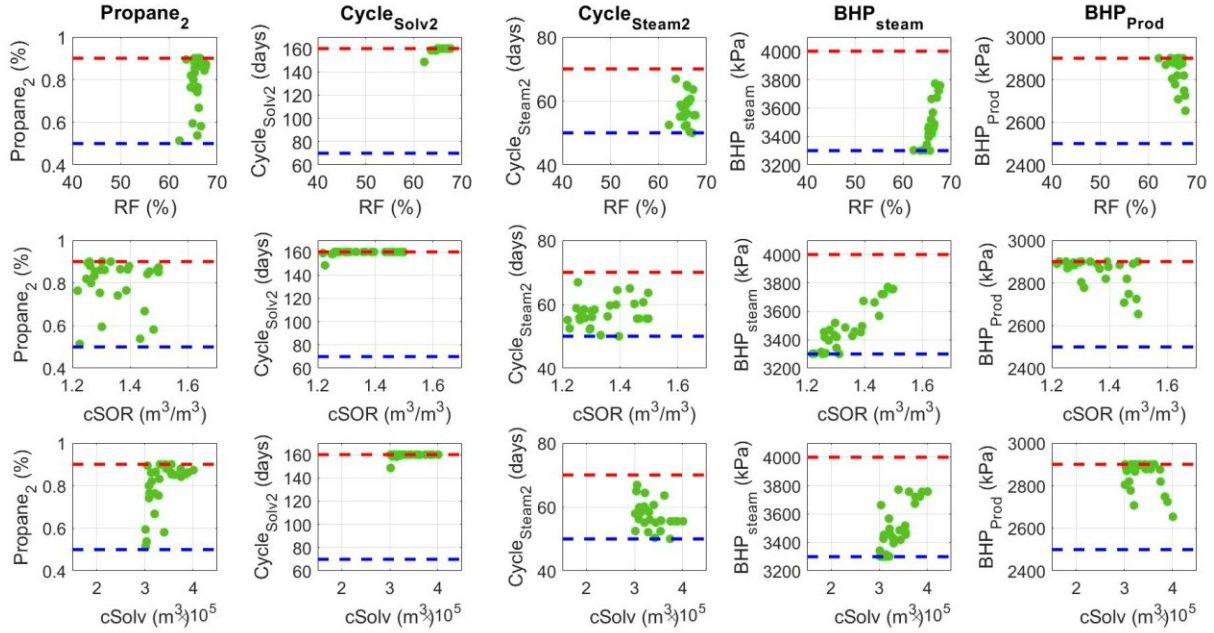
Figure 22. Final optimal ranges of the controllable operational parameters obtained using SPEA-II for the second period vs. the objective functions in the green section.

4.5. General Remarks

Among the results, some interesting findings were observed:

- Overall, if more steam is to be injected (i.e. magenta section) is preferred longer steam injection cycles ($Cycle_{steam1}, Cycle_{steam2}$) instead of increase the BHP_{steam} drastically.

- Moreover, if more solvent needs to be injected, such as in the magenta and green sections, it seems to be more effective to add, in the first period, high propane concentrations over short cycles. Then, for the second period, switch to low propane concentrations over long cycles because the solvent has to travel further to the chamber edge during the later production stage. This assumption is in accordance with lab observations reported by Zhao et al. (2005); they found that when a considerable amount of propane is injected into the

reservoir, the temperature in areas away from the wells drops below the dew point of the solvent mixture, making the favourable condition to create a liquid-liquid phase due to propane condensation. Thus, the mass transfer of propane into the oil phase is enhanced, and consequently, the oil recovery would increase.

- Results revealed that when propane concentration is increased, higher BHP_{steam} is usually accompanied; this to achieve a higher temperature in the reservoir to remain the solvent in the vapour phase.

- Somehow BHP_{prod} appears to be related to BHP_{steam}. From the results graphs can be seen that if BHP_{steam} increases, BHP_{prod} generally decreases; this might be to allow more liquid (either oil or solvent) to be produced.

- The objective of dividing the cycling phase into two periods, first (early) and second (late), is based on the sensitivity analysis results. As is well-known from field-scale applications, as the chamber advances away from the wells pair after a while, more time is required for the injected fluids to reach the chamber edge. Although results showed it is more optimal to implement short cycles initially, at some point, this strategy may not be efficient anymore. The oil rate might start to drop more rapidly, and this may be an indicator to switch to the longer cycles, which are generally recommended for the second period.

- All three used MOEAs showed that some trade-offs need to be considered between the targets (objective functions) when optimizing the SAS process. One example is Figure 20; if a higher BHP_{steam} is needed for more propane to be injected, this strategy might be compensated by reducing the steam cycle duration to maintain a balance between the objectives. Moreover, this would help keep, for instance, $cSOR$ at reasonable levels while RF and $cSolv$ somehow increase.

- Regarding the concordance among the results between the used MOEAs, small differences compared with SPEA-II results were identified. For example, 1) MOPSO, in the magenta section, gives slightly wider $Propane_1$ (Figure 47) and $Cycle_{solv2}$ (Figure 48) optimal ranges and in the blue section also on $Cycle_{solv1}$ (Figure 45). Besides, in the green section, the solutions distribution is different [$Cycle_{solv1}$, $Cycle_{steam1}$ (Figure 49) and $Propane_2$ (Figure 50)]. 2) Using PESA-II, narrow optimal ranges in terms of $Cycle_{solv1}$ in the magenta (Figure 53) and green (Figure 55) sections are observed.

Chapter 5: Heterogeneous case – Modelling, results and discussions

This chapter presents the modelling methodology, how the heterogeneities (i.e. shale barriers) are parameterized, the experimental design construction process (super-imposed methodology), and the proposed modified optimization workflow for heterogeneous reservoirs. Additionally, the sensitivity and proxy analysis, the solution Pareto fronts, and the optimal operational parameters of the four most impactful heterogeneous models accounting for two and three objective functions are detailed.

5.1. Modelling Methodology

The 2-D numerical model described in section 3.1 was used as a base model to build the heterogeneous reservoir models. The reservoir, input conditions, grid, rock and fluid properties used are listed in Table 1. Similar to the homogeneous case (section 3.1), the data was collected from the Suncor's Firebag project (Zheng et al., 2017) and the Surmont project (Li, 2006) located in the Fort McMurray formation in the Athabasca region in Alberta, Canada and from SAGD studies done by Ma et al. (2015).

A total simulation duration of 5,475 days (15 years) is considered in the study, and the entire simulation period is divided into three phases as in section 3.1.

5.2. Parameterization and super-imposed methodology

In this study, heterogeneities such as shale barriers are incorporated since these types of formations are commonly found in heavy oil reservoirs. Shale barriers have particular characteristics, such as low porosity, permeability and thermal conductivity (Huang et al., 2015, Luo et al., 2015, Middleton et al., 2017). The shale permeability was found to be excessively smaller than the oil sands permeability, typically reported in the range of 10^{-6} to $10^{-3}\ mD$ (Magara, 1968; Borst, 1983). Due to these factors, oil production is negatively affected due to the

slow steam/solvent chamber evolution, and the migration fluid behaviour might change (Zhang et al., 2021). The shale properties used in this study are listed in Table 9 and were taken from data reported by Zheng et al. (2017).

Table 9. Shale properties

Description	Parameters	Values
	Shale porosity (fraction)	0.25
	Shale Permeability in I and J direction (mD)	$3x10^{-5}$
	Shale Permeability in K-direction (mD)	$1x10^{-5}$
	Oil Saturation in Shale (S_o)	0
Shale Properties	Water Saturation in Shale (S_w)	1
		$K_{rw} = 0.2, K_{row} = 0.75$
		$K_{rg} = 0.95, K_{rog} = 0.75$
	Relative permeability end points (Shale)	

To assess the impacts of the shale barriers according to their location, size, and proportion on the SAS process, a similar modelling strategy as in Zheng et al. (2016, 2017, and 2021) is adopted. This strategy, basically super-impose, on the numerical homogeneous base-model (section 3.1), shale barriers different in size, proportion and location; this might be facilitated by dividing the simulation domain into three zones, as illustrated in Figure 23. Zone 1 (red area) is where the wells are located and is extended 14 m on the I-axis and 9 m on the K-axis and is considered a critical zone. Next to this area, zone 2 is found. This zone corresponds to the yellow area a bit away from the wells pair, where the effects of any shale barriers are less critical. The rest of the reservoir, zone 3, is considered a non-critical zone where the impacts of most shale barriers are generally not significant and encompass the green area. The categorization of each zone lies under the theory that as the shale barrier (with a particular size) distance from the wells pair increases, the impact in the production performance diminishes; thus, in zone 2 and 3, just larger

and thicker shale barriers will impact the performance. The shale barrier unit represents the minimum geometry a shale can have to be considered as a barrier. The experiments showed that a shale barrier with a thickness below 20 cm would not impede steam-solvent chamber advancement and dramatically affect production performance; hence, they are not considered barriers; this fact is in concordance with the results presented by Zheng et al., 2016.
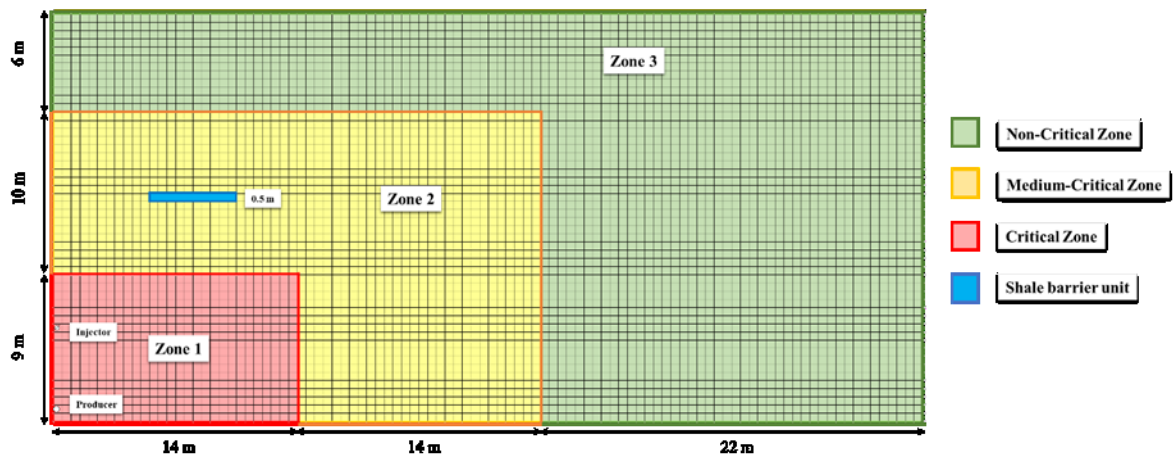
Figure 23. Reservoir zone distributions and basic shale unit representation.

5.2.1. Experimental design

A total of 250 experimental models are constructed, varying the geometry and location of the shale barriers. Four different sets of models are generated where the shale barrier length ranges are between 5 m to 13 m, while its thickness varies from 0.5 m to 2 m. The first set corresponds to models with up to ten shale barriers in zone 1. In the second set, just shale barriers in zone 2 were superimposed. And finally, the third set contains models with shale barriers in zone 3 only. These sets tend to show a sort of transition from a reservoir where no shale barriers exist to a more complex and realistic heterogeneous reservoir. Among all three groups, four representative models are selected and described next, as they capture the ranges of response observed in those 250 models.

- Model (a) is the base-homogeneous model.

- Model (b) corresponds to a simple heterogeneous model where just one shale barrier of 5 m in length is imposed in zone 1 right above the injector.

- Model (c) is a semi-complex heterogeneous model constructed super-imposing four shale barriers at different locations and geometries within zone 1.

- Model (d) refers to a complex heterogeneous model where many shale barriers are spread from bottom to top onto the entire reservoir (zone 1, 2 and 3), and their geometries are varied. All the graphic models are presented in Figure 24.
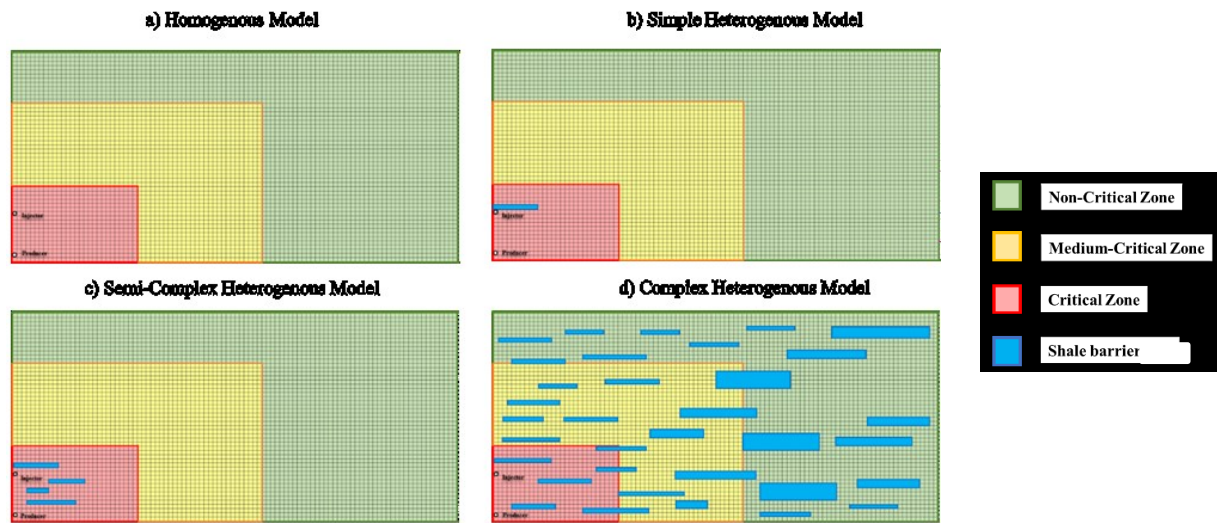
Figure 24. Experimental design models.

5.3. Simulation results

The temperature (T) profiles for the experimental design models described in section 5.2.1 are plotted at different SAS elapsed times and are presented in Figures 25. Regarding the homogenous case (a) can be seen that the steam-solvent chamber growth is uniformly from the injector to the top of the reservoir. Once the chamber reaches the top, it continues going forward to the right-bottom of the reservoir; the oil swept is smooth and uniform. Inversely, in the presence of shale barriers, especially near the wells, the steam-solvent chamber growth and its shape change drastically depending on the heterogeneity's geometry and location. The migration behaviour

might also be affected (Zhang et al., 2021). Respecting models b and c, as can be noticed, the chamber growth is impeded by the shale barrier located right above the injector. This barrier is causing a considerable pressure increase; thus, steam and solvent injection need to be reduced and sometimes need to be stopped; this is until the pressure is relieved, and it is optimal to continue with the injection. This phenomenon happens especially when the steam or solvent has contact with the barrier for the first time; after a while, the pressure does not increase exponentially. Once the chamber in scenario (b) has advanced beyond the shale barrier, its growth follows the exact behaviour of scenario (a) ought to no more shale barriers are found in the rest of the reservoir. For case (c), since more than one shale barrier is located in the critical area, it takes more time for the chamber to surpass these heterogeneities so that its growth is slower, compared with case (b), and less of the reservoir is reached. Case (d) showed a slightly different behaviour of (b) and (c). It was expected that since many shale barriers with different geometries and locations were superimposed, the chamber would not grow easily, but it grew. This significant growth at the end of the SAGD operation phase is because the shale barrier above the injector was located not at 0.5 m like the others but 1 m away from it. So, although there were more heterogeneities in that area, it is evident that barriers that impact the most are those located at a short distance from the injector. Then, similarly to all cases, the chamber flows to the top of the reservoir and then to the right-bottom. As can be seen, since the shale barriers in the pathway to the top of the reservoir are relatively small in thickness and length, the chamber has no flowing problems. However, when the chamber contacts larger and thicker barriers, its speed flow is reduced, and its growth is somehow braked (i.e. end of cycling phase). This observation confirms the previous statement that says that only larger shale barriers located away from the wells would impact the production performance. Seemingly, due to the presence of heterogeneities, the chamber temperature

distribution is not uniform, which may be due to the amount of steam and solvent injected and the time it takes for these fluids to travel into the reservoir. As a result of these facts, the oil viscosity reduction is less; thus, less oil can be recovered.
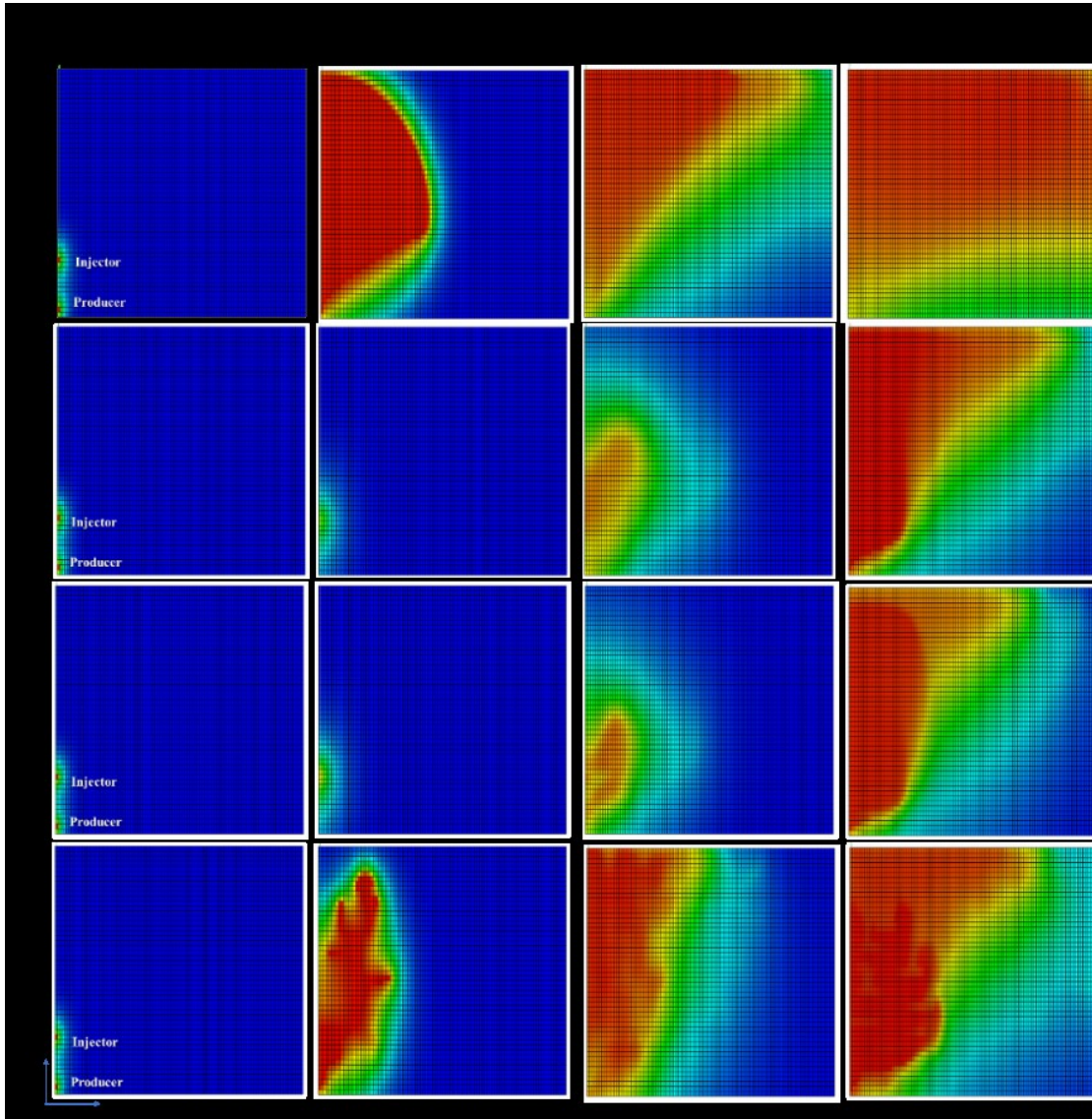
Figure 25. Temperature distribution profile of four different scenarios at different SAS elapsed times.

Figure 26 shows the cumulative Oil Production ($cumOP$) profiles for each of the models described previously (section 5.2.1). Concerning how the steam-solvent chamber propagates into the reservoir, as expected, the homogenous case (a) is where more oil can be recovered. In this scenario, a considerable amount of oil is produced during the first two years (2011-2013) because

just pure steam is injected (pre-heating and SAGD phase), and the oil viscosity is reduced

substantially. After that, the production seems to be constant until 2021. Then, since most of the

reservoir has been swept, the oil production starts to decrease. The heterogeneous cases, (b) and

(c), have very similar behaviour. For these particular cases, the shale barrier imposed right above

the injector does not allow the steam and solvent to be injected so that the oil production in the

first year is almost null. Once that shale barrier is surpassed, steam and solvent might be injected

with certain restrictions, but according to the graph, it seems that the steam and solvent injections

are constant until the end of the simulation. Evidently, in the presence of shale barriers, oil

production is reduced. Case (d), differently, produces less oil than the homogenous cases but pretty

much the same as cases (b) and (c); this is due to the previous explanation of the shale location

above the injector. After three years, the chamber starts to flow in the green zone, where larger

and thicker shale barriers are super-imposed, and that is why, after 2014, the oil production begins

to decline and end up recovering almost the same amount of oil than scenario (b) and (c).
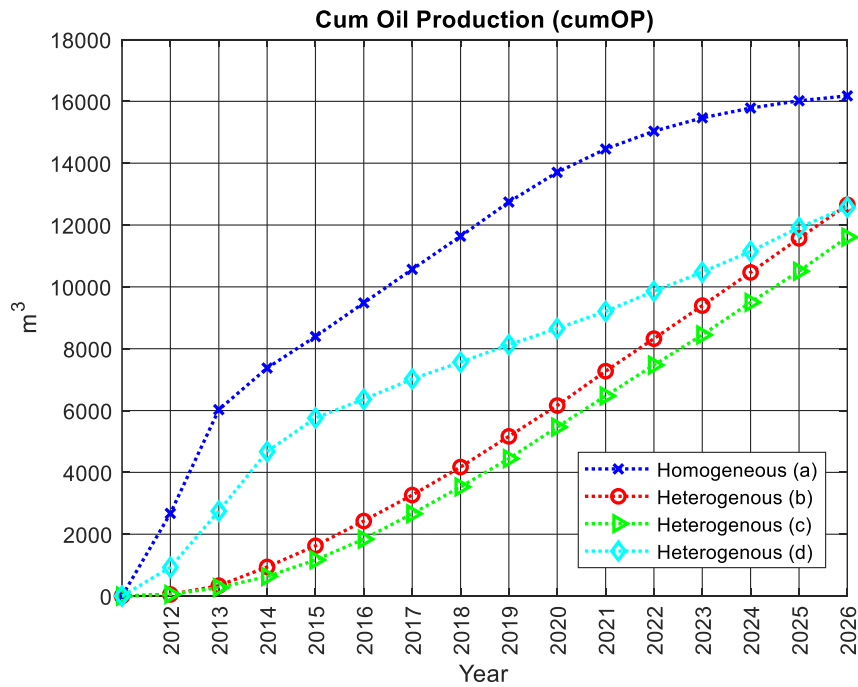
Figure 26. The cumulative Oil Production profile of four different scenarios.

5.4. Sensitivity Analysis

Differently than section 3.3, for the heterogeneous cases, just a global sensitivity analysis (SA) applying RSM was performed. The study was carried out using a built-in optimization tool, CMOST, within CMG (2019) package.

Similarly to section 3.3, the cycling injection phase (from day 601 to 5,475) was divided into two equal periods. In these periods, the operational parameters remained constant; there are multiple cycles within each period. Also, the solvent composition (i.e. $\%mol\ propane$) and duration of steam and solvent cycles in each period are varied.

The sensitivity analysis contemplates 14 potential decision variables such as solvent composition ($Propane_1$ and $Propane_2$), bottom-hole pressure in the injector when either steam (BHP_{steam1} and BHP_{steam2}) or solvent (BHP_{solv1} and BHP_{solv2}) are injected, cycle steam ($Cycle_{steam1}$ and $Cycle_{steam2}$) and solvent ($Cycle_{solv1}$ and $Cycle_{solv2}$) duration time for each period within the cycling phase, the minimum operational bottom-hole pressure in the producer (BHP_{prod}) and steam quality. Also, two operational constraints are incorporated, such as steam trap and bottom-hole gas (BHG); this is illustrated on the left graph in figure 27. The subscript 1 and 2 refer to either the first or second period of the cycling phase, respectively. The parameters without subscript are kept constant for the entire simulation.

The SA results identified the nine most impactful decision variables in the SAS heterogeneous process and are shown on the right side of Figure 27:

- Solvent composition: propane fraction in the solvent mixture for each period ($Propane_1$ and $Propane_2$).
- Cycle duration: duration of steam and solvent injection within each period ($Cycle_{steam1}, Cycle_{solv1}, Cycle_{steam2}$ and $Cycle_{solv2}$)

- Maximum injector bottom-hole pressure when steam is being injected (BHP_{steam}): this pressure should always be greater than the initial reservoir pressure and is kept constant throughout the entire simulation.

- Maximum injector bottom-hole pressure when the solvent is being injected: the difference in operating pressures is less than 200 kPa than BHP_{steam} and it is also kept constant at 96% of BHP_{steam} during the simulation.

- Producer constraints: steam trap and BHG play a key role in the optimization.

- The values for BHP_{prod} and steam quality are 2,900 kPa and 95%, respectively, and are consistent with another study of warm solvent injection by Ma and Leung (2019).
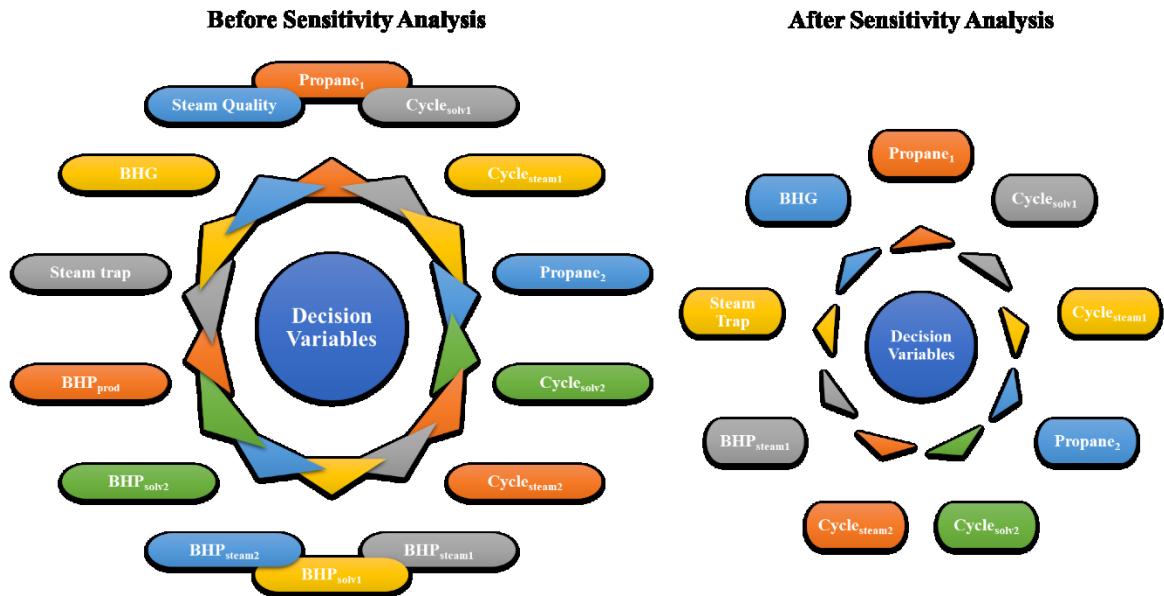
Figure 27. Initial and final chosen decision variables for the heterogeneous optimization SAS process.

The SA has been repeated for the homogeneous (base) model as well, and the considered ranges for all the decision variables for both the homogeneous and heterogeneous models are listed in Table 10.

Table 10. Decision variables and their ranges of the SAS process in a homogenous (a) and heterogeneous (b) reservoir.

a) Homogeneous Reservoir			b) Heterogeneous Reservoir		
Decision Variable	**Min**	**Max**	**Decision Variable**	**Min**	**Max**
$Propane_1$ (%)	50	70	$Propane_1$ (%)	10	90
$Cycle_{Solv1}$ (days)	60	120	$Cycle_{Solv1}$ (days)	60	90
$Cycle_{Steam1}$ (days)	45	60	$Cycle_{Steam1}$ (days)	45	60
$Propane_2$ (%)	50	90	$Propane_2$ (%)	10	90
$Cycle_{Solv2}$ (days)	70	160	$Cycle_{Solv2}$ (days)	70	120
$Cycle_{Steam2}$ (days)	50	70	$Cycle_{Steam2}$ (days)	55	70
BHP_{Steam} (kPa)	3,300	4,000	BHP_{Steam} (kPa)	2,700	3,500
			$Steam\,Trap$ (°C)	2	10
			BHG (m^3/m^3)	3	10

5.5. Objective functions

Two sets of objective functions were formulated in this study. The first set contemplated two objective functions: Recovery Factor (RF) and cumulative Steam-Oil Ratio ($cSOR$) and can be formulated as shown in equation (18). Similarly, to equation (4), for the second set, cumulative Solvent consumption ($cSolv$) was added.

$$F(\vec{x}) = \{f_1(\vec{x}), f_2(\vec{x}), \dots, f_i(\vec{x})\} = \left\{\frac{1}{RF}, cSOR\right\}$$

(18)

where $\vec{x}$ is the decision variable vector, and F denotes the objective function. The RF and $cSOR$ are estimated according to section 3.4.

5.6. Multi-Objective Evolutionary Algorithms (MOEAs) and Proxy models

Identically to section 3.5, MOEAs are used to optimize each of the selected heterogeneous models described previously in section 5.2.1. The same widely used algorithms were applied: SPEA-II, MOPSO and PESA-II. A brief description of each scheme can be found in sections 3.5.1, 3.5.2 and 3.5.3, respectively. The settings configuration used for the three algorithms is shown in Table 4, section 3.5.4.

Regarding the proxy models, similar to section 3.6, CMOST, an optimization tool of the Computing Modelling Group (CMG, 2019), is incorporated to formulate the equation to approximate the objective functions of the chosen heterogeneous realizations. To train the proxies in this study, 90 SAS experimental designs on average are usually required, of which 90% of those were training and 10% verification files. The training data set is constructed by first assigning random values to the decision variables listed and according to the ranges of table 2. Then, a numerical simulation is performed to record the output of each individual; same as for the base-case model (section 3.6), the least-square method is applied to generate the proxy model.

5.7. Modified Multi-Objective Optimization work-flow

A minor modification of the proposed multi-objective workflow presented in section 3.7 to optimize the Steam Alternating Solvent (SAS) process in the presence of shale barriers with different geometries and locations is carried out. The steps are listed below and are shown in Figure 28:

1. A base case (homogeneous) simulation model is built using Builder, CMG, 2019 tool and a few representative heterogeneity realizations are constructed.

2. As described in section 5.4, a sensitivity analysis is performed to identify the key decision variables considering both the homogeneous and heterogeneous models. Also, the experimental design to build the proxy model is generated.

3. Results from the simulation run in the SA are used to compute the objective function values (section 5.5).

4. The results from the previous step, together with some additional runs, are used to train a set of proxy models; for each heterogeneity scenario, three proxies for each objectives function are constructed.

5. The proxy models are incorporated into each of the three chosen MOEA methods described in sections 3.5.1, 3.5.2 and 3.5.3 to seek the optimal Pareto solution set. The MOEAs used in this study were adapted from various MATLAB open code sources developed by Mostapha, 2015.
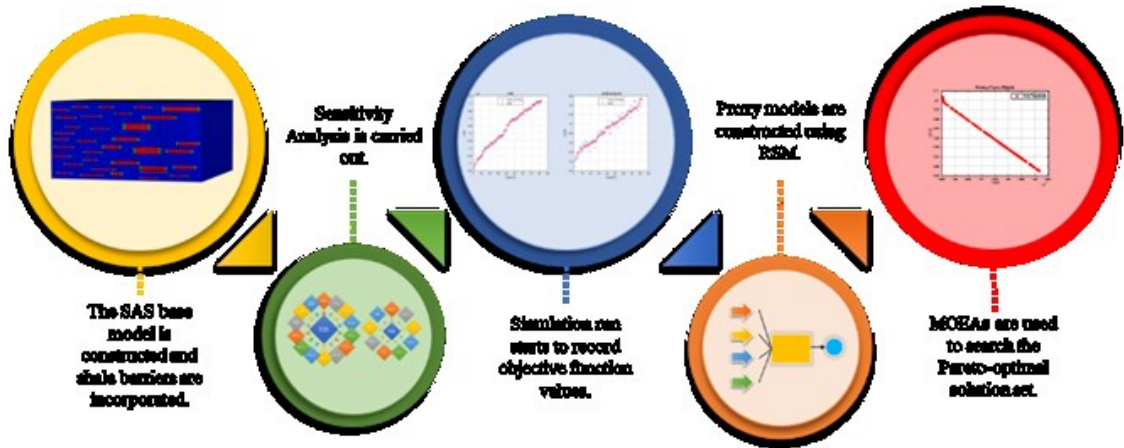
Figure 28. Proposed workflow scheme for the Steam Alternating Solvent Optimization Process in heterogeneous reservoirs.

5.8. Result and discussion

For this section, the results are divided into two parts. First, the analysis of models (b) and (d) accounting for two objective functions (RF and $cSOR$) is presented (section 5.8.2). Then the results accounting for three objective functions ($RF, cSOR$ and $cSolv$) of the four models and their respective optimization results are shown (section 5.8.3); the chosen realizations are explained in section 5.2.

5.8.1. Proxy model analysis - Response Surface Methodology

Similar to section 4.2, the accuracy of the proxy model is assessed by comparing the simulated versus the estimated results from the mathematical equation obtained using RSM for each objective. Figure 29 shows this comparison of all four models (a, b, c and d). The slight variation in the results might be due to the increment in the heterogeneities in the reservoir; the more the

barriers, the more complex the non-linear relationship between the objective functions and the decision variables becomes. To get a more accurate proxy model, more experiments may be needed, but the computational time will increase.
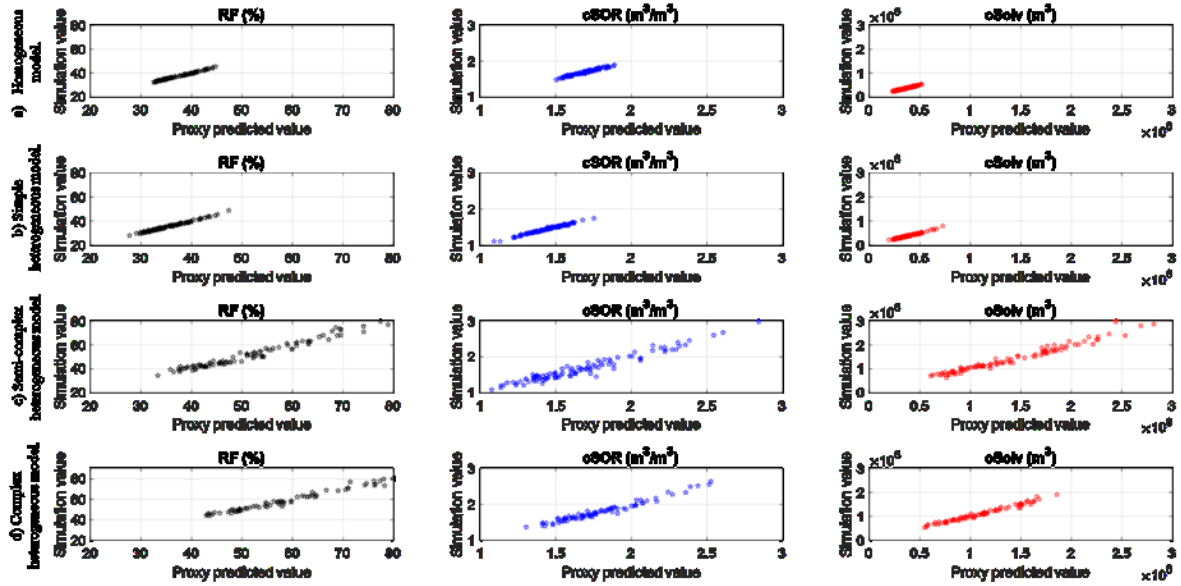
Figure 29. Comparison between the simulated and RSM results for cases b and d accounting two objectives.

The agreement of the predicted values with the true simulated results using the proxy model equations is acceptable since the coefficient (R^2) and the adjusted coefficient ($R^2_{adjusted}$) of determination for each objective function is close to one, and the mean square (MSE) for all cases is close to zero. The R^2 and $R^2_{adjusted}$ accounting two and three objectives are quite similar. So that, just the results considering three objectives are presented in table 11. The RSM coefficients needed to calculate the objective functions can be found in Appendix A.

Table 11. R^2 and $R^2_{adjusted}$ of the RSM proxy models.

Model	Objective Function	R^2	$R^2_{adjusted}$
	RF	0.9500	0.9490
a)	$cSOR$	0.9500	0.9470
	$cSolv$	0.9430	0.9380
b)	RF	0.9895	0.9863

	cSOR	0.9859	0.9824
	cSolv	0.9812	0.9775
c)	RF	0.9724	0.9641
	cSOR	0.9522	0.9456
	cSolv	0.9774	0.9706
d)	RF	0.9872	0.9807
	cSOR	0.9650	0.9545
	cSolv	0.9801	0.9694

5.8.2. Two objective functions (RF and $cSOR$) analysis.

For each algorithm used to optimize the SAS process accounting RF and $cSOR$ as objective functions, the initial population and the Pareto fronts are presented for model (b) in Figure 30 and model (d) in Figure 31. As is noted, in both models, the PESA-II and SPEA-II solution-front show wider optimal solutions that extend along the x and y-axis; the front of MOPSO lacks solutions in the y-axis for model b and in the x-axis for model d. Also, comparing the Pareto front of models (b) and (d), a considerable change in shape is observed due to the complicated non-linear relationship between the objectives and the decision variables; the more complex the problem is, the smoother the front is.
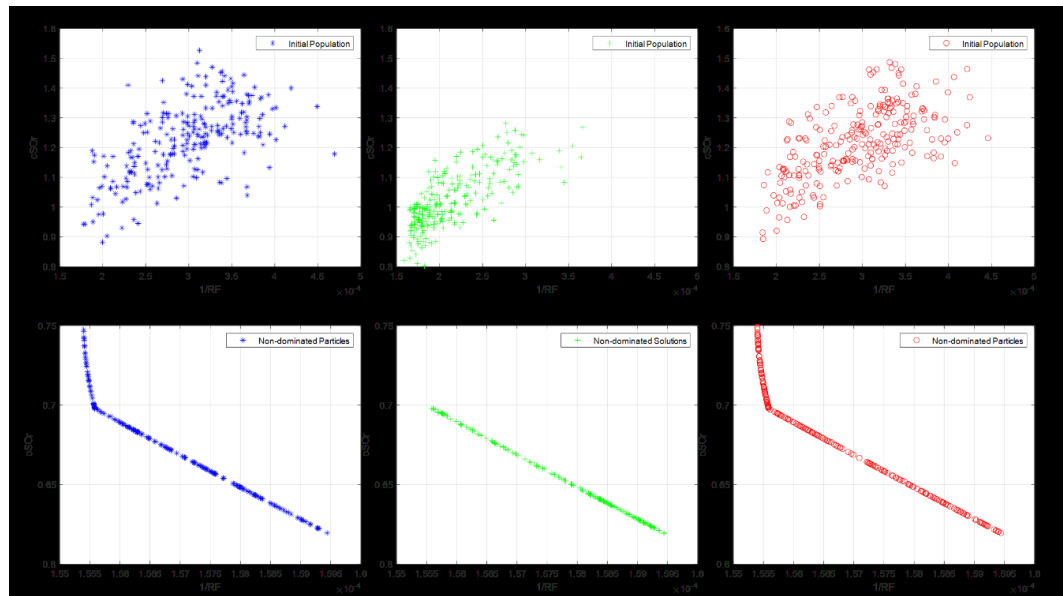
Figure 30. Simple heterogeneous model initial population and Optimal Pareto-front for each MOEAs accounting for two objective functions.

Regarding the computational time, the MOPSO algorithm runs in less than a minute while the others vary up to 2 minutes. Furthermore, when MOPSO is performed, the Pareto front is fully developed after 13 generations and using PESA-II and SPEA-II after 60 and 80 generations, respectively.
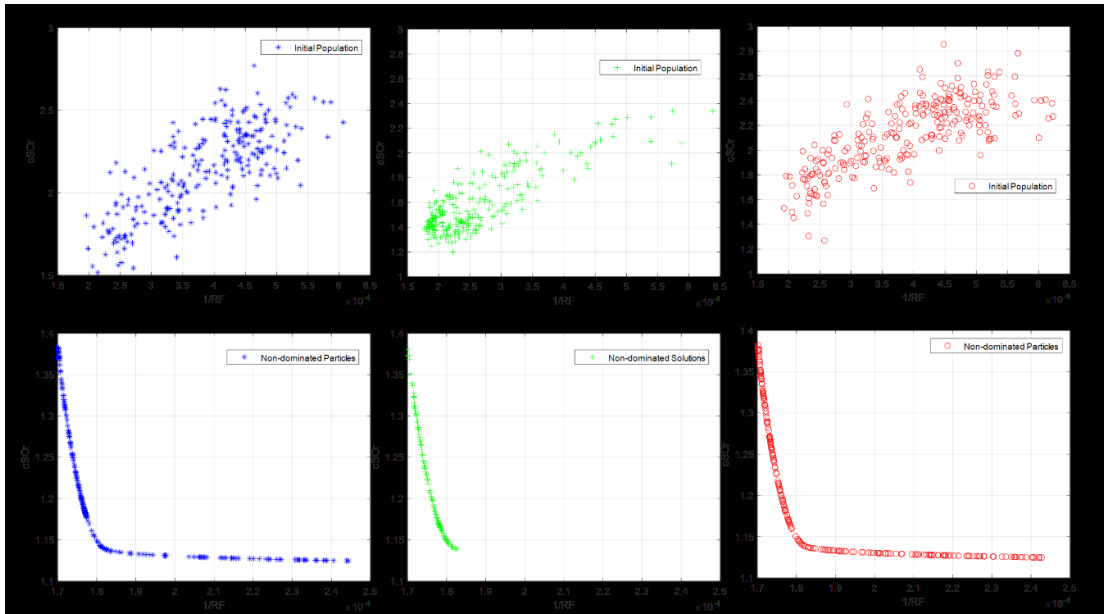
Figure 31. Complex heterogeneous model initial population and Optimal Pareto-front for each MOEAs accounting two objective functions.

5.8.2.1.   Pareto front analysis – Optimal operational results

For this specific study, the results obtained from PESA-II are used since it is a more robust algorithm, and its results are in good concordance with those in SPEA-II. The optimal operational ranges for models (b) and (d) are shown in Figure 32; the x-axis refers to the ranges listed in Table 10, and the y-axis corresponds to the frequency. It is vital to point out that when many barriers exist in the reservoir, the production performance's major impact occurs when these barriers are located near the wells (zone 1) and at the near edges of zone 2.

For the simple heterogeneous model (b) in the first period is observed that:

1) When a shale barrier is located near the injector and steam is injected, the surrounding area's pressure increases rapidly. Thus, the operational strategy might include short steam

cycles (45-50 days) combined with a high bottom-hole pressure in the injector to allow a considerable amount of steam to be injected, accounting for the shale's fracture pressure. The increment in pressure is relieved with high propane concentrations (70% - 90%); a higher propane concentration leads to higher pressure and temperature reductions since the BHP is reduced when the solvent is injected.

2) The solvent injection is more optimal to last less than 70 days since the reservoir still has a suitable temperature after the SAGD operation time and also to avoid a high-temperature reduction.

3) At the end of the first period (1,522 days), the steam/solvent chamber has a sort of path, so the fluids injected into the reservoir (in the second period) will travel faster to the edge of the chamber where the reservoir temperature decreases and this may lead to a better SAs performance.

For the same model in the second period:

4) Since the fluids need to travel long distances to reach the edge of the steam-solvent chamber, the steam injection is recommended to be longer (66-70 days) to also re-heat the reservoir. Interestingly, after this heterogeneity is exposed for a while to the steam and solvent, the shale's pressure does not increase exponentially; this might be due to some fluids penetrating this formation.

5) The solvent concentration is preferable to be kept at high propane concentrations, similar to the first period. The solvent duration cycles, since more steam is pouring into the reservoir, might last less (70-80 days) to keep the $cSOR$ balance. As mentioned before, the injector's bottom-hole pressure needs to stay constant at a higher value to allow, when possible, the maximum fluid to be injected.

6) The minimum bottom-hole in the producer must keep it low (2,600 kPa) to allow fluid production.

7) Concerning the steam trap production constraint, it needs to be set at its maximum value to maximize the production and to prevent the production of live steam; thus $cSOR$ is maintained low. This optimum operational strategy is in accordance with the study done by Edmunds (1998), where if the steam trap is set below a higher steam saturation temperature, more oil is produced. However, the penalization is a more pressure drawdown.

8) The bottom-hole gas (BHG) constraint, the same as the steam trap, needs to be set at its maximumly allowable limit to avoid gas concentration in the area near the wells and early solvent production.

For the complex heterogeneous model (d) in the first period:

- Solvent composition and its duration follow the same trend described above for model (b); high propane concentration over a short solvent injection period.

- Conversely, it is more likely to keep the steam bottom-hole pressure in the injector low to avoid high pressures in the wells surrounding area. Thus, longer steam injection cycles are more optimal .

For the same model in the second period:

- The optimization results indicate that high propane concentrations are needed, and the duration of solvent cycles should be between 70 to 80 days, the same as the model (b).

- The steam injection was expected to behave similarly to model (b); however, after performing the run simulation of model d, the results threw the opposite. Therefore, the duration of steam injection should last less than 60 days.

- It was observed that the bottom-hole pressure in the injector must be increased somehow to maintain a balance between the conflicting objectives.

- Similar to the previous adjustment, to prevent gas production, BHG needs to be reduced to a value between 5 and 8. This happens because more barriers are found in the reservoir and pressure increases considerably. As a result, the injected fluid (either steam or solvent) cannot spread easily in the reservoir, causing both gas and liquid to accumulate in the area near the wells.

- The steam trap needs to be used with relatively small values to produce the fluid. This would avoid steam accumulating in the area near the wells and prevent its production without having fulfilled the objective of transferring the heat to the reservoir.
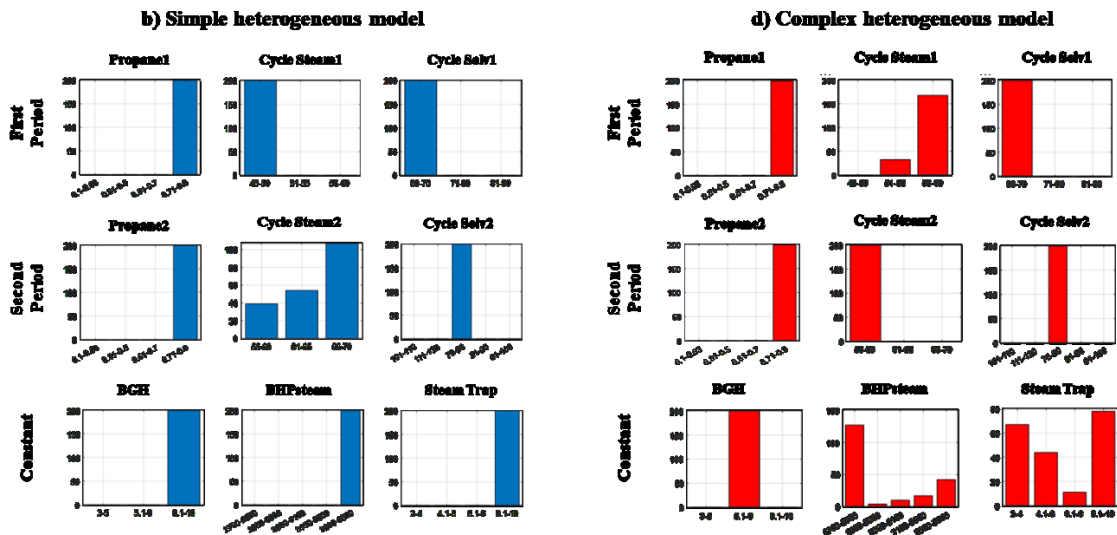
Figure 32. Optimal ranges for models b and d for all controllable parameters in the SAS process accounting two objective functions.

5.8.2.2.   General remarks

- It is noticeable from Figure 25 that shale barriers notably impact production performance and water usage. For example, oil production in model (b) is high, and the $cSOR$ might be reduced significantly. In contrast, as shale barriers number increase into the reservoir, the production tends to be low, and the water usage (steam) increases, thus $cSOR$ is high.

- The steam injection duration in the second period for model (b) seems to have more controllable flexibility. In model (d), conversely, this flexibility is related to the bottom-hole pressure and steam trap when steam is injected.

- The lack of optimal solutions using MOPSO and the slight variation among the results might be due to the reproduction operators that each algorithm implies (i.e., mutation) to maintain the diversity or due to how each individual's fitness is calculated.

5.8.3. Three objective functions (RF, $cSOR$ and $cSolv$) analysis

The SAS models described in section 5.2.1 accounting for three objective functions (RF, $cSOR$ and $cSolv$) are optimized. The workflow presented in section 5.7 is used for this analysis. Figure 33 illustrates the Pareto front obtained using MOPSO, SPEA-II, and PESA-II algorithms. The Pareto front is divided into four (blue, red, green and magenta) quadrants. Some minor differences are observed:

- The number of solutions in each quadrant and its distribution varied among the three algorithms.

- Different from the two objective Pareto front analysis (section 5.8.2), more even and less scattered solutions are observed when SPEA-II is used compared with the solutions obtained using the other algorithms. Therefore, only the results from SPEA-II are presented in the following sections.

Overall, significant variability in all four models is viewed. For example, as the number of shale barriers increases into the reservoir, as expected, solutions cluster in zones where less oil is produced and more steam and solvent are needed.
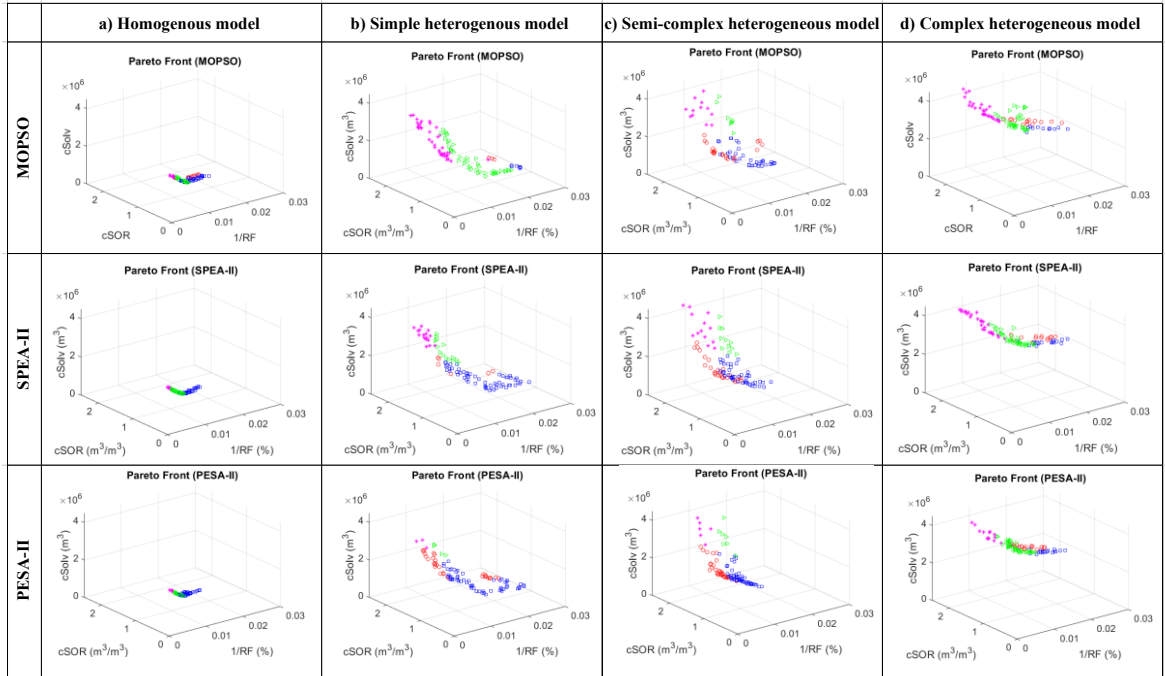
Figure 33. Pareto-front for all four models using different MOEAs.

The 3-D Pareto front, to better visualize the trade-off between the objective functions, could be projected onto a series of 2-D Pareto front. Figure 34 illustrates the initial population and the final Pareto front in 3-D and 2-D using the SPEA-II algorithm for each model.

The computational requirements to perform the optimization of each model are assessed. A summary of the computational time to complete the SAS optimization with or without using a proxy model is presented in Table 12. Each of the MOEAs uses 80 iterations that include in each one a population of 50 individuals. A single flow simulation and to compute the objective functions if the proxy modelling is not employed on average takes approximately 140 minutes. As can be seen, a significant saving in computational time is achieved using proxy models, despite the frontloading costs of calibrating the proxy models.
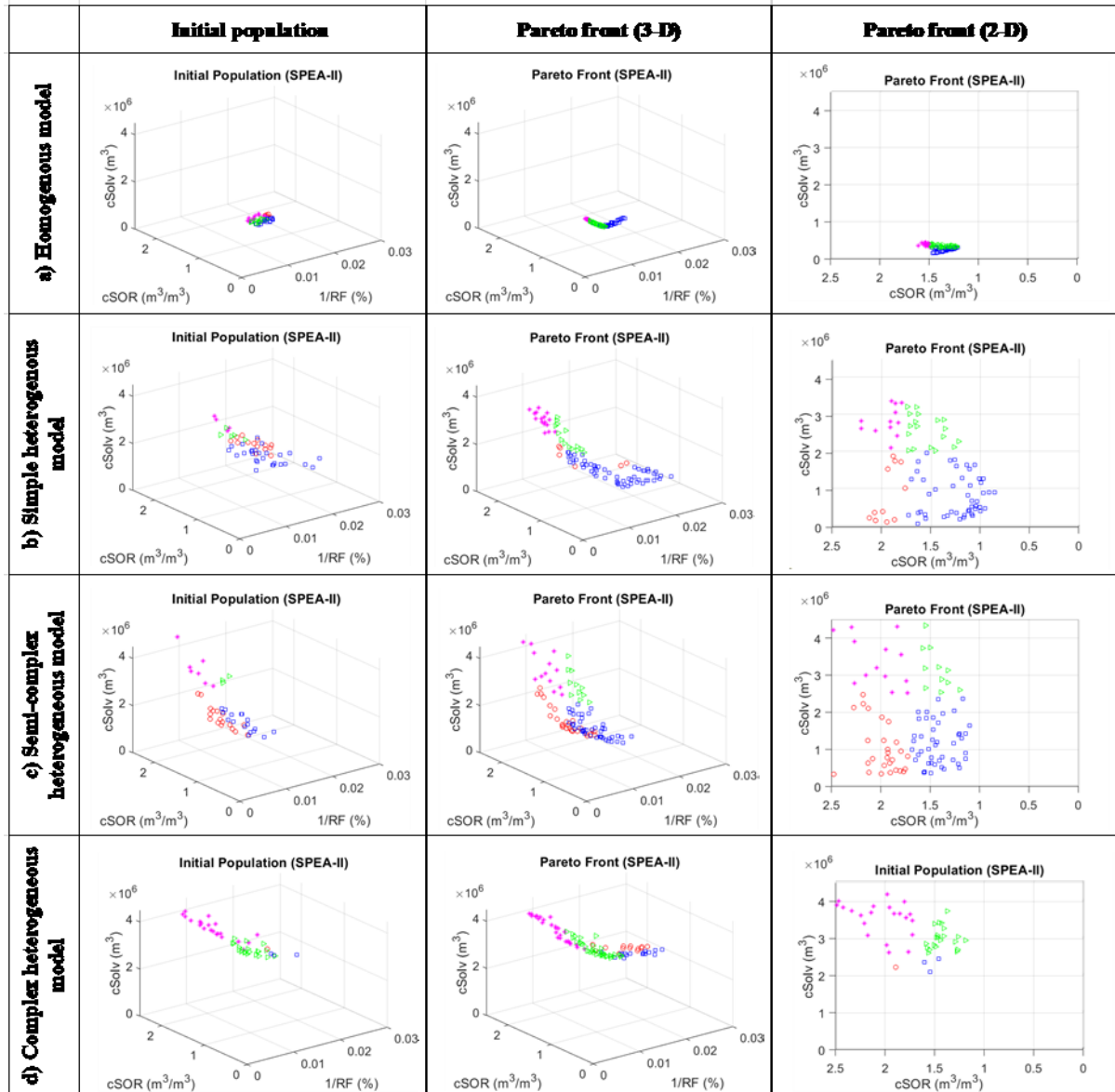
Figure 34. Initial population and the final Pareto-front (2-D and 3-D) for all four models using SPEA-II.

Table 12. Comparison of the total computing time with and without using proxy models.

	Steps	No proxy	Proxy
a) Homogeneous model	Building time (min)	N/A	3,361.12
	Objective Function Calculation (min)	64 min × 50 individuals × 80 iterations = *256,000*	0.0001053 min × 50 individuals × 80 iterations = *0.4212*
	Rest of MOEA (min)	0.86	0.86
	Total Time (min)	*256,000.86*	*3,362.40*
b) Simple hetero	Building time (min)	N/A	4,500

71

	Objective Function Calculation (min)	90.2 min × 50 individuals × 80 iterations = *360,800*	0.0001098 min × 50 individuals × 80 iterations = *0.4392*
	Rest of MOEA (min)	0.86	0.86
	Total Time (min)	***360,800.86***	***3,362.42***
c) Semi-complex heterogeneous model	Building time (min)	N/A	5,900
	Objective Function Calculation (min)	118 min × 50 individuals × 80 iterations = 472,000	0.0001124 min × 50 individuals × 80 iterations = *0.4496*
	Rest of MOEA (min)	0.86	0.86
	Total Time (min)	***472,000.86***	***3,362.43***
d) Complex heterogeneous model	Building time (min)	N/A	10,450
	Objective Function Calculation (min)	209 min × 50 individuals × 80 iterations = 836,000	0.0001188 min × 50 individuals × 80 iterations = *0.4752*
	Rest of MOEA (min)	0.86	0.86
	Total Time (min)	***836,000.86***	***3,362.45***

In the following sections, the optimum operational strategy for each model and each zone (i.e. blue, red, green and magenta) is described first. Then, general remarks and observations among all four models are listed. The results of the optimal operational ranges using MOPSO and PESA-II are shown in Appendix C.

5.8.3.1.   Homogeneous Model

a) **Low $cSOR$ – Low $cSolv$ (Blue quadrant):** The average RF is the lowest among all the quadrants between 45% to 65%, as can be seen in Figure 34. Results revealed, as is shown in Figure 35 that it is more optimal to inject lower propane concentration ($Propane_1 < 60\%$) over short cycles ($Cycle_{solv1} < 70$ days) during the first period (early stages of the cycling phase), while in the second period (later stages of the cycling phase), also injecting low propane concentration (i.e. $Propane_2 < 60\%$) but in longer cycles ($Cycle_{solv2} > 140$

days) is recommended. The bottom-hole pressure (BHP_{steam}) is generally set at lower values to minimize steam and solvent injection (characteristic of this quadrant).

Figure 35. Optimal operational ranges of the decision variables for the homogeneous model using the SPEA-II.

b) **High $cSOR$ – High $cSolv$ (Magenta quadrant):** in this quadrant the highest objectives values are achieved ($RF: 60 - 70\%$, $cSOR: 1.2 - 1.7 \frac{m^3}{m^3}$, $cSolv$ 0.1 to $0.5 \times 10^5 m^3$). As shown in Figure 36, different from the Blue quadrant (Figure 11), it is more optimal to inject higher propane concentration ($Propane_1 \cong 70\%$) in shorter cycles ($Cycle_{solv1} < 70$ days) during the first period. However, for the second period, higher propane concentration ($Propane_2$) and very long cycles ($Cycle_{solv2}$) are implemented to increase solvent injection. The steam injection duration ($Cycle_{steam}$) and BHP_{steam} are adjusted to inject more steam.

c) **High $cSOR$ – Low $cSolv$ (Red quadrant)** – Interestingly, no optimal solutions were found for this model in this section.
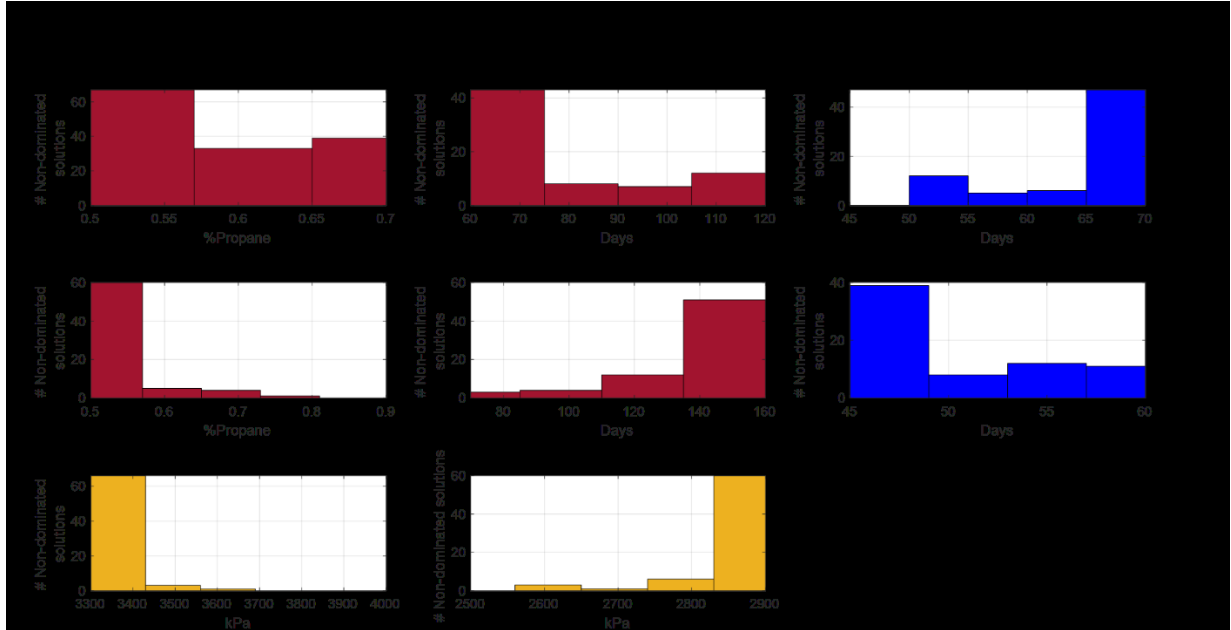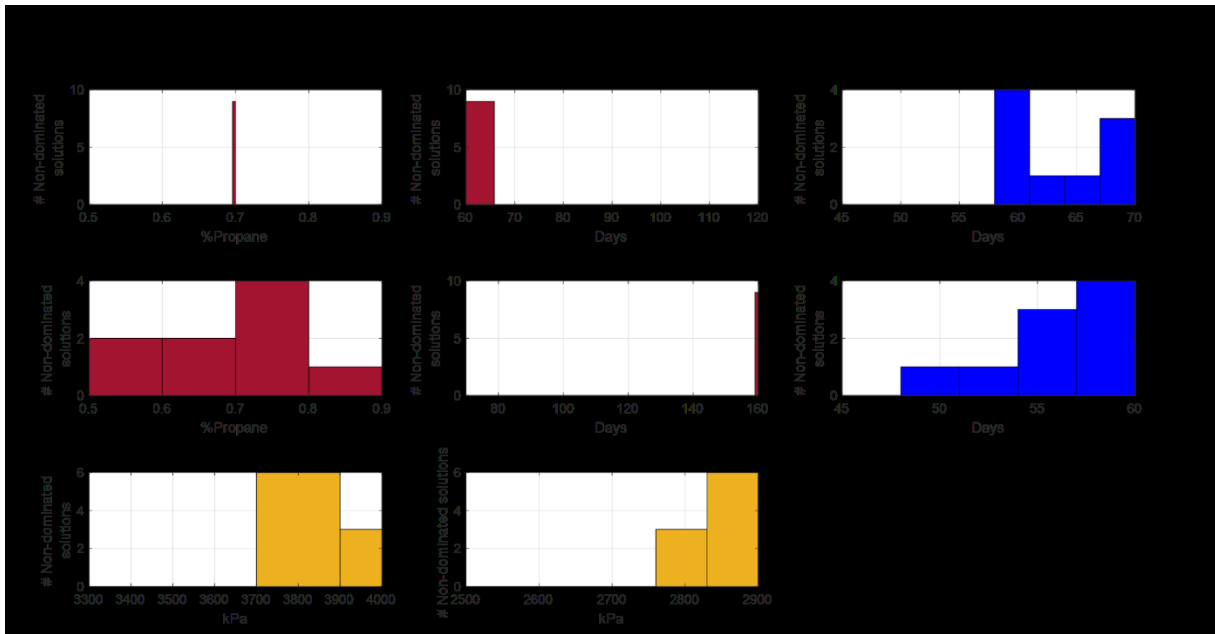
Figure 36. Optimal operational ranges of the decision variables for the homogeneous model using the SPEA-II.

d) **Low $cSOR$ – High $cSolv$ (Green quadrant)** – The solvent injection strategy (Figure 37) is similar to the Magenta quadrant (Figure 36): inject higher propane concentration ($Propane_1 \cong 70\%$) in shorter cycles ($Cycle_{solv1} < 70$ days) during the first period and higher propane concentration ($Propane_2 > 80\%$) with longer solvent cycles ($Cycle_{solv2} > 150$ days) in the second period. Since $cSOR$ is to be minimized in this section, steam should be injected in short cycles. Also, low BHP_{steam} are implemented.

Results from all four quadrants would suggest that injecting high propane concentration over short solvent cycles during the first period is better. Lower propane concentrations and longer solvent cycles should be used in the second period if more solvent is to be injected. It is observed that it is more optimal to maintain BHP_{steam} at a minimum, if less steam is to be used. Steam trap ($5\,°C$) and BHG ($5\,m^3/m^3$) values for this homogeneous model are kept constant because, according to the performed SA, these parameters do not significantly impact the results.
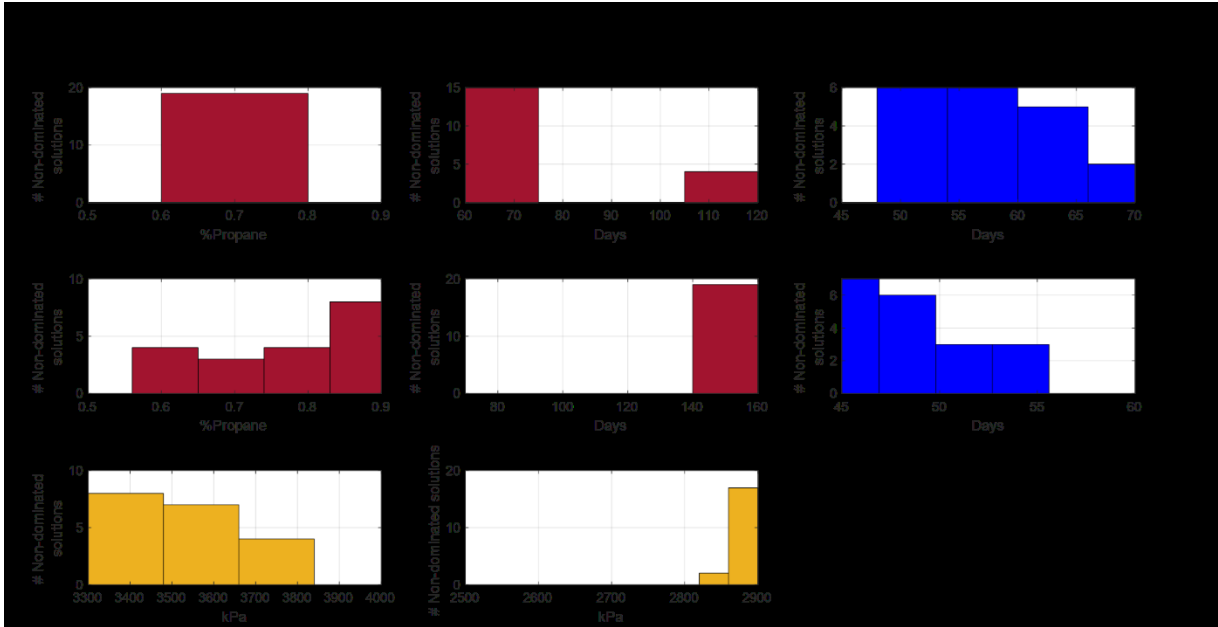
Figure 37. Optimal operational ranges of the decision variables for the homogeneous model using the SPEA-II.

5.8.3.2. Simple Heterogeneous Model

a) **Low $cSOR$ – Low $cSolv$ (Blue quadrant):** The results are shown in Figure 38. The average RF has a wide range between 33 to 80%. Some interesting comparisons with the homogeneous model can be made: 1) For the first period, it is more optimal to inject also low propane concentrations ($Propane_1 < 40\%$) and shorter cycles ($Cycle_{solv1} < 70$ days), while in the second period, injecting higher (instead of lower) propane concentration (i.e. $Propane_2 > 70\%$) in shorter (instead of longer) cycles ($Cycle_{solv2} < 80$ days) seems to be optimal. To minimize steam and solvent injection, bottom-hole pressure (BHP_{steam}) is generally set at lower values. 2) It is vital to control the steam trap due to the presence of the shale barrier: for example, the shorter the cycles, the higher the steam trap ($> 8°C$) is required for preventing early live steam production. 3) BHG is more optimal to be kept relatively low, considering that $cSOR$, $cSolv$, and RF in this quadrant is characterized to be at low values.
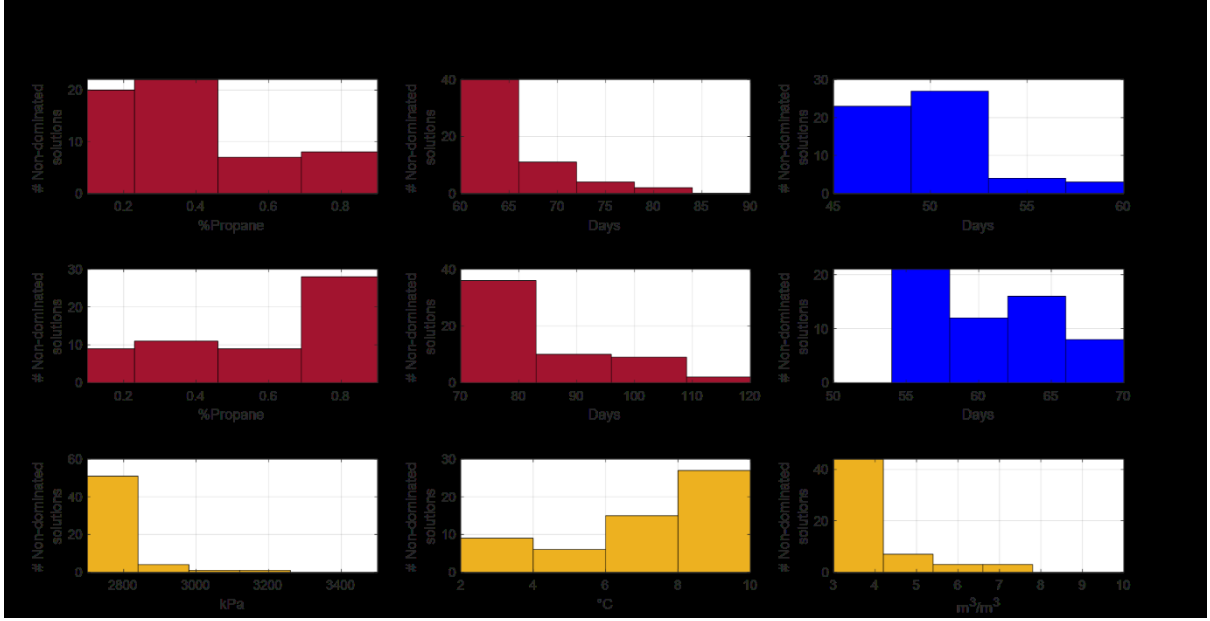
75

Figure 38. Optimal operational ranges of the decision variables for the simple heterogeneous model using the SPEA- II.

b) **High $cSOR$ – High $cSolv$ (Magenta quadrant):** In this quadrant, the highest objective values are achieved ($RF: 60 - 80\%, cSOR: 1.8 - 2.3 \frac{m^3}{m^3}$, and $cSolv$ 2 to $3.5 \times 10^5 \ m^3$) among the other solutions. Similar to the homogeneous model, results revealed, as shown in Figure 39, that it is more optimal during the first period to inject high propane concentration over short cycles; however, for the second period, low propane concentration and long solvent cycles ($Cycle_{solv2} > 100 \ days$) are optimal. To inject and allow more steam and solvent into the reservoir, the steam injection duration ($Cycle_{steam}$) and BHP_{steam} are adjusted at higher values.

c) **High $cSOR$ – Low $cSolv$ (Red quadrant):** The average recovery for this quadrant is the lowest with $RF: 35 - 50\%$. $cSOR$ is between $1.8 - 2.2 \frac{m^3}{m^3}$, and $cSolv$ $0.1 - 2 \times 10^5 \ m^3$. As shown in Figure 39, it seems more beneficial to inject high propane concentration ($Propane_1 > 60\%$) and short solvent cycle ($Cycle_{solv1} < 65$ days) in the first period. For

76

the second period, high propane concentrations ($Propane_2 > 70\%$) and shorter solvent

cycles ($Cycle_{solv2} < 80$ days) are also beneficial. The steam injection strategy is also

similar to the Blue quadrant (Figure 38). Interestingly, this section has the least number of
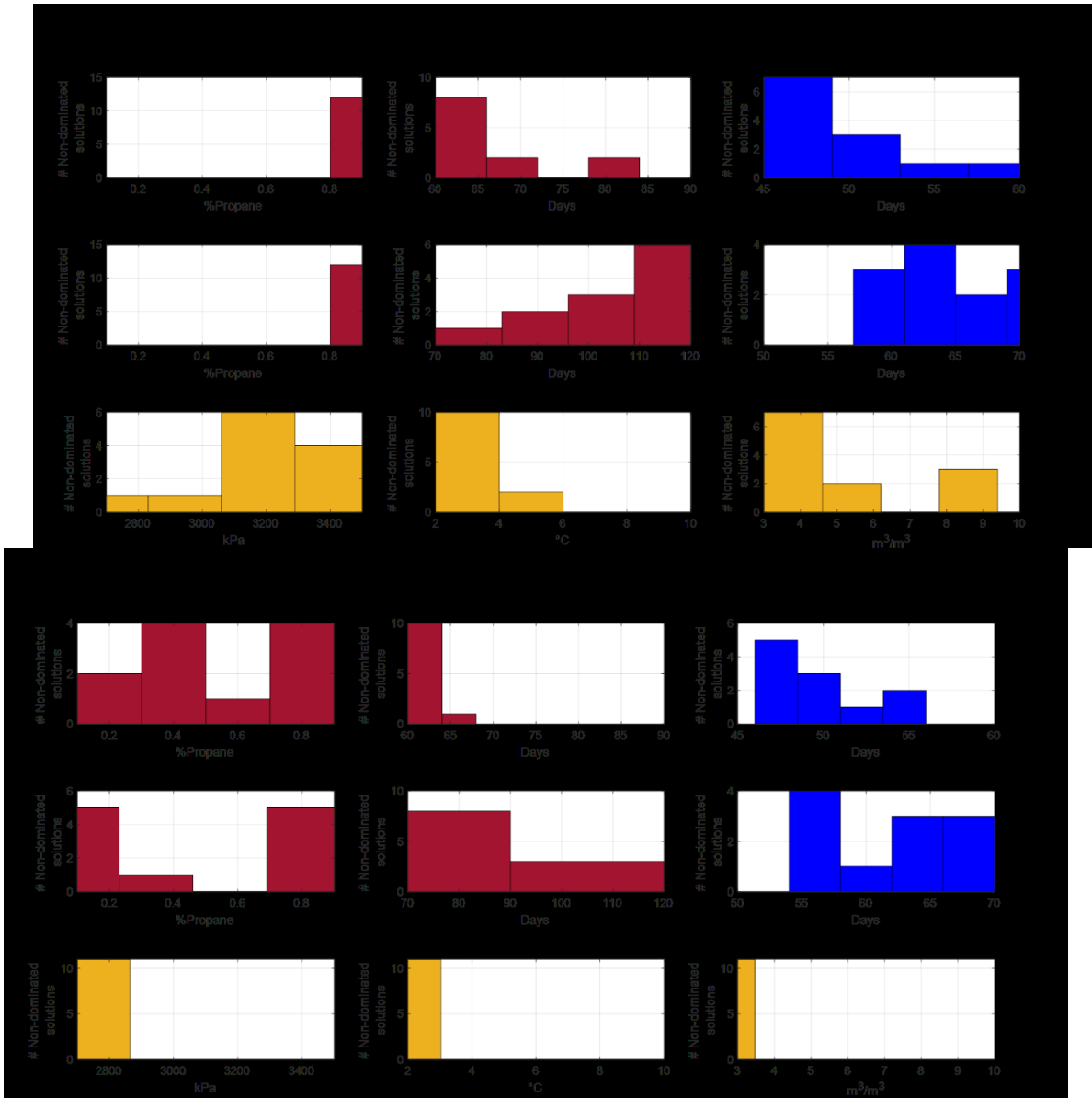
solutions.

Figure 39.Optimal operational ranges of the decision variables for the simple heterogeneous model using the SPEA- II.

d) **Low $cSOR$ – High $cSolv$ (Green quadrant):**. The ranges of the objective function in this quadrant are: RF in average is $65 - 80\%$, $cSOR$ between $1-1.7 \frac{m^3}{m^3}$, and $cSolv$ 2 to $3.5\times 10^5 \ m^3$. The solvent injection strategy and recovery are similar to the Magenta quadrant (Figure 39). The differences, as can be observed in Figure 40, are: 1) The $Cycle_{solv2}$ should be shorter (instead of longer). 2) The steam injection pressure and steam trap should be increased between 3,200 to 3,400 kPa and between 6 to 8 $°C$, respectively, to reduce $cSOR$ and accomplish the characteristic of this quadrant.
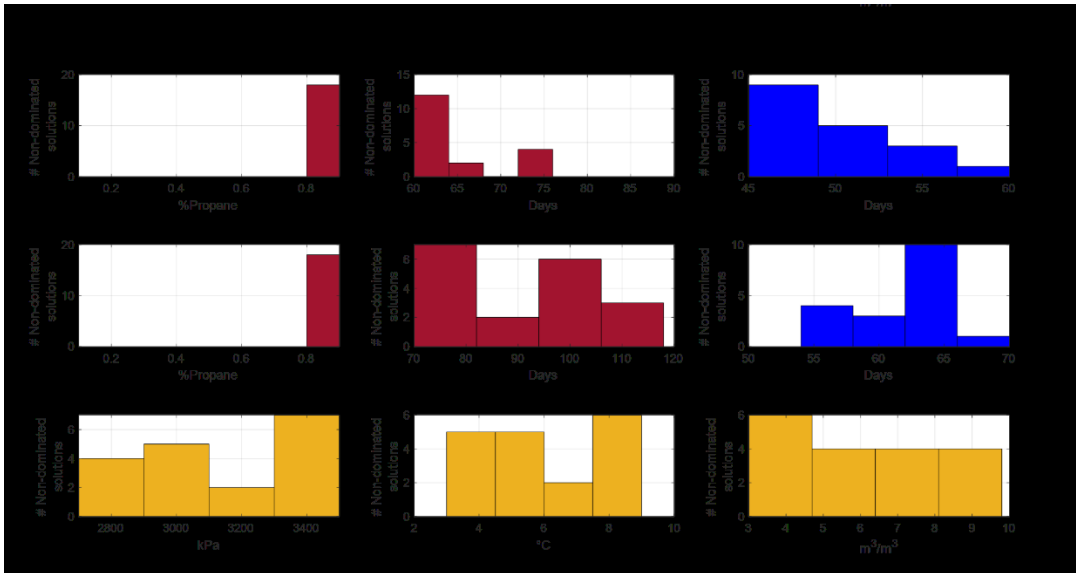
Figure 40. Optimal operational ranges of the decision variables for the simple heterogeneous model using the SPEA- II.

Overall, results from all four quadrants would suggest (similar to the homogeneous case) that instead of switching to lower propane concentrations and longer solvent cycles during the second period, it is more optimal to inject high propane concentration over short solvent cycles during both the first and second periods.

5.8.3.3. Semi-Complex Heterogeneous Model

a) **Low cSOR – Low cSolv (Blue quadrant):** Because of the characteristic of this group, the average RF is the lowest (45 – 80%), while $cSOR$ ranges between $1-1.8 \frac{m^3}{m^3}$ and $cSolv = 0.2 - 2.5\times 10^5 \ m^3$, as expected. The results are illustrated in Figure 41. The optimal strategy for the first period is different from that for the homogeneous model. It is observed that it is more optimal to inject higher propane concentration ($Propane_1 > 70\%$) over shorter cycles ($Cycle_{solv1} < 65$ days); this is because there is no long shale barrier above the injector, as in the simple heterogeneous case. The optimal strategy for the second period is similar to all the simple heterogeneous cases detailed in the previous section: 1) It is better to inject higher propane concentration (i.e. $Propane_2 > 70\%$) in shorter cycles ($Cycle_{solv2} < 75$ days). 2) The shale barriers located farther away from the wells pair have similar impacts than the simple heterogeneous cases. To minimize steam injection, bottom-hole pressure (BHP_{steam}) is generally set at lower values. BHG is quite low to stick to the characteristic of this quadrant.

b) **High $cSOR$ – High $cSolv$ (Magenta quadrant):** The average objective function values are 1) $RF = 61-85\%$, 2) $cSOR = 1.8-2.4 \frac{m^3}{m^3}$, and 3) $cSolv = 2.5 - 4.5\times 10^5 \ m^3$. As can be seen in Figure 41, similar to the homogeneous and simple heterogeneous model results, it is more optimal to inject high propane concentration ($Propane_{1,2} > 80\%$) over short solvent cycles ($60 < Cycle_{solv1,2} < 75$ days) for both periods. BHP_{steam} is set at higher values (i.e. $BHP_{steam} > 3,100 \ kPa$) with lower steam trap levels to prevent accumulation that might impact the pressure of the reservoir.

Figure 41. Optimal operational ranges of the decision variables for the semi-complex heterogeneous model using the SPEA-II.

c) **High $cSOR$ – Low $cSolv$ (Red quadrant):** The objective function values are $RF = 50 - 87\%$, $cSOR = 1.8 - 2.3 \frac{m^3}{m^3}$, and $cSolv = 0.2 - 2.5 \times 10^5\ m^3$. The results shown in Figure 42 revealed that the optimum operational strategy for both periods is similar to that for the simple heterogeneous case. The only difference is that longer (rather than shorter) steam injection ($Cycle_{steam1}$) cycles are more optimal.

d) **Low $cSOR$ – High $cSolv$ (Green quadrant):** The objective function values in this

quadrant are: $RF = 75-85\%$, $cSOR = 1.2-1.7 \frac{m^3}{m^3}$, and $cSolv = 2.5 - 4.5 \times 10^5\ m^3$. The

optimal operating strategy for this quadrant (Figure 42) is similar to that of the Magenta

quadrant (Figure 41); the difference is that larger steam traps are more optimal.

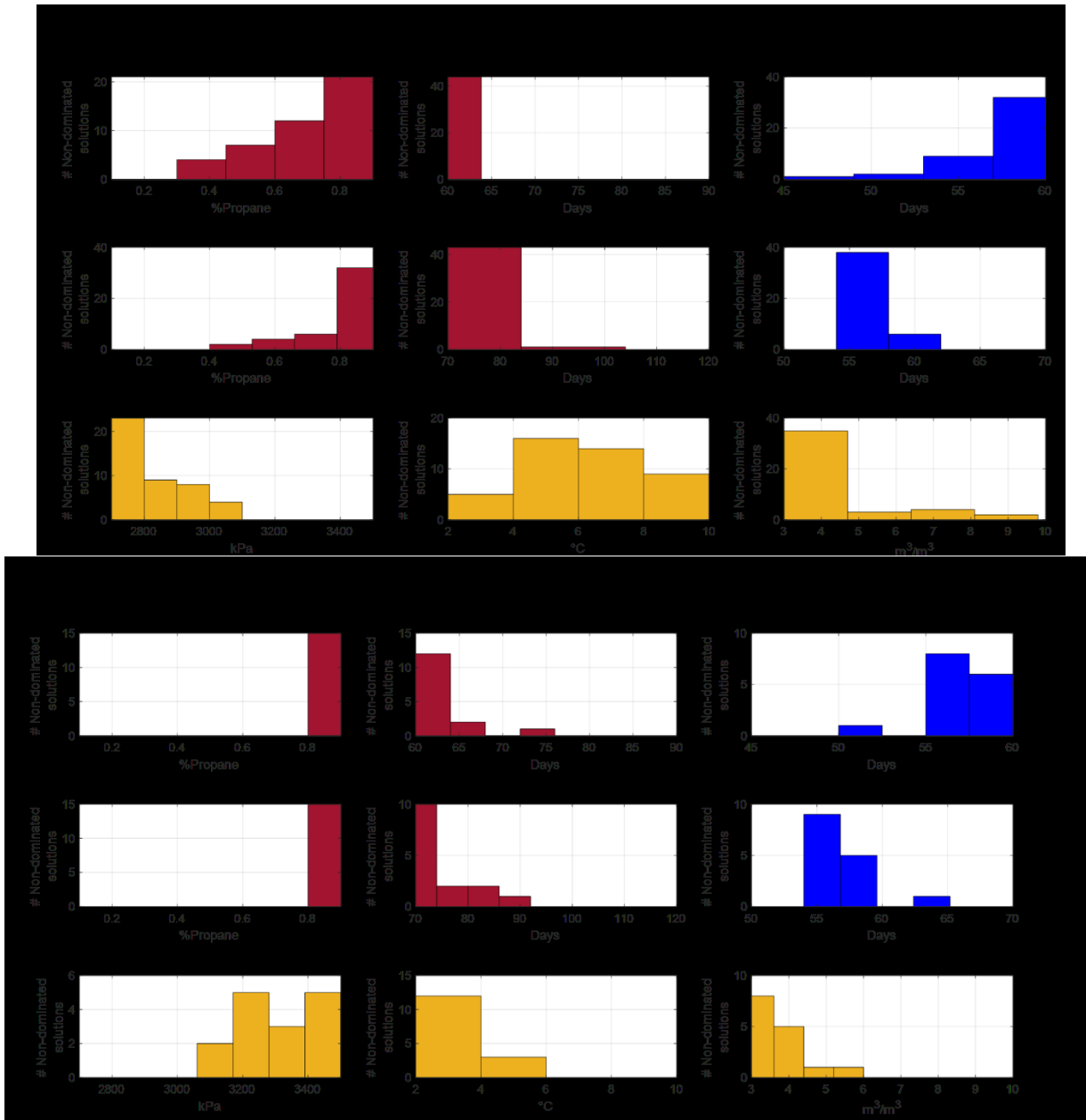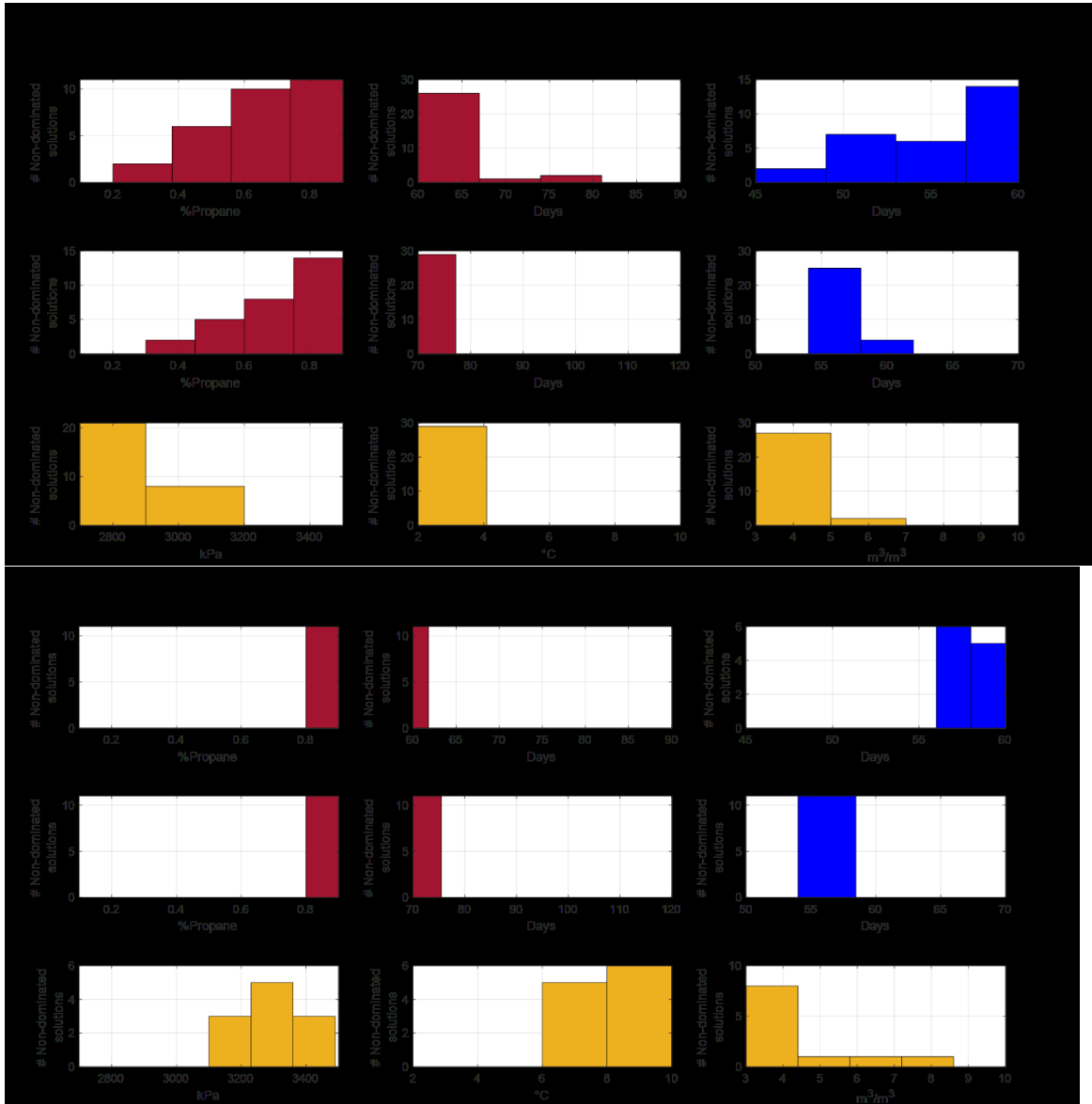**Figure 42. Optimal operational ranges of the decision variables for the semi-complex heterogeneous model using the SPEA-II.**

Results from all four quadrants would suggest that the optimal operating strategy is very similar to the simple heterogeneous case; during both the first and second periods, it is better to inject high propane concentration over short solvent cycles.

5.8.3.4. Complex Heterogeneous Model

a) **Low $cSOR$ – Low $cSolv$ (Blue quadrant):** The average objective functions are $RF = 35-65\%$, $cSOR = 1.25 - 1.7 \frac{m^3}{m^3}$, and $cSolv = 1.8 - 2.5 \times 10^5 \ m^3$. The optimal scheme results are shown in Figure 43. Similar to the simple heterogeneous case, for the first period is recommended to inject low propane concentrations (i.e. $Propane_1 < 40\%$) over short solvent cycles ($Cycle_{solv1} < 65$ days). Flexibility in the adjustment of steam injection duration has been used. Similar to the homogeneous case, for the second period, lower propane concentration ($Propane_2 < 50\%$) and longer solvent cycles ($Cycle_{solv2}$) are needed since the edge of the chamber is far away from the wells pair. Also, due to the large number of shale barriers located throughout the entire domain, longer steam cycles (i.e. $Cycle_{steam2} \sim 68$ days) are more optimal. The bottom-hole pressure (BHP_{steam}) is generally set at lower values to minimize steam injection. BHG is relatively low, considering the characteristic of this quadrant.

b) **High $cSOR$ – High $cSolv$ (Magenta quadrant):** The average objective functions are $RF = 65-85\%$, $cSOR = 1.6 - 2.5 \frac{m^3}{m^3}$, and $cSolv = 2.5 - 4.3 \times 10^5 \ m^3$. The optimal operating strategy (Figure 43) is similar to all the other heterogeneous cases: injecting high propane concentration over short cycles during both periods. More steam is injected (i.e., higher values of $Cycle_{steam1,2}$ and BHP_{steam}) due to the characteristics of this quadrant.

Figure 43. Optimal operational ranges of the decision variables for the complex heterogeneous model using the SPEA-II.

c) **High $cSOR$ – Low $cSolv$ (Red quadrant):** The average objective functions are $RF = 35 - 55\%$, $cSOR = 1.7 - 2 \frac{m^3}{m^3}$, and $cSolv = 1.9$ to 2.5×10^5 m^3. The operating strategy is presented in Figure 44 and is similar to the blue quadrant (Figure 43), where both cases represent low $cSolv$. The main difference is that more steam is needed here, which is achieved by adjusting the steam trap at lower levels.

d) **Low $cSOR$ – High $cSolv$ (Green quadrant):** The average objective functions are $RF = 60 - 85\%$, $cSOR = 1 - 1.5 \frac{m^3}{m^3}$, and $cSolv = 2.5 - 4 \times 10^5 \ m^3$. Similar to other heterogeneity scenarios, this quadrant (Figure 44) is similar to the magenta quadrant (Figure 43). The main difference is that less steam is injected (characteristic of this quadrant); hence, higher steam trap levels are used.
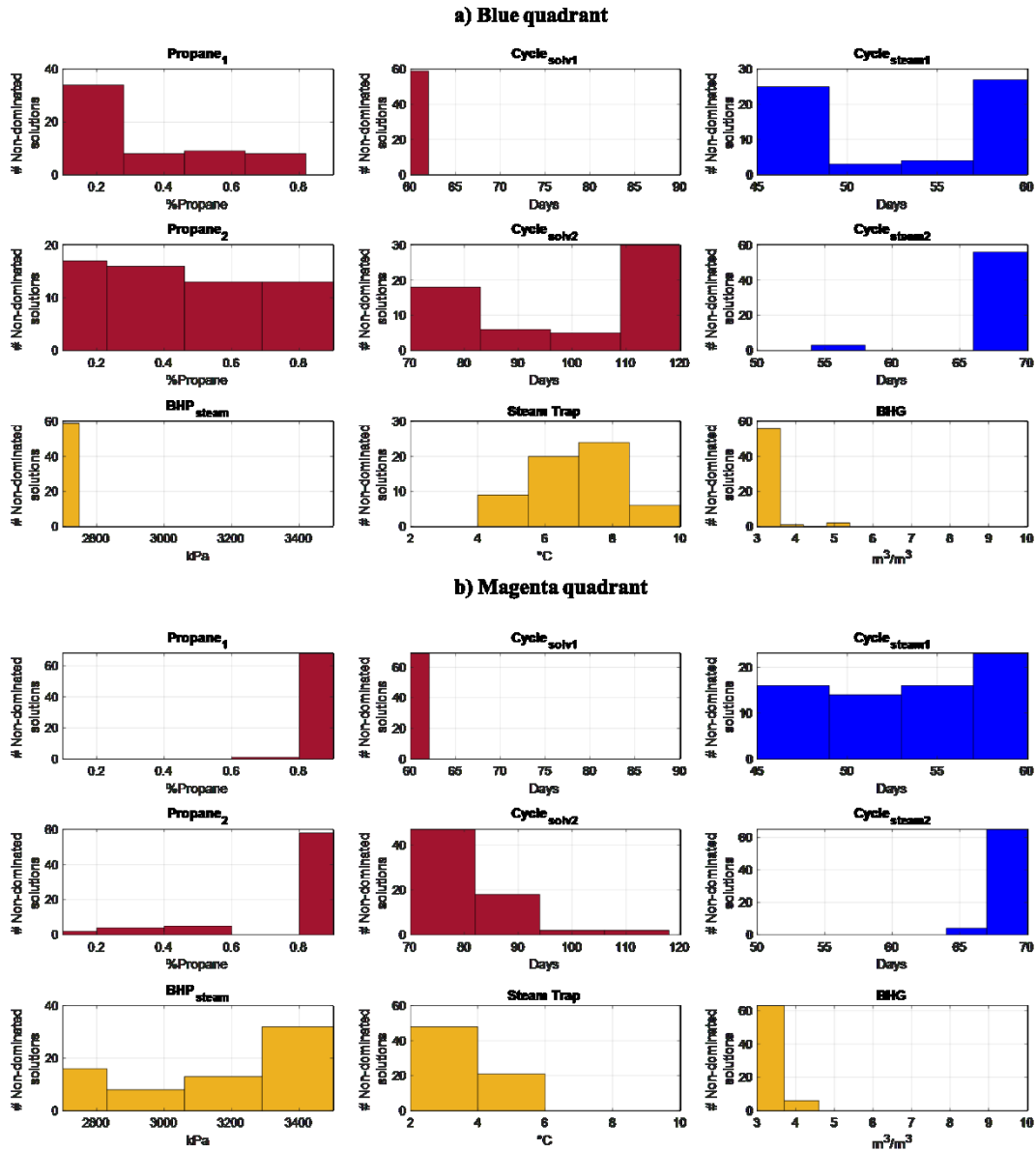

Figure 44. Optimal operational ranges of the decision variables for the complex heterogeneous model using the SPEA-II.

84

Results from all four quadrants would suggest that the optimal operating strategy is to inject high propane concentration over short solvent cycles if more solvent is used. Conversely, propane concentration should be reduced if $cSolv$ must be kept low. Steam usage can be adjusted primarily through steam trap levels and steam cycle durations.

5.8.3.5.   General Remarks

- The recommended optimum strategy on average for most scenarios consists of injecting high propane concentrations over short cycles. If $cSolv$ is to be minimized, the propane concentration can be reduced. It seems that the solvent injection time might be extended to help to maintain a balance between the objectives.

- It is observed that BHP_{steam} should be reduced if heterogeneities are found in the near-well area to avoid over-pressurization and fluid accumulation in that zone.

- In the presence of many shale barriers, extending the steam injection periods during the later stages ($Cycle_{steam2}$) helps to enhance the steam-solvent chamber growth. This is unnecessary if the shale barriers are mostly discontinuous and not overly extensive laterally.

- The Steam trap constraint imposed in the SAS process in heterogeneous reservoirs is important to be adjusted and seems to have a close relationship with the steam injection duration. The shorter the cycles ($Cycle_{steam1,2}$), the larger the steam trap is required for preventing the production of live steam. Similar strategies can also be used to reduce $cSOR$ (i.e. BHG).

- It is observed that the solvent in the SAS process is preferable to be kept into the reservoir as long as possible; thus, BHG is recommended to be kept low for all heterogeneity scenarios to prevent early solvent production.

- An increase in solvent usage would lead to better steam-solvent chamber development and oil production in the presence of shale barriers into the reservoir. This is evidenced by more optimal solutions located in the high *cSolv* zones (i.e. green and magenta quadrants), as is illustrated in Figure 34.

- Similar to section 4.5, the split between the first (early) and second (late) periods in the cycling phase should also be optimized. Overall short cycles are feasible initially, but at some point, the oil rate would start to drop rapidly, which could indicate that longer cycles should be commenced.

- Minor differences in the results among the three MOEAs are noted.

CHAPTER 6: CONCLUDING REMARKS

This section presents a summary and the conclusion of the SAS process research project. Moreover, the contributions and recommendations for future work are listed.

6.1. Summary and Conclusions

This research project explores, analyzes, and develops a practical workflow to optimize the Steam Alternating Solvent (SAS) process. The work is conducted 1) to identify the relevant parameters that intervene when this process is applied to homogeneous and various heterogeneous reservoirs and 2) to propose their optimal operational ranges depending on the characterization of the reservoir. The data used in this project is compiled from public domain data of Suncor's Firebag and Surmont projects.

One homogeneous base model and different heterogeneous realization in 2-D are constructed. The heterogeneous dataset is built by superimposing idealized shale barriers onto the homogeneous model, whose properties are in accordance with previous SAS studies done by Coimbra et al. (2019) and Coimbra (2020). The four more representative and impactful models are selected to be analyzed.

A detailed and robust sensitivity analysis is performed to determine relevant operational parameters (decision variables) that intervene in the SAS process for each constructed and selected model. Two widely used methodologies are incorporated, OPAAT and RSM. Additionally, a set of three different objective functions is formulated for this study. For the homogenous case, two different analyses are performed. The first one accounts for two objective functions and the second one for three objective functions. Also, to select the proper grid size for the simulations, a mesh sensitivity analysis is performed.

A different set of proxy models are constructed to reduce the computational effort and time. These models predict the values of the objective functions by approximating the non-linear relationship between the targets and the selected decision variables adopting the Response Surface Methodology. Also, the optimization of the different model datasets is performed by adopting the Pareto optimality theory. Three widely used different Multi-Objective Evolutionary Algorithms (MOEAs) are used: SPEA-II, MOPSO, and PESA-II.

A Multi-Objective workflow to optimize the SAS process depending on the reservoir characterization is proposed and consists of six main steps: 1) A simulation homogeneous base model is constructed. 2) If heterogeneities (i.e. shale barriers) exist, these particular formations are added to the reservoir using the superimposing methodology. 3) A detailed sensitivity analysis is performed. 4) The simulation is run, and based on the results, three objective functions are formulated. 5) Results from step four, together with additional runs, are used to train a set of proxy models for each reservoir model. 6) The proxy models are incorporated into any of the three MOEAs to perform the optimization and analyze the results.

The results for the homogenous case revealed that it is more optimal to start (first period) with high propane concentrations in the solvent over short solvent cycles and then switch, in the second period, to low propane concentrations in long cycles. Also, if more steam is to be injected, it is recommended to do so over long cycles instead of increase dramatically the bottom-hole (BHP_{steam}) injection pressure. Moreover, if more solvent is to be injected, more steam would be needed to compensate and increase the steam-solvent chamber temperature. Production constraints such as steam trap and bottom-hole gas do not impact the SAS performance under this reservoir characterization.

For the heterogeneous cases, several conclusions are observed:

1) The production performance of the SAS process is highly affected depending on the shale barrier's location and geometry.

2) Shale barriers at any location and with any length into the reservoir with thickness less than 0.5 m barely affect the production performance and may not be considered barriers.

3) The shale barriers location and geometry rule the steam-solvent chamber shape and growth.

4) Heterogeneities allocated in zone 1 (near the wells pair) have a more critical impact on the SAS process than those located far away (i.e. edges of zone 2 and 3). Also, the shale barriers situated in zone 1 might highly determine the optimization strategy to follow.

5) Special attention is needed in zone 1 in terms of pressure to avoid fractures in the shale formations. The pressure increase near the wells might be caused by fluid accumulation, high bottom-hole injection pressure, and an incompatible production well constraint (i.e. steam trap and BHG) setting.

6) The SAS performance in the presence of heterogeneities would be enhanced by, similar to the homogenous case, injecting high propane concentrations in the solvent mixture over short cycles and also followed by short steam cycles during the first period. Also, depending on the heterogeneities location (mainly those found near the wells), switching to lower propane concentrations over long cycles and longer steam (instead of short) cycles is more optimalfor the second period. This is since the fluids need to travel long distances to the developed steam-solvent chamber.

7) Conversely to the homogeneous case, special attention to the production constraints is needed. For example, to better $cSOR$ results, the steam trap needs to be adjusted depending on the length of the steam cycles. BHG, when the solvent is injected is recommended to keep it low at all times to maintain as long as possible the solvent in the reservoir and to avoid early solvent production.

8) It is crucial to determine the targets to be incorporated in the SAS optimization study. It was observed that when performing the optimization accounting for two objective functions ($i.e\ RF\ and\ cSOR$), some critical insights and trade-offs were missed compared to when three objectives were incorporated in the optimization. Even though the complexity of the problem and the result analysis increase, having a more in-depth study and a better understanding of the relationship between the objectives and the controllable operational parameters (decision variables) would positively highly impact the SAS performance and the economics of the project.

Regarding the MOEAs used in this study, the performance among all three algorithms is compared. The result trends for each model and each selected decision variable are similar and in good agreement. Some minor differences are observed. Overall, MOPSO compared with SPEA-II results gives a slightly wider $Propane_1$ and $Cycle_{solv2}$ optimal ranges in the low $cSOR$ – low $cSOlv$ zone. Contrarily, narrow $Propane_2$ optimal ranges in the same zone. Interestingly, $Cycle_{solv1}, Cycle_{steam1}$ and $Propane_2$ solution trends, in the Low $cSOR$ – High $cSolv$ zone, are distributed differently. When using PESA-II, just narrow optimal ranges of $Cycle_{solv1}$ in the High $cSOR$ – High $cSolv$ and $cSOR$ – High $cSolv$ zones are observed. SPEA-II computational time is the lowest in most of the scenarios used and shows a more even and smooth distribution of the solutions.

The SAS process is a promising environmental-friendly alternative to many widely used traditional steam-based methods, such as the SAGD process and its many proposed modifications. Also, it has the potential to reduce water usage and GHG emissions. However, the SAS implementation might be more complex since more operational parameters must be considered.

6.2. Contributions

The main contributions of this study are listed as follows:

1) The extensive sensitivity analysis results identified the most impactful variables that should be considered for proper and better optimization of the SAS process incorporating two widely used methodologies. Also, Response Surface Methodology (RSM) was successfully implemented as an alternative 1) to reduce the high computational effort and time that a typical simulation process implies and 2) to facilitate a SAS targets forecast. The results obtained with the proxy models are reliable and efficient in capturing the complex non-linear relationship between the targets and the operational parameters.

2) The parameterization and superimposed scheme used in this study allowed a more in-depth understanding of the impact of shale barriers in different zones instead of having them in a smooth and following a Gaussian distribution such as the work done by Coimbra (2020).

3) The study provides the optimum operational ranges of the selected controllable parameters of the SAS process that could be used in reservoirs located in the Fort McMurray formation in the Athabasca region in Alberta, Canada. Additionally, an optimum operational strategy, depending on the targets (i.e. either steam or solvent needs to be minimized, maximized or both), is provided for particulars scenarios. Also,

this study is the first that utilizes a Multi-Objective Optimization approach for systematically determining an optimal SAS operational strategy accounting for two and three objective functions. Moreover, to determine whether one or more MOEAs would be suitable for particular heterogeneous scenarios, this study is the first that incorporates and compare different MOEAs for optimizing a wide range of operational parameters of the SAS process.

4) This study illustrates how a MOO workflow that incorporates MOEAs can be utilized to design optimally and accurately any hybrid, solvent-thermal operations under different constraints. Moreover, this research work explicitly shows how to parameterize solvent-based processes for homogeneous and complex heterogeneous reservoirs. Additionally, it illustrates how a complex engineer problem could be implemented by accounting for many decision variables and many objective functions instead of integrating them into a simple NPV objective function.

5) Even the Steam Alternative Solvent (SAS) process currently is not a commercial method, this study incorporates many elements that are used in many other commercial hybrid solvent-based methods. Thus, this research work might be used as a guide to optimizing those parameters (i.e. cycle duration, bottom-hole pressure) in other processes depending on the reservoir characterization.

6.3. Recommendations

Future studies should focus on:

1) Considering to incorporate other proxy modelling methodologies such as Polynomic, Kriging, Splines, and Neural Networks Models to compare their performance.

2) Extending the workflow to 3D reservoirs. However, numerical simulation involving complex heterogeneities in 3D would be extremely computationally intensive. Thus, the use of proxy models would be essential.

3) Incorporating 1) an economic analysis to assess the profitability of the application of the SAS process in the field scale and 2) an Environmental, Social and Governance (ESG) analysis to ensure the positive impact of the implementation of the SAS process.

References

Adams B. M., Bauman, L. E., Bohnhoff, W. J., Dalbey, K. R., Eddy, J. P., Ebeida, M. S., Eldred, M. S., Hough, P. D., Hu, K. T., Jakeman, J. D., Rushdi, A., Swiler, L. P., Stephens, J. A., Vigil, D. M. and Wildey, T. M. (2015). "Dakota, a multilevel parallel object-oriented framework for design optimization, parameter estimation, uncertainty quantification, and sensitivity analysis: Version 6.2 users manual". Technical Report SAND2014-4633, Sandia National Laboratories, Albuquerque, NM. http://dakota.sandia.gov/documentation.html.

Al-Gosayir, M., Leung, J., & Babadagli, T. (2012, November 1). "Design of Solvent-Assisted SAGD Processes in Heterogeneous Reservoirs Using Hybrid Optimization Techniques". Society of Petroleum Engineers. doi:10.2118/149010-PA.

Ali, S. M., & Blunschi, J. (1983). "Cyclic Steam Stimulation with Formation Parting". In Annual Technical Meeting. Petroleum Society of Canada, Banff, Canada. https://doi.org/10.2118/83-34-45.

Ali, M., Siarry, P. & Pant, M. (2012). "An efficient Differential Evolution based algorithm for solving multi-objective optimization problems," European Journal of Operational Research, vol. 217, no. 2, pp. 404–416.

Alonso, G., Del Valle, E. & Ramírez, J. R. (2020). "Chapter 5 - Optimization methods". In Woodhead Publishing Series in Energy, Desalination in Nuclear Power Plants, Woodhead Publishing. Pages 67-76, ISBN 9780128200216. https://doi.org/10.1016/B978-0-12-820021-6.00005-3.

Alvarez-Benitez, J., Everson, R. & Fieldsend, J. (2005). "A MOPSO Algorithm Based Exclusively on Pareto Dominance Concepts". Lecture Notes in Computer Science. 3410. 459-473. 10.1007/978-3-540-31880-4_32.

Arora, J.S. (2012). "Chapter 10 - Numerical Methods for Unconstrained Optimum Design". Introduction to Optimum Design (Third Edition), Academic Press. Pages 411-441, ISBN 9780123813756. https://doi.org/10.1016/B978-0-12-381375-6.00010-3.

Al-Bahlani, A., & Babadagli T. (2011). "Steam-over-solvent injection in fractured reservoirs (SOS-FR) technique as a new approach for heavy-oil and bitumen recovery: an overview of the method." Energy & Fuels 25.10 4528-4539.

Babadagli, T. & Al-Bahlani, A.M. (2008). "Hydrocarbon Recovery Process for Fractured Reservoirs". Canadian Patent Application, Serial No: 2,639,997.

Bevillon, D., & Mohagerani, S. (2015, September 14). "A Miscible EOR Project in a Mature, Offshore, Carbonate Middle East Reservoir – Uncertainty Analysis with Proxy Models Based on Experimental Design of Reservoir Simulations". Society of Petroleum Engineers. doi:10.2118/175642-MS.

Borst, R. L. (1983, January 1). "Methods for Calculating Shale Permeability". Society of Petroleum Engineers.

Box, G.E.P & Wilson K.B. (1951). "On the Experimental Attainment of Optimum Conditions". Journal of the Royal Statistical Society, Series B.13(1): 1-45. doi:10.1111/j.2517-6161.1951.tb00067.x.

Butler, R. M., McNab, G. S. & Lo, H. Y. (1981). "Theoretical-Studies on the Gravity Drainage of Heavy Oil During Insitu Steam Heating". Canadian Journal of Chemical Engineering. 59: 455-460.

Butler, R.M. (1987). "Rise Of Interfering Steam Chambers". Journal of Canadian Petroleum Technology 26(03): 70-75.

Butler, R. M. & Mokrys I. J. (1991) "A new process (VAPEX) for recovering heavy oils using hot water and hydrocarbon vapour." Journal of Canadian Petroleum Technology 30.01.

Cenovus (2020). https://www.cenovus.com/.

Coello Coello C. A. & Lechuga M. S. (2002). "MOPSO: a proposal for multiple objective particle swarm optimization," Proceedings of the 2002 Congress on Evolutionary Computation. CEC'02 (Cat. No.02TH8600). Honolulu, HI, USA. pp. 1051-1056 vol.2, doi: 10.1109/CEC.2002.1004388.

Coello Coello C. A. (2018). "Multi-objective Optimization. In: Martí R., Panos P., Resende M. (eds) Handbook of Heuristics". Springer, Cham. https://doi.org/10.1007/978-3-319-07153-4_17-1.

Coimbra, L., Ma, Z., & Leung, J. Y. (2019, April 22). "Practical Application of Pareto-Based Multi-Objective Optimization and Proxy Modeling for Steam Alternating Solvent Process Design". Society of Petroleum Engineers. doi:10.2118/195247-MS.

Coimbra, L. (2020). "A-Multi-Objective Optimization Work-flow for Steam-Alternating-Solvent Heavy Oil Process Design". University of Alberta (Thesis).

Computer Modelling Group, 2019. Calgary, Canada. https://www.cmgl.ca/

Corne D.W., Knowles J.D. & Oates M.J. (2000). "The Pareto Envelope-Based Selection Algorithm for Multiobjective Optimization". In: Schoenauer M. et al. (eds) Parallel Problem Solving from Nature PPSN VI. PPSN 2000. Lecture Notes in Computer Science, vol 1917. Springer, Berlin, Heidelberg. https://doi.org/10.1007/3-540-45356-3_82.

Corne, W. David, Jerram, R. Nick, Knowles, D. Joshua & Oates, J. Martin. (2001). "PESA-II: Region-based selection in evolutionary multi-objective optimization". Proc. 6th Int. Conf. Parallel Prob. Solving from Nature PPSN-VI.

Deb, K., Pratap, A., Agarwal, S. & Meyarivan, T. (2002). A Fast and Elitist Multi-Objective Genetic Algorithm: NSGA -II. IEEE Transactions on Evolutionary Computation 6 (0): 182–97.

Deb K. (2014). "Multi-objective Optimization. In: Burke E., Kendall G. (eds) Search Methodologies". Springer, Boston, MA.

Edmunds, Neil R. (1998). "Investigation of SAGD Steam Trap Control in Two and Three Dimensions." Paper presented at the SPE International Conference on Horizontal Well Technology, Calgary, Alberta, Canada. doi: https://doi.org/10.2118/50413-MS.

Eiben, A.E. & Smith, J. E. (2003). "Introduction to evolutionary computing". Springer, Berlin. ISBN:3- 540-40184-9.

Emission Reduction Alberta, 2020. https://eralberta.ca/projects/details/n-solv-best-pilot-plant-suncor-dover/.

Farouq Ali, S.M.; Bayestehparvin, B. (2018, March 13-14). "Electrical Heating—Doing the same thing over and over again." In Proceedings of the SPE Canada Heavy Oil Technical Conference, Calgary, AB, Canada.

Fonseca, C.M. & Fleming, P.J. (1993, July 17-22). "Genetic algorithms for multi- objective optimization: formulation, discussion and generalization". Proceedings of the 5th International Conference on Genetic Algorithms, San Francisco, CA, Morgan Kaufmann Publishers Inc.   San Mateo, 416-423

Fonseca, C. M., and Fleming. P J.   (2011). "Genetic Algorithms and Multi-objective Optimization". Multi-objective Genetic Algorithms for Clustering, no. July: 25–50. https://doi.org/10.1007/978-3-642-16615-0_2.

Frauenfeld, T.W., Jossy, C., Bleile, J., Krispin, D., & Ivory, J. (2009). "Experimental and Economic Analysis of the Thermal Solvent and Hybrid Solvent Processes." *J Can Pet Technol* 48: 55–62. doi: https://doi.org/10.2118/130445-PA.

Goldberg D. E. & Deb K. (1991). "A comparison of selection schemes used in genetic algorithms". In: Rawlins GJE (ed) Foundations of genetic algorithms. Morgan Kaufmann, San Mateo, pp 69–93.

Government of Canada, 2020. https://energy-information.canada.ca/en/subjects/crude-oil.

Gunantara, N. (2018). "A review of multi-objective optimization: Methods and its applications". Cogent Engineering. 5. 10.1080/23311916.2018.1502242.

Gupta, S. C., & Gittins, S. D. (2005). "Christina Lake solvent aided process pilot." Canadian International Petroleum Conference. Petroleum Society of Canada.

Gutek, H., Harshnitz, B., Myers R. D. & Okazaka, T. (2003, December 16). "Combined steam and vapor extraction process (SAVEX) for in situ bitumen and heavy oil production." U.S. Patent No. 6,662,872.

Horn, J., Nafpliotis, N., & Goldberg, D.E. (1994). "Niched Pareto Genetic Algorithm for Multiobjective Optimization". IEEE Conference on Evolutionary Computation - Proceedings 1: 82–87. https://doi.org/10.1109/icec.1994.350037.

Huang, S.J., Kang, B.T., Cheng, L.S., Zhou, W.S. & Chang, S.P. (2015). "Quantitative characterization of interlayer interference and productivity prediction of directional wells in the multilayer commingled production of ordinary offshore heavy oil reservoirs". Petrol Explor. Dev 42(4):533-40.

Hunyinbo, S., Ma, Z. & Leung J.Y. (2020, March 17-19). "Incorporating phase behavior constraints in multi-objective optimization of warm vaporized solvent injection process". SPE

Paper 198925 presented at the Latin America and Caribbean Petroleum Engineering Conference, Bogota, Colombia.

Ipek, G., Frauenfeld, T., & Yuan, J. Y. (2008, January 1). "Numerical Study of Shale Issues in SAGD". Petroleum Society of Canada. doi:10.2118/2008-150.

James, L. (2009). "Mass Transfer Mechanisms during the Solvent Recovery of Heavy Oil". UWSpace. http://hdl.handle.net/10012/4478

Jiang, Q., Butler, R., & Yee, C.T. (1998, June 8-10). "The Steam and Gas Push (SAGP)-2: Mechanism Analysis and Physical Model Testing". Paper 98-43, presented at proceedings of the petroleum society 49th Annual Technical Meeting, Calgary, AB.

Knowles, J. & Corne, D. (1999, July). "The pareto archived evolution strategy: a new baseline algorithm for Pareto multi-objective optimisation," in Proceedings of the Congress on Evolutionary Computation (CEC '99), vol. 1, pp. 98–105.

Leaute, R. P., & B. S. Carey. (2007) "Liquid addition to steam for enhancing recovery (LASER) of bitumen with CSS: Results from the first pilot cycle." Journal of Canadian Petroleum Technology 46.09.

Leung, J.Y. (2014). "Scale-up of effective mass transfer in vapor extraction process accounting for field-scale reservoir heterogeneities". Journal of Canadian Petroleum Technology, 53(05), 275-289. https://doi.org/10.2118/153862-PA.

Li, P. (2006). "Numerical simulation of the SAGD process coupled with geomechanical behavior". Doctoral dissertation, University of Alberta, Canada.

Lima, D. M.S. de B., Araújo, E. A., Diniz, A, A.R., Gurgel, A. R. & Da Mata, W. (2016). "Analysis of the intermittency of the steam alternating solvent process (SAS) applied to a heavy oil reservoir". Editor(s): Zdravko Kravanja, Miloš Bogataj, Computer Aided Chemical

Engineering, Elsevier, Volume 38, Pages 1743-1748, ISSN 1570-7946, ISBN 9780444634283. https://doi.org/10.1016/B978-0-444-63428-3.50295-2.

Luo, X.R., Hu, C.Z., Xiao, Z.Y., Zhao, J., Zhang, B.S., Yang, W., Zhao, H., Zhao, F.Y., Lei Y.H. & Zhang, L.K. (2015). "Effects of carrier bed heterogeneity on hydrocarbon migration". MarPetrol Geol 68:120-31.

Ma, Z., Liu, Y., Leung, J. Y., & Zanon, S. (2015). "Practical Data Mining and Artificial Neural Network Modeling for SAGD Production Analysis". Society of Petroleum Engineers. doi:10.2118/174460-MS.

Ma, Z., & Leung, J. Y. (2019, March). "Design of Warm Solvent Injection Processes for Heterogeneous Heavy Oil Reservoirs: A Hybrid Work-flow of Multi-Objective Optimization and Proxy Models". In SPE Reservoir Simulation Conference. Society of Petroleum Engineers. https://doi.org/10.2118/193842-MS.

Magara, K. (1968, January 1). "Porosity-Permeability Relationship Of Shale ". Society of Petroleum Engineers.

Middleton, R.S., Gupta, R., Hyman, J.D. & Viswanathan, H.S. (2017). "The shale gas revolution: barriers, sustainability, and emerging opportunities". Appl Energy 199:88-95.

Miettinen, K. (1999). "Nonlinear Multiobjective Optimization". Boston, MA: Kluwer Academic Publishers.

Mirjalili S & Lewis A (2015). "Novel performance metrics for robust multi-objective optimization algorithms". Swarm Evolut Comput 21:1–23.

Mokheimer, E., Hamdy, M., Abubakar, Z., Shakeel, R., Habib, M. A. & Mahmoud, M. (2019). "A Comprehensive Review of Thermal Enhanced Oil Recovery: Techniques Evaluation". Journal of Energy Resources Technology, Transactions of the ASME. 141. 10.1115/1.4041096.

Mostapha K. H. (2015). "PESA-II, MOPSO and SPEA-II in MATLAB" (URL: https://yarpiz.com/86/ypea123-pesa2), Yarpiz.

Motameni, H. (2016). "PSO for multi-objective problems: Criteria for leader selection and uniformity distribution". Journal of AI and Data Mining, 4, 67-76.

Nasr, T.N. & Isaacs, E.E. (2001, May). "Process for Enhancing Hydrocarbon Mobility Using a Steam Additive". US patent 6,230,814.

Naqvi, S. (2012). "Enhanced Oil Recovery of Heavy Oil by Using Thermal and Non-Thermal Methods". MS thesis, Dalhousie University, Halifax, NS, Canada.

Nenniger J. &Nenniger E. (2005, July). "Method and Apparatus for Stimulating Heavy Oil Product". US Patent 20050145383A1, N-Solv Corp.

Nnamdi, D. (2020, August). "Conceptual Reservoir Development and Short-Term Forecasting Using Material Balance Based Integrated Asset Models and Neural Network Proxy Models." Paper presented at the SPE Nigeria Annual International Conference and Exhibition, Virtual. doi: https://doi-org.login.ezproxy.library.ualberta.ca/10.2118/203682-MS

Pareto, V. (1896). "Cours D'Economie Politique". Vol I and II. F. Rouge, Lausanne.

Pichery, C. (2014). "Encyclopedia of Toxicology". Third edition. Elsevier Inc. ISBN 978-0-12-386455-0.

Rakhshani, H. (2020, May 15). "Interplay of Machine Learning and Metaheuristics". Universite de Haute-Alsace (Thesis).

Saka, M.P, Doğan, E. & Aydogdu, I. (2013). "Analysis of Swarm Intelligence–Based Algorithms for Constrained Optimization". Swarm Intelligence and Bio-Inspired Computation, Elsevier, Pages 25-48. ISBN 9780124051638. https://doi.org/10.1016/B978-0-12-405163-8.00002-8.

Sarapardeh, A., Kiasari, H. H., Alizadeh, N., Mighani, S., & Kamari, A. (2013). "Application of Fast-SAGD in Naturally Fractured Heavy Oil Reservoirs: A Case Study". SPE Middle East Oil and Gas Show and Conference, Manama, Bahrain, Mar. 10–13, SPE Paper No. 164418.

Schaffer, J. D. (1985). "Multiple Objective Optimization with Vector Evaluated Genetic Algorithms". In Proceedings of First International Conference on Genetic Algorithms, 93–100. https://doi.org/10.1017/CBO9781107415324.004.

Souraki, Y., Torsater, O., Jahanbani Ghahfarokhi, A., & Ashrafi, M. (2013, April 19). "Application of Solvent Alternating SAGD Process to Improve SAGD Performance in Athabasca Bitumen Reservoir". Society of Petroleum Engineers. doi:10.2118/165327-MS

Speight, J.G. (2009). "Enhanced Recovery Methods for Heavy Oil and Tar Sands". Gulf Publishing Company, Houston.

Suncor Energy Inc (2020). Project: "Solvent+". https://www.suncor.com.

Yadali J. & Ben, B. (2013). "Enhanced Cyclic Solvent Process (ECSP) for Thin Heavy Oil Reservoirs". Diss. The University of Calgary.

Zandvliet, M., Handels, M., Van Essen, G., Brouwer, R. and Jan-Dirk Jansen. (2008) "Adjoint-Based Well-Placement Optimization Under Production Constraints." SPE J. 13: 392–399. doi: https://doi.org/10.2118/105797-PA

Zhao, L., Nasr, T. N., Huang, H., Beaulieu, G., Heck, G., & Golbeck, H. (2005, September 1). "Steam Alternating Solvent Process: Lab Test and Simulation". Petroleum Society of Canada. https://doi.org/10.2118/05-09-04.

Zhao, L. (2007). "Steam Alternating Solvent Process". SPE Reservoir Evaluation & Engineering, 10(02), 185-190. https://doi.org/10.2118/86957-PA.

Zhang, L., Li, J., Sun, L. & Yang, F. (2021). "An influence mechanism of shale barrier on heavy oil recovery using SAGD based on theoretical and numerical analysis". Energy, Volume 216, 119099, ISSN 0360-5442. https://doi.org/10.1016/j.energy.2020.119099.

Zheng, J., Leung, J. Y., Sawatzky, R. P., & Alvarez, J. M. (2016, June 7). "A Proxy Model for Predicting SAGD Production from Reservoirs Containing Shale Barriers". Society of Petroleum Engineers. doi:10.2118/180715-MS.

Zheng, J., Leung, J.Y., Sawatzky, R. P. & Alvarez J. M. (2017, February). "An AI-Based Work-flow for Estimating Shale Barrier Configurations from SAGD Production Histories." Paper presented at the SPE Canada Heavy Oil Technical Conference, Calgary, Alberta, Canada. doi: https://doi-org.login.ezproxy.library.ualberta.ca/10.2118/184984-MS.

Zheng, J., Leung, J.Y., Sawatzky, R.P., Alvarez, J.M. (2021). A cluster-based approach for visualizing and categorizing the impacts of shale barrier configurations on SAGD production. Journal of Petroleum Science and Engineering 203: 108664.

Zhou A., Qu, B.Y., Li, H., Zhao S. Z., Suganthan, P. N. & Zhang Q. (2011). "Multi-objective evolutionary algorithms: A survey of the state of the art". Swarm and Evolutionary Computation, Volume 1, Issue 1. Pages 32-49, ISSN 2210-6502, https://doi.org/10.1016/j.swevo.2011.03.001.

Zitzler, E., Laumanns, M. & Thiele, L. (2001). "SPEA2: Improving the Strength Pareto Evolutionary Algorithm ". TIK-Report. 103.

Zolpakar, N., Singh-Lodhi, S., Pathak, S. & Sharma, M. (2019). "Application of Multi-objective Genetic Algorithm (MOGA) Optimization in Machining Processes." 10.1007/978-3-030-19638-7_8.

Zubarev, D. I., January 1, 2009. "Pros and Cons of Applying Proxy-models as a Substitute for Full

Reservoir Simulations". Society of Petroleum Engineers. doi:10.2118/124815-MS

Appendix A

In this section, the RSM coefficients needed to calculate the objective function of section 5.8.1 are presented. Coefficients in tables 13, 14, 15 and 16 refer to models a, b, c and d, respectively.

Table 13. RSM coefficients to calculate the objective functions of the homogeneous model.

Term	RSM Coefficient RF	Term	RSM Coefficient $cSOR$	Term	RSM Coefficient $cSolv$
Interception (β_0)	44.26	Interception (β_0)	3.4759	Interception (β_0)	1,512,900
Propane$_1$ (β_1)	-92.43	Propane$_1$ (β_1)	0.1629	Propane$_1$ (β_1)	-2,375,300
Propane$_2$ (β_2)	11.23	Propane$_2$ (β_2)	0	Propane$_2$ (β_2)	238,867
Cycle$_{solv1}$ (β_3)	-0.0804	Cycle$_{solv1}$ (β_3)	0.0010	Cycle$_{solv1}$ (β_3)	-1,706.02
Cycle$_{steam1}$ (β_4)	0	Cycle$_{steam1}$ (β_4)	0.0021	Cycle$_{steam1}$ (β_4)	-19,461.80
Cycle$_{steam2}$ (β_5)	0.3669	Cycle$_{steam2}$ (β_5)	0.0012	Cycle$_{steam2}$ (β_5)	5,724.81
Cycle$_{solv2}$ (β_6)	0.0208	Cycle$_{solv2}$ (β_6)	-0.0012	Cycle$_{solv2}$ (β_6)	1,168.80
BHP$_{steam1}$ (β_7)	0.0013	BHP$_{steam1}$ (β_7)	-0.0008	BHP$_{steam1}$ (β_7)	2.44
BHP$_{prod}$ (β_8)	-0.0043	BHP$_{prod}$ (β_8)	-0.0007	BHP$_{prod}$ (β_8)	-400.49
$(\beta_1)^2$	55.9839	$(\beta_1)*(\beta_3)$	-0.0037	$(\beta_1)^2$	1,242,600.00
$(\beta_1)*(\beta_3)$	0.10	$(\beta_7)^2$	1.0741E-07	$(\beta_1)*(\beta_3)$	2,873.72
$(\beta_1)*(\beta_7)$	0.0039	$(\beta_8)^2$	1.3875E-07	$(\beta_1)*(\beta_7)$	228.91
$(\beta_1)*(\beta_8)$	0.0058			$(\beta_2)*(\beta_3)$	-1,830.97
$(\beta_2)*(\beta_3)$	-0.0485			$(\beta_3)*(\beta_5)$	31.02
$(\beta_2)*(\beta_5)$	-0.0871			$(\beta_4)*(\beta_8)$	6.79
$(\beta_3)*(\beta_5)$	0.0006			$(\beta_5)^2$	-68.11
$(\beta_5)^2$	-0.0026			$(\beta_5)*(\beta_6)$	-8.26
$(\beta_5)*(\beta_6)$	-0.0004				

Table 14. RSM coefficients to calculate the objective functions of the simple heterogeneous model

Term	RSM Coefficient **RF**	Term	RSM Coefficient **cSOR**	Term	RSM Coefficient **cSolv**
Interception (β_0)	-2.04	Interception (β_0)	1.0722	Interception (β_0)	129,270
Propane$_1$ (β_1)	-25.23	Propane$_1$ (β_1)	0.4384	Propane$_1$ (β_1)	-810,102
Cycle$_{solv1}$ $(\beta2)$	0.07	Cycle$_{solv1}$ $(\beta2)$	-0.0020	Cycle$_{solv1}$ $(\beta2)$	440
Cycle$_{steam1}$ $(\beta3)$	-0.02	Cycle$_{steam1}$ $(\beta3)$	-0.0217	Cycle$_{steam1}$ $(\beta3)$	-1,863
Propane$_2$ $(\beta4)$	13.0886	Propane$_2$ $(\beta4)$	-0.2152	Propane$_2$ $(\beta4)$	293,584
Cycle$_{solv2}$ (β_5)	0.0469	Cycle$_{solv2}$ (β_5)	-0.0018	Cycle$_{solv2}$ (β_5)	-406.30

Term	Coefficient	Term	Coefficient	Term	Coefficient
Cycle$_{steam2}$ (β_6)	0.0673	Cycle$_{steam2}$ (β_6)	0.0134	Cycle$_{steam2}$ (β_6)	0
BHP$_{steam1}$ (β_7)	0.0135	BHP$_{steam1}$ (β_7)	0.00016	BHP$_{steam1}$ (β_7)	68.51
Steam trap (β_8)	-0.0905	Steam trap (β_8)	-0.0219	Steam trap (β_8)	0
BHG (β_9)	-0.2990	BHG (β_9)	-0.0015	BHG (β_9)	-8,790.04
(β_9)*(β_1)	-0.0446	(β_4)*(β_9)	0.00048	(β_7)*(β_9)	6.87
(β_5)*(β_9)	0.0034	(β_8)*(β_9)	-8.54E-06	(β_1)*(β_9)	-2,880.66
(β_7)*(β_7)	-1.56E-06	(β_1)*(β_1)	-0.3833	(β_1)*(β_7)	134.43
(β_1)*(β_7)	0.0032	(β_1)*(β_8)	-0.01944	(β_1)*(β_1)	304,130
(β_7)*(β_8)	0.0002	(β_1)*(β_3)	-0.004536	(β_1)*(β_4)	152,886
(β_1)*(β_1)	15.6566	(β_4)*(β_4)	-0.1612	(β_1)*(β_3)	4,664.02
(β_1)*(β_4)	5.1848	(β_4)*(β_5)	0.001761	(β_4)*(β_4)	290,464
(β_1)*(β_8)	0.2257	(β_8)*(β_8)	0.0028761	(β_2)*(β_4)	-3,167.78
(β_1)*(β_3)	0.1221	(β_3)*(β_5)	7.44E-05	(β_4)*(β_5)	-2245.4600
(β_4)*(β_4)	9.2940	(β_3)*(β_3)	0.000313		
(β_2)*(β_4)	-0.0817	(β_3)*(β_6)	-0.000215		
(β_4)*(β_5)	-0.0355				
(β_4)*(β_6)	-0.1325				
(β_3)*(β_5)	-0.0006				

Table 15. RSM coefficients to calculate the objective functions of the semi-complex heterogeneous model

Term	RSM Coefficient	Term	RSM Coefficient	Term	RSM Coefficient
	RF		**cSOR**		**cSolv**
Interception (β_0)	4.56	Interception (β_0)	6.2087	Interception (β_0)	4.29E+06
Propane$_1$ (β_1)	-30.56	Propane$_1$ (β_1)	0.7870	Propane$_1$ (β_1)	-5.70E+06
Cycle$_{solv1}$ (β_2)	1.42	Cycle$_{solv1}$ (β_2)	0	Cycle$_{solv1}$ ($\beta2$)	71785.50
Cycle$_{steam1}$ ($\beta3$)	-0.3934	Cycle$_{steam1}$ ($\beta3$)	0	Cycle$_{steam1}$ ($\beta3$)	-111437
Propane$_2$ ($\beta4$)	-30.8062	Propane$_2$ ($\beta4$)	-0.9396	Propane$_2$ ($\beta4$)	-2.57E+06
Cycle$_{solv2}$ (β_5)	-0.2610	Cycle$_{solv2}$ (β_5)	0.0031	Cycle$_{solv2}$ (β_5)	3581.44
Cycle$_{steam2}$ (β_6)	0.3803	Cycle$_{steam2}$ (β_6)	0.0032	Cycle$_{steam2}$ (β_6)	71989.80
BHP$_{steam1}$ (β_7)	-0.0105	BHP$_{steam1}$ (β_7)	-0.0031	BHP$_{steam1}$ (β_7)	-3717.23
Steam trap (β_8)	-1.2760	Steam trap (β_8)	-0.2937	Steam trap (β_8)	-27780.30
BHG (β_9)	0.8771	BHG (β_9)	0	BHG (β_9)	91133.70
(β_9)*(β_9)	-0.06	(β_7)*(β_7)	5.64E-07	(β_5)*(β_9)	-485.10
(β_4)*(β_7)	0.0.3351	(β_4)*(β_7)	0.0004	(β_7)*(β_7)	0.068
(β_2)*(β_7)	-0.0003	(β_1)*(β_8)	-0.0788	(β_1)*(β_7)	1379.45
(β_3)*(β_7)	0.0005	(β_4)*(β_4)	-0.3423	(β_4)*(β_7)	1378.32
(β_1)*(β_1)	49.1765	(β_8)*(β_8)	0.01807	(β_2)*(β_7)	-9.1544
(β_1)*(β_4)	6.6975			(β_1)*(β_1)	2.69E+06
(β_4)*(β_4)	58.4522			(β_4)*(β_4)	1.36E+06

Term	RSM Coefficient	Term	RSM Coefficient
$(\beta_2)*(\beta_4)$	-0.2660	$(\beta_2)*(\beta_4)$	-4688.14
$(\beta_3)*(\beta_4)$	-0.7026	$(\beta_3)*(\beta_4)$	-32221.30
$(\beta_4)*(\beta_6)$	-0.57651	$(\beta_2)*(\beta_2)$	-262.02
$(\beta_2)*(\beta_3)$	-0.01055	$(\beta_3)*(\beta_3)$	1173.12
$(\beta_5)*(\beta_5)$	0.00124	$(\beta_6)*(\beta_6)$	-618.75

Table 16. RSM coefficients to calculate the objective functions of the complex heterogeneous model.

Term	RSM Coefficient RF	Term	RSM Coefficient cSOR	Term	RSM Coefficient cSolv
Interception (β_0)	-238.21	Interception (β_0)	0.4281	Interception (β_0)	-9.24E+06
Propane$_1$ (β_1)	-107.41	Propane$_1$ (β_1)	-1.1698	Propane$_1$ (β_1)	-1.80E+06
Cycle$_{solv1}$ ($\beta2$)	-0.84	Cycle$_{solv1}$ ($\beta2$)	0	Cycle$_{solv1}$ ($\beta2$)	-32,837.8
Cycle$_{steam1}$ ($\beta3$)	-0.5828	Cycle$_{steam1}$ ($\beta3$)	-0.0110	Cycle$_{steam1}$ ($\beta3$)	20,058.30
Propane$_2$ ($\beta4$)	-29.2263	Propane$_2$ ($\beta4$)	-2.7905	Propane$_2$ ($\beta4$)	1.03E+06
Cycle$_{solv2}$ (β_5)	0.6998	Cycle$_{solv2}$ (β_5)	0.0232	Cycle$_{solv2}$ (β_5)	19,091.70
Cycle$_{steam2}$ (β_6)	8.0751	Cycle$_{steam2}$ (β_6)	-0.00049	Cycle$_{steam2}$ (β_6)	234,858
BHP$_{steam1}$ (β_7)	0.0299	BHP$_{steam1}$ (β_7)	0.00066	BHP$_{steam1}$ (β_7)	9.55.487
Steam trap (β_8)	-0.7990	Steam trap (β_8)	0.03986	Steam trap (β_8)	46,561
BHG (β_9)	5.2277	BHG (β_9)	0.0703	BHG (β_9)	245,038
$(\beta_7)*(\beta_9)$	-0.0020	$(\beta_7)*(\beta_9)$	-2.48E-05	$(\beta_7)*(\beta_9)$	-48.40
$(\beta_1)*(\beta_9)$	0.9778	$(\beta_8)*(\beta_9)$	-4.14E-05	$(\beta_1)*(\beta_9)$	31,465.10
$(\beta_4)*(\beta_7)$	0.0110	$(\beta_1)*(\beta_8)$	-0.0655	$(\beta_3)*(\beta_9)$	-1,778.41
$(\beta_7)*(\beta_8)$	-0.0016	$(\beta_1)*(\beta_6)$	0.0232	$(\beta_4)*(\beta_7)$	398.96
$(\beta_1)*(\beta_1)$	46.8455	$(\beta_3)*(\beta_4)$	0.02504	$(\beta_7)*(\beta_8)$	-49.64
$(\beta_1)*(\beta_8)$	0.7365	$(\beta_4)*(\beta_6)$	0.01996	$(\beta_1)*(\beta_1)$	848,250
$(\beta_1)*(\beta_6)$	1.4870	$(\beta_8)*(\beta_8)$	0.01415	$(\beta_1)*(\beta_3)$	-17,598.40
$(\beta_4)*(\beta_4)$	24.9726	$(\beta_6)*(\beta_8)$	-0.0002046	$(\beta_1)*(\beta_6)$	40840.1
$(\beta_2)*(\beta_4)$	-0.140332	$(\beta_5)*(\beta_5)$	-0.0001205	$(\beta_4)*(\beta_4)$	542100
$(\beta_8)*(\beta_8)$	0.144108			$(\beta_2)*(\beta_4)$	-4705.39
$(\beta_6)*(\beta_8)$	0.04151			$(\beta_4)*(\beta_6)$	1268.84
$(\beta_2)*(\beta_3)$	0.02933			$(\beta_8)*(\beta_8)$	2152.1
$(\beta_2)*(\beta_6)$	-0.0099			$(\beta_6)*(\beta_8)$	835.23
$(\beta_5)*(\beta_5)$	-0.00401			$(\beta_2)*(\beta_3)$	717.177
$(\beta_3)*(\beta_6)$	-0.0222			$(\beta_5)*(\beta_5)$	-106.757
$(\beta_6)*(\beta_6)$	-0.05754			$(\beta_3)*(\beta_6)$	-833.406
				$(\beta_6)*(\beta_6)$	-1781.47

Appendix B

This section presents the optimization ranges for the homogeneous model for each of the

selected decision variables using MOPSO and PESA-II.
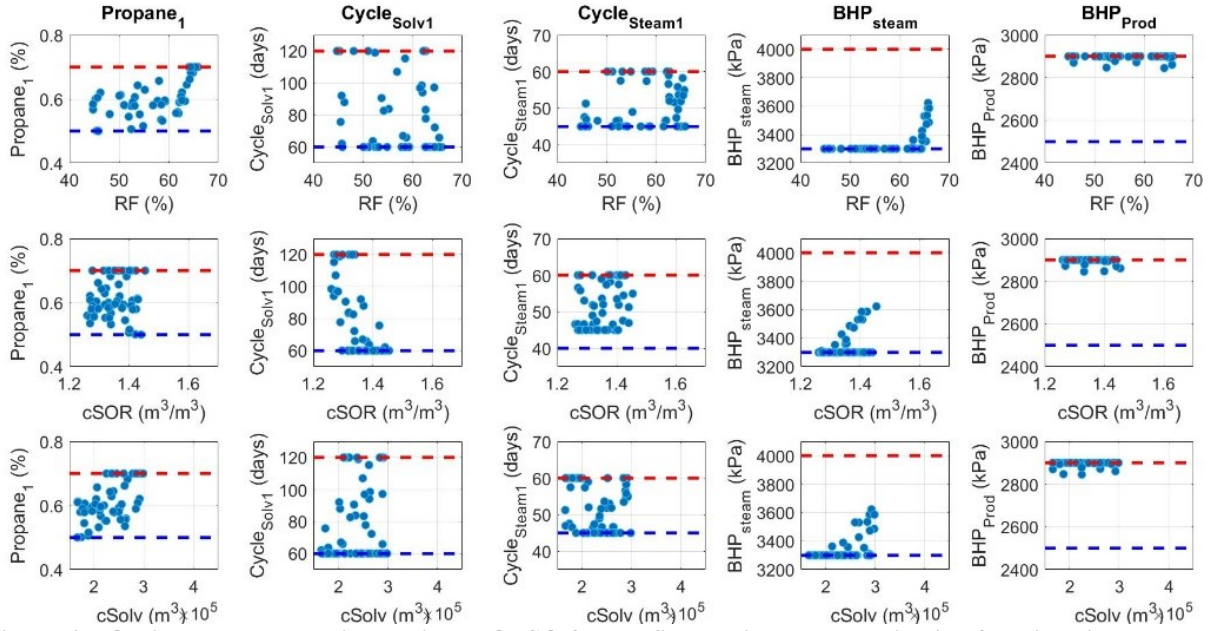
Figure 45. Optimal ranges obtained using MOPSO for the first period vs. the objective functions in the blue section.
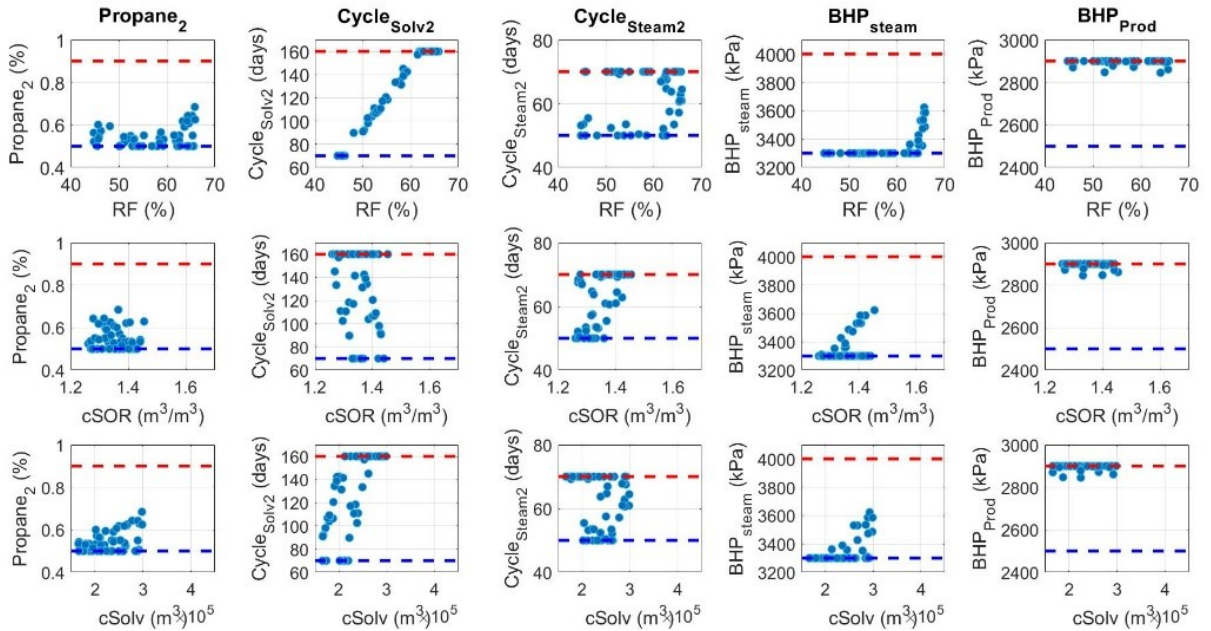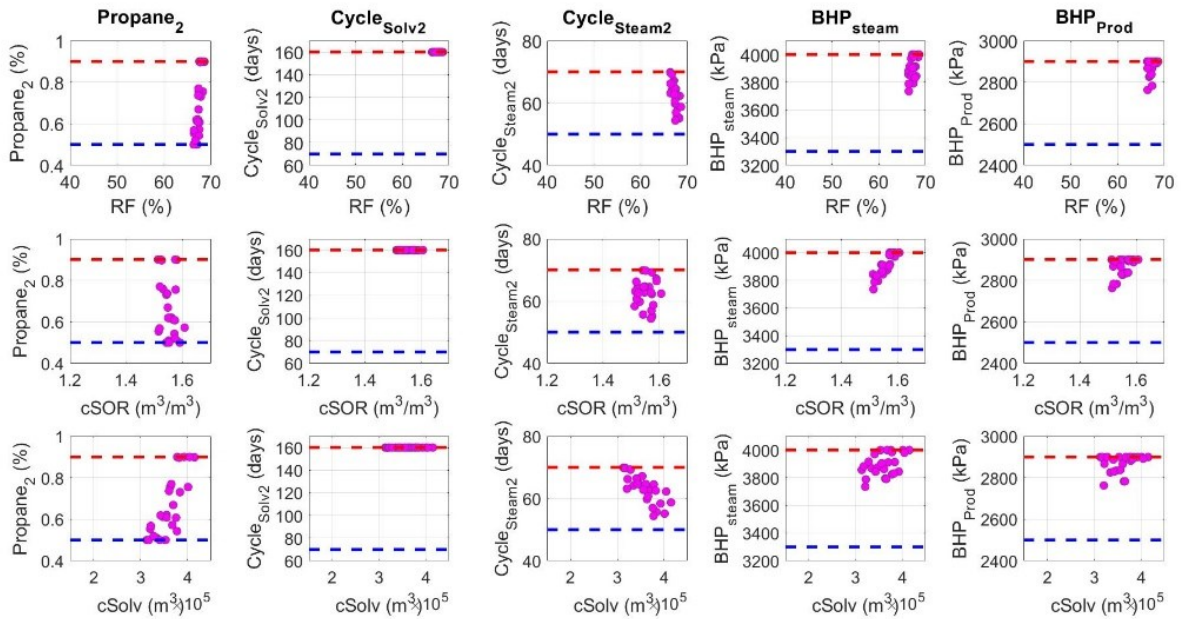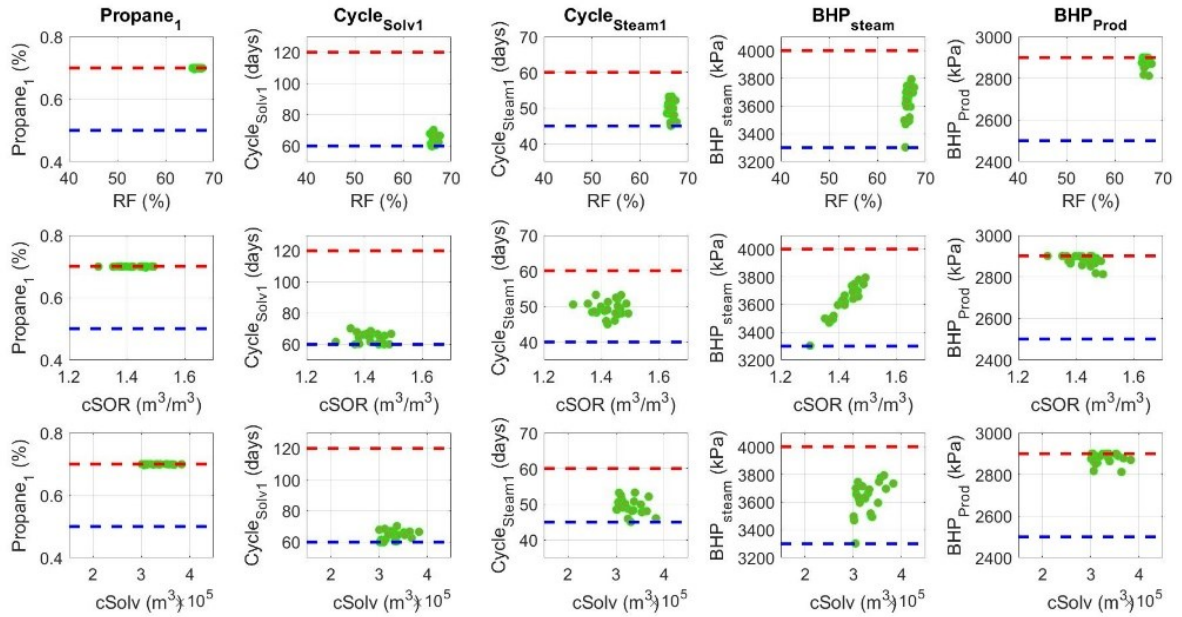

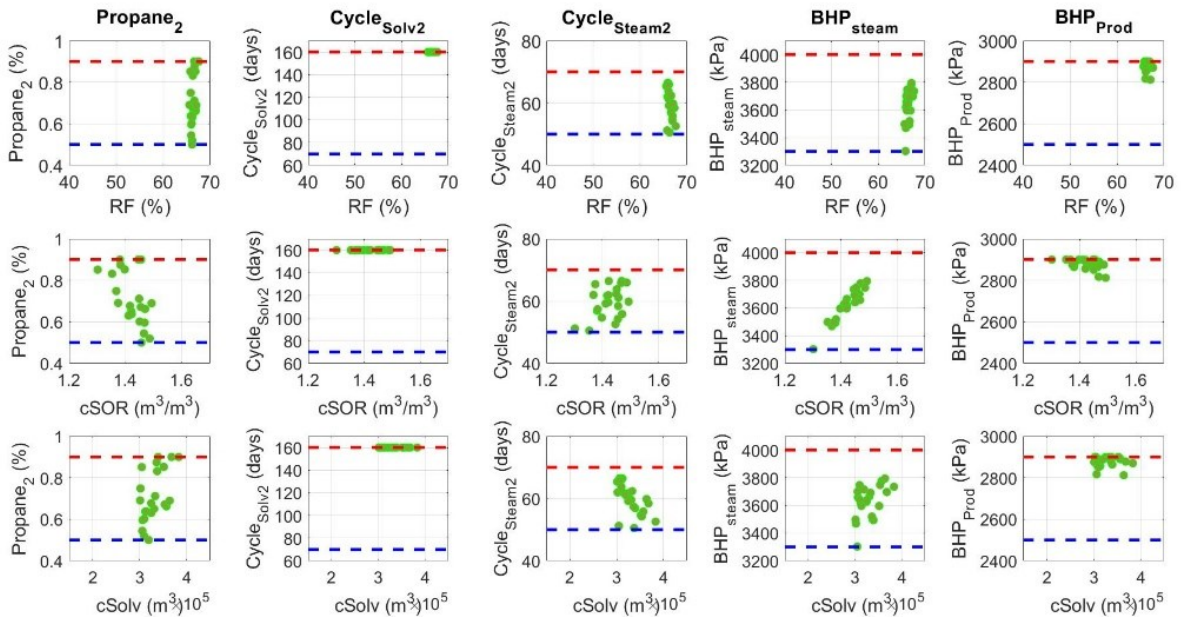**Figure 46. Optimal ranges obtained using MOPSO for the second period vs. the objective functions in the blue section.**
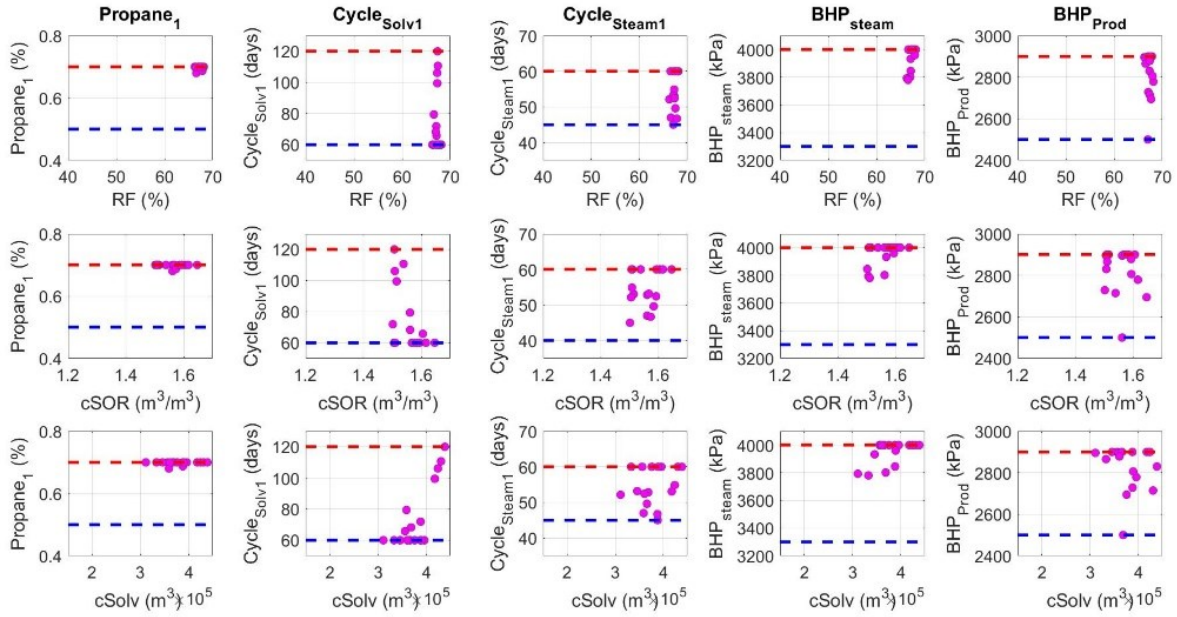
Figure 47. Optimal ranges obtained using MOPSO for the first period vs. the objective functions in the magenta section.
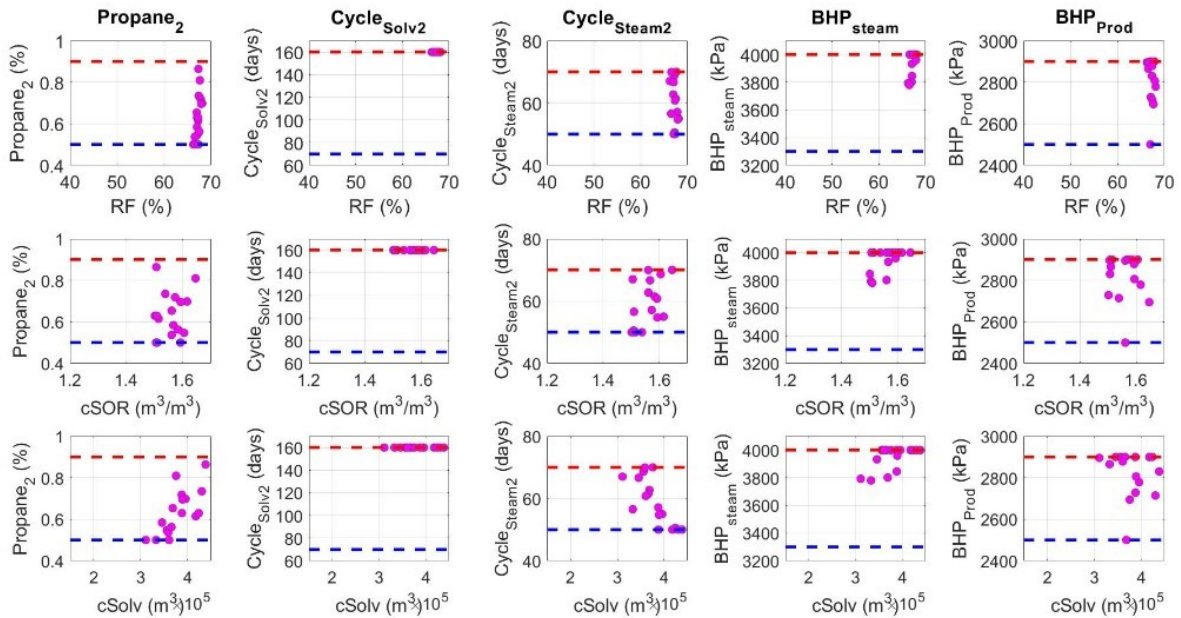
Figure 48. Optimal ranges obtained using MOPSO for the second period vs the objective functions in the magenta section.

109
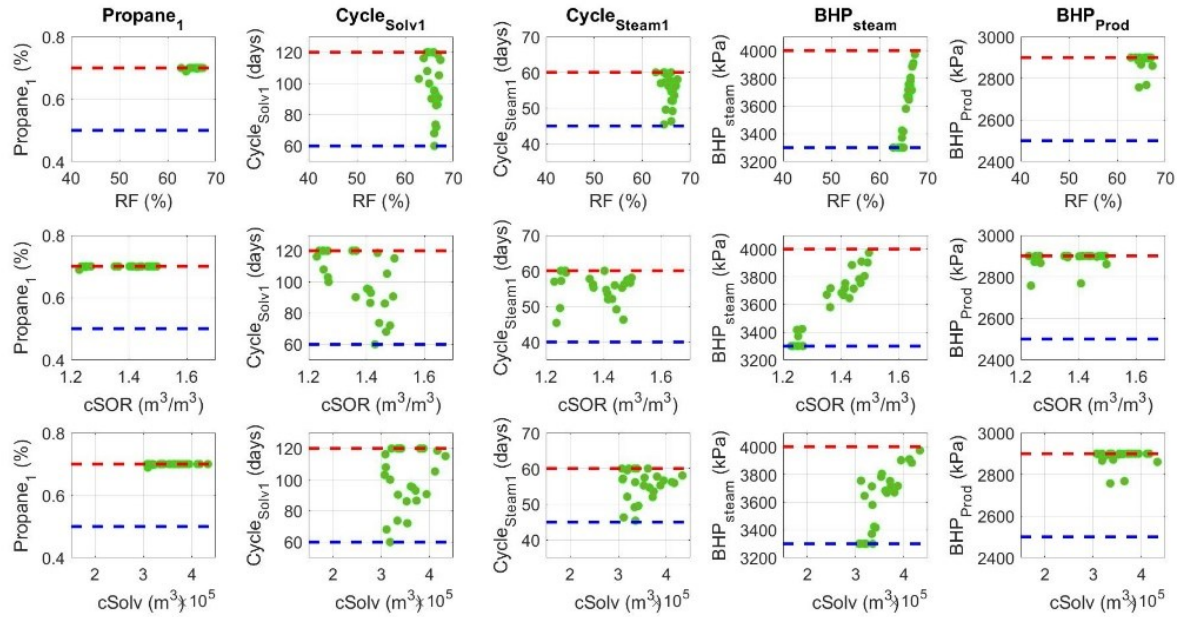
Figure 49. Optimal ranges obtained using MOPSO for the first period vs. the objective functions in the green section.
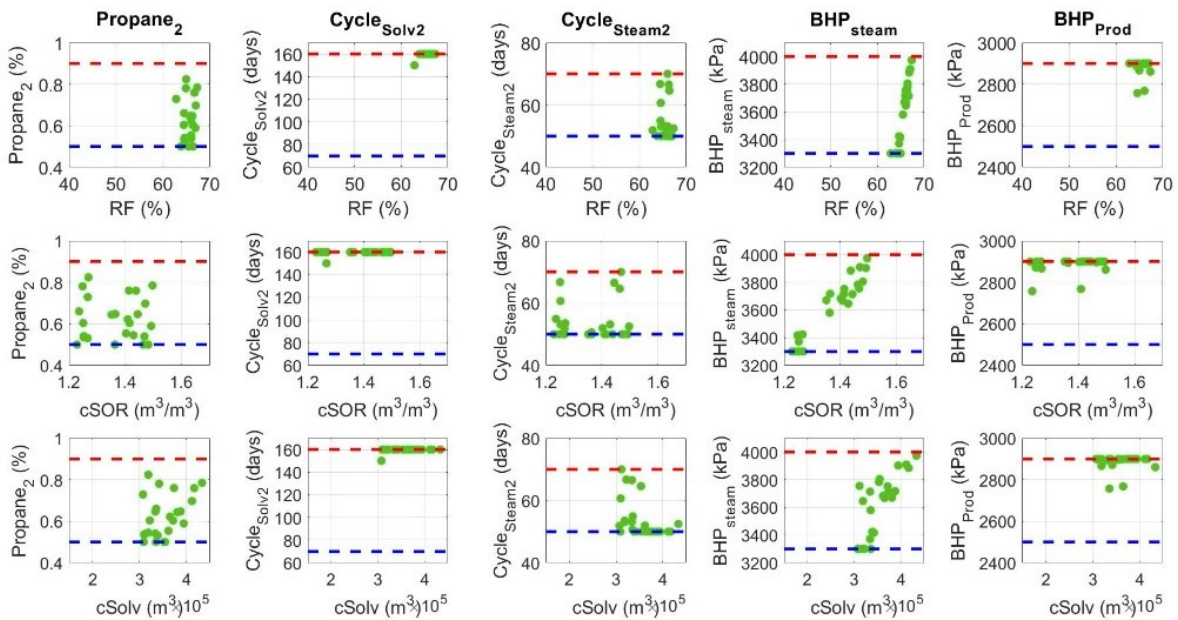
Figure 50. Optimal ranges obtained using MOPSO for the second period vs. the objective functions in the green section.

110
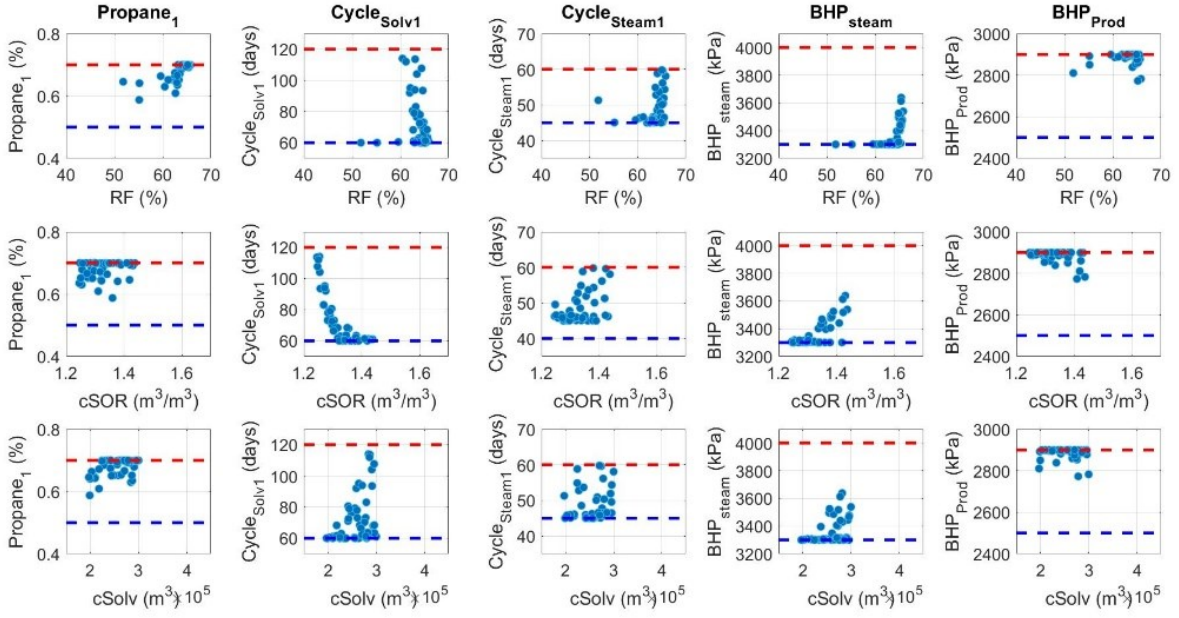
Figure 51. Optimal ranges obtained using PESA-II for the first period vs. the objective functions in the blue section.
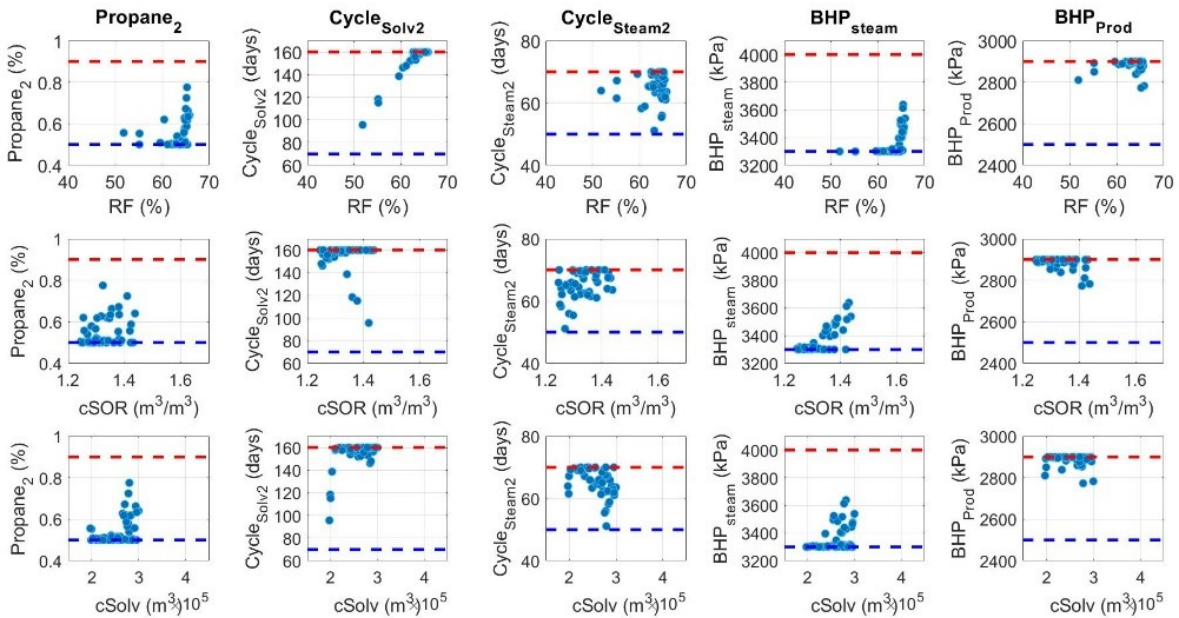
Figure 52. Optimal ranges obtained using PESA-II for the second period vs. the objective functions in the blue section.

111
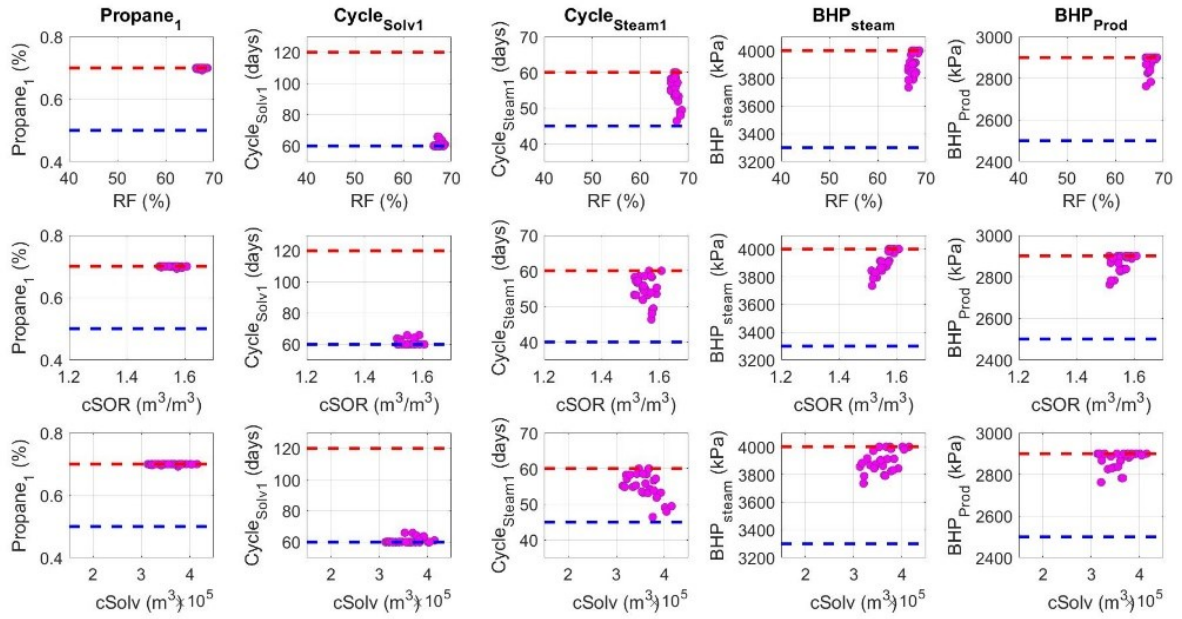
Figure 53. Optimal ranges obtained using PESA-II for the first period vs. the objective functions in the magenta section.

Figure 54. Optimal ranges obtained using PESA-II for the second period vs the objective functions in the magenta section.

Figure 55. Optimal ranges obtained using PESA-II for the first period vs. the objective functions in the green section.

Figure 56. Optimal ranges obtained using PESA-II for the second period vs. the objective functions in the green section.

Appendix C

This section presents the optimization ranges for the homogeneous, simple heterogeneous, semi-complex heterogeneous and complex heterogeneous for each of the selected decision variables using MOPSO and PESA-II.
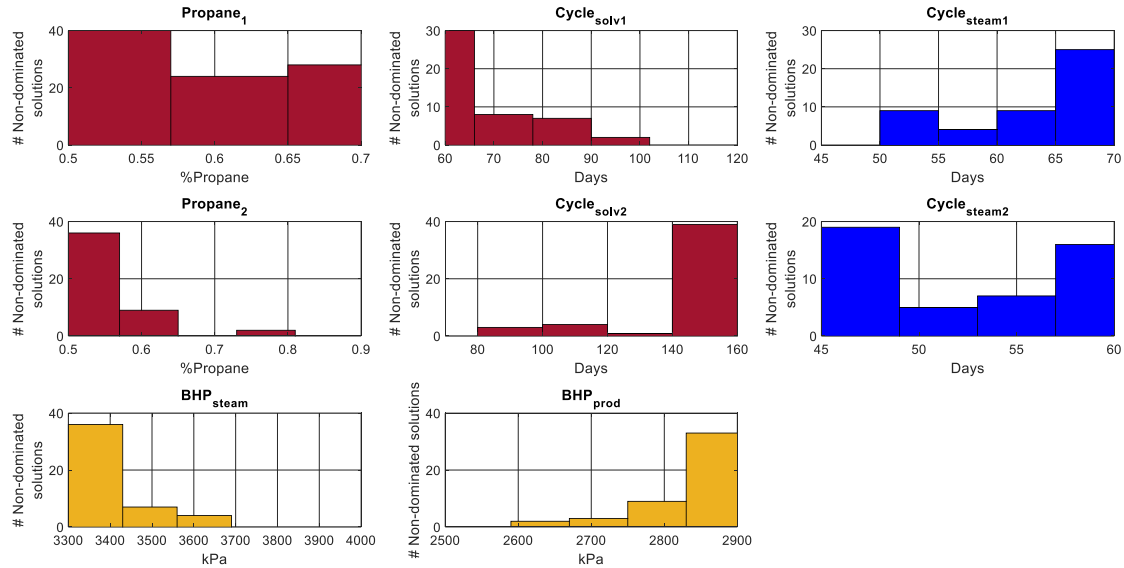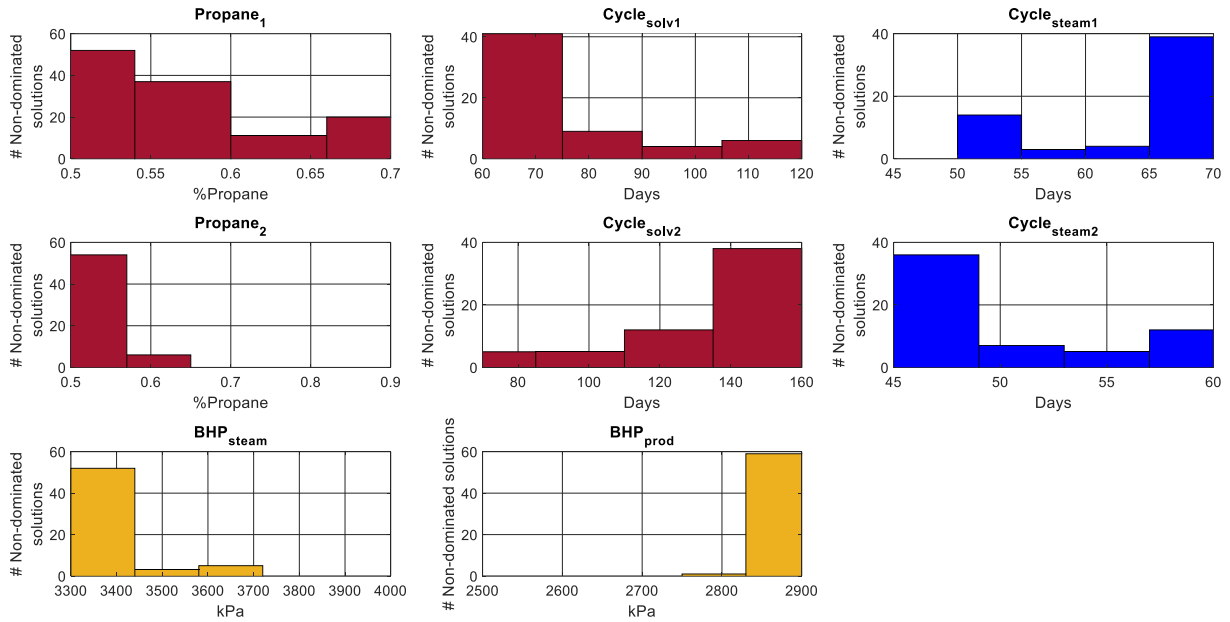

Figure 57. Optimal ranges using PESA-II for the homogeneous model in the blue quadrant.
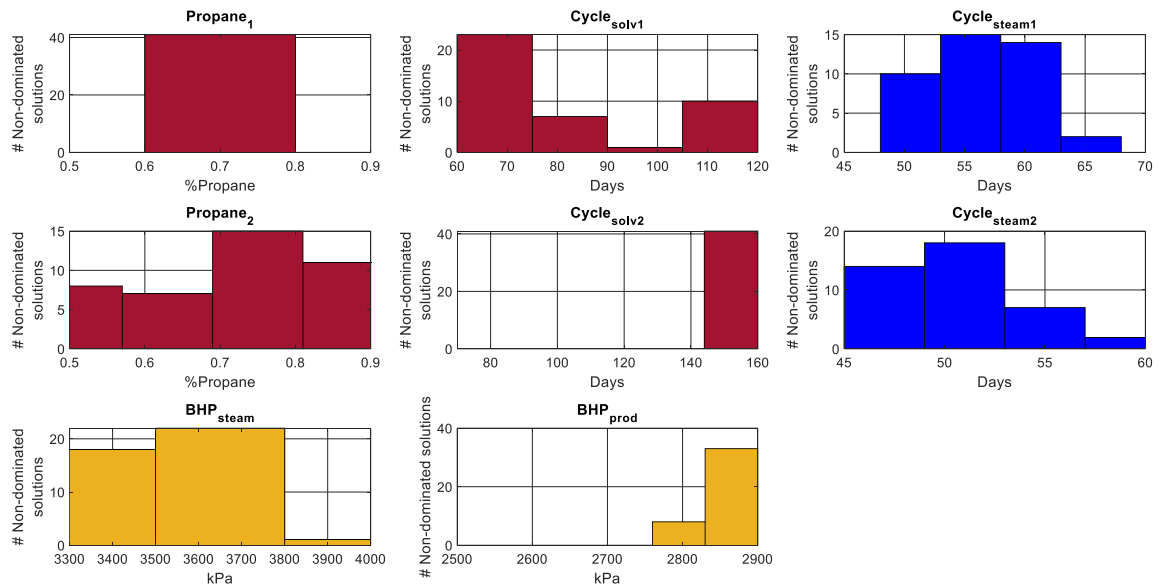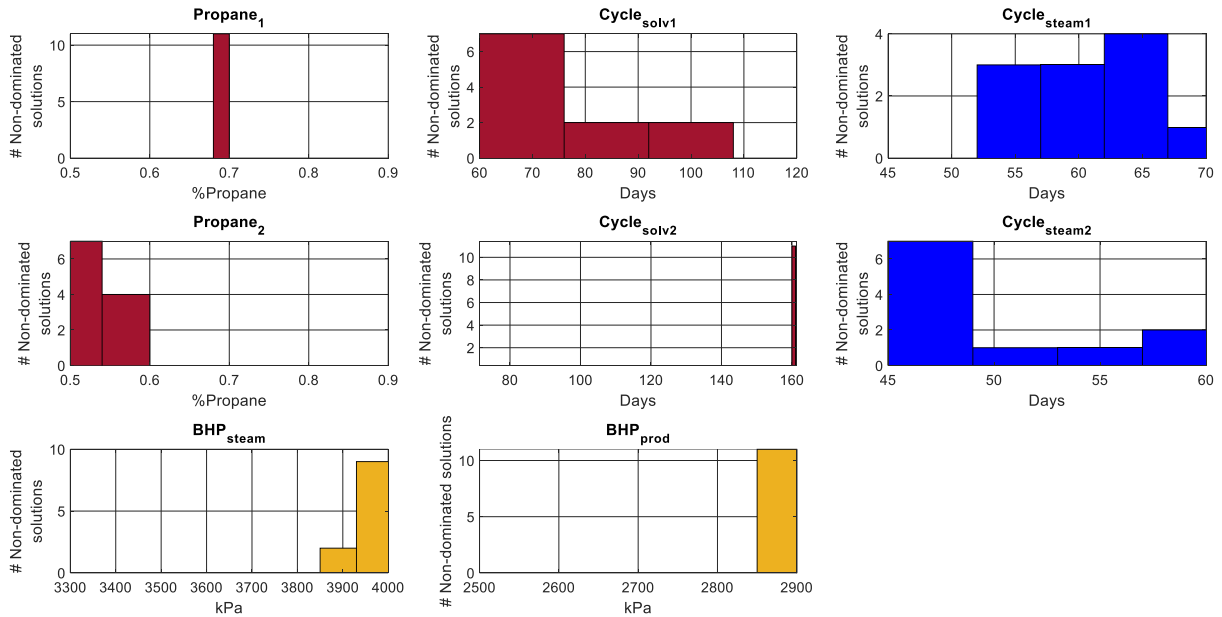

Figure 58. Optimal ranges using PESA-II for the homogeneous model in the magenta quadrant.
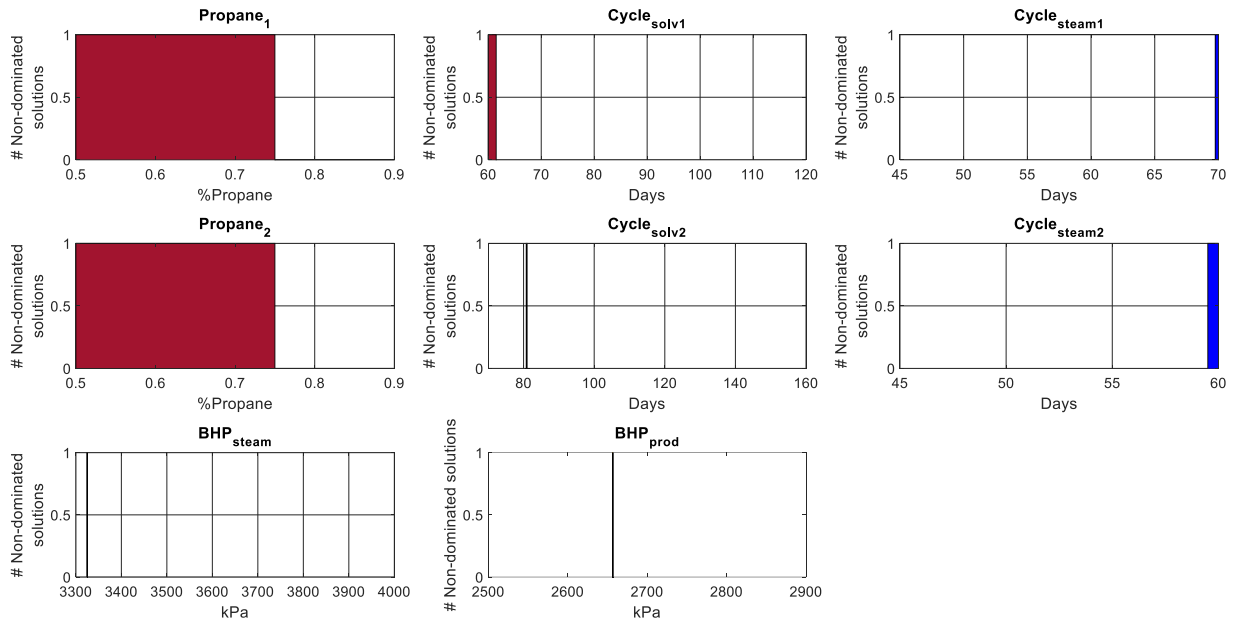
Figure 59. Optimal ranges using PESA-II for the homogeneous model in the red quadrant.
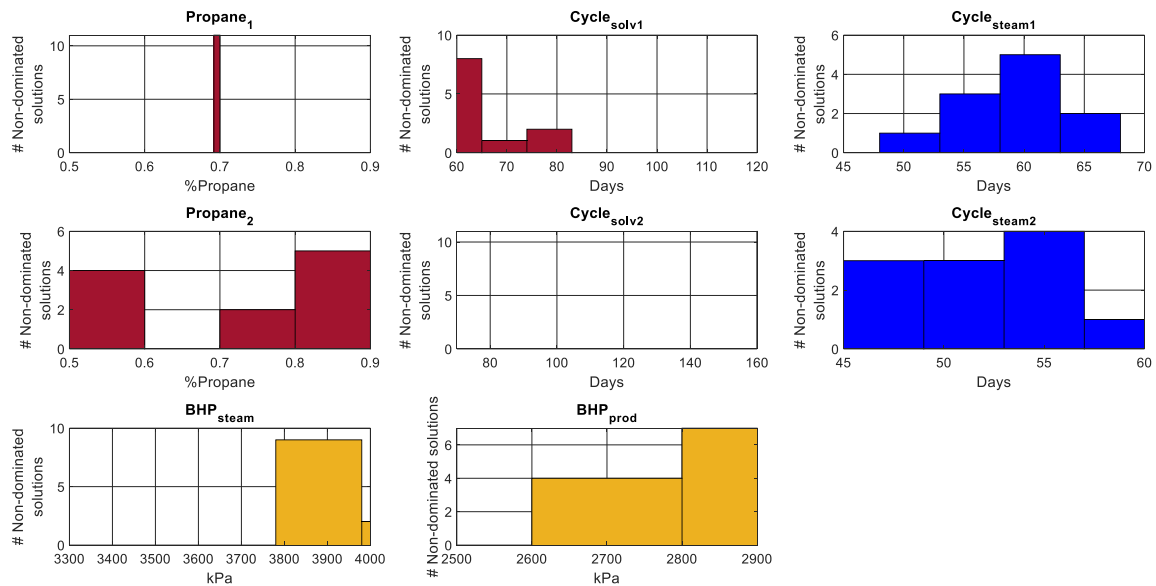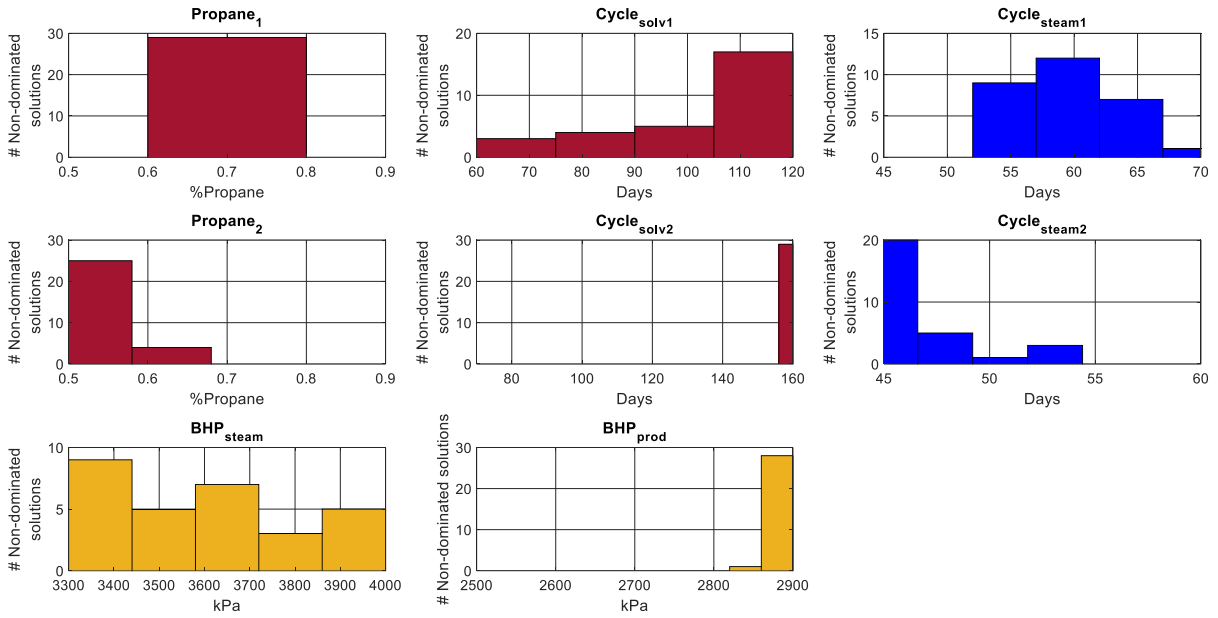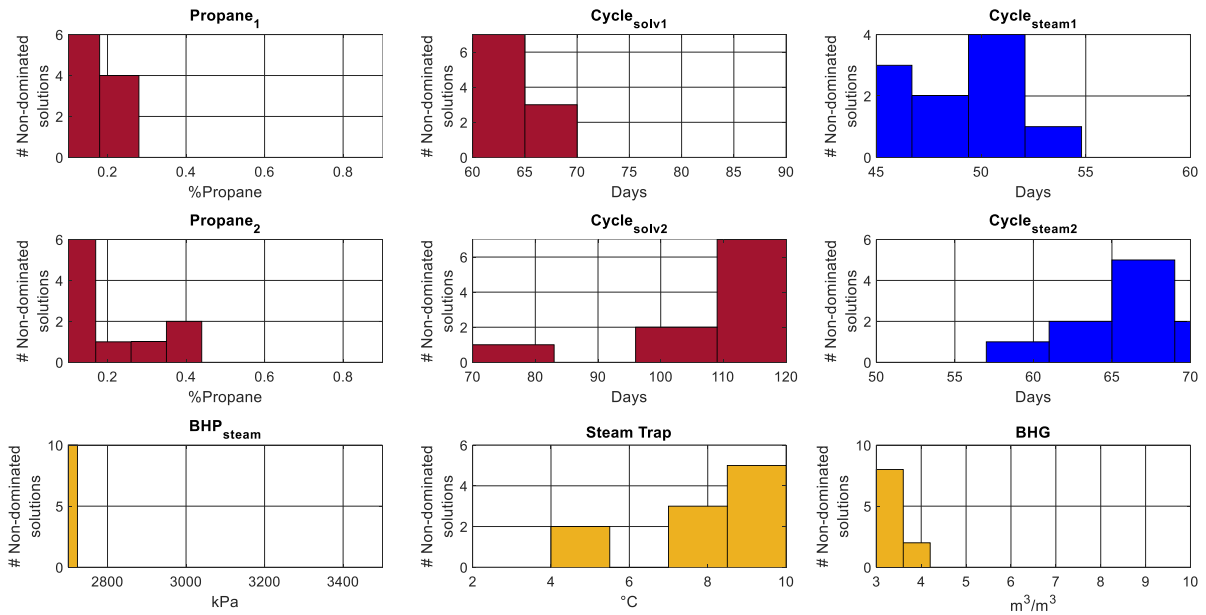

Figure 60. Optimal ranges using PESA-II for the homogeneous model in the green quadrant.
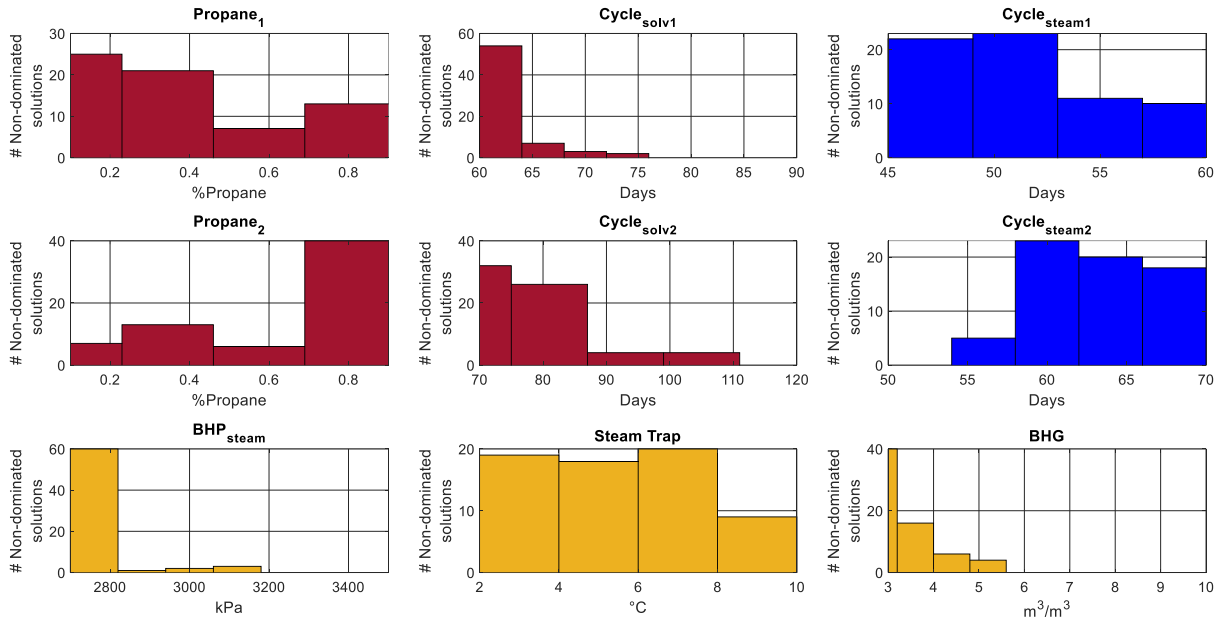
Figure 61. Optimal ranges using PESA-II for the simple heterogeneous model in the blue quadrant.
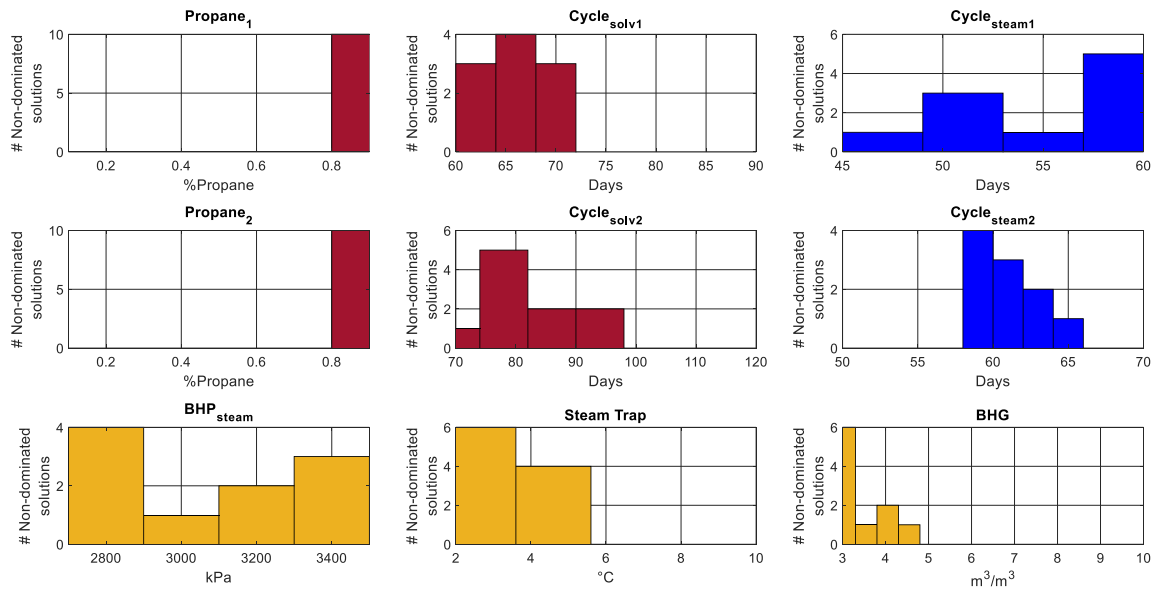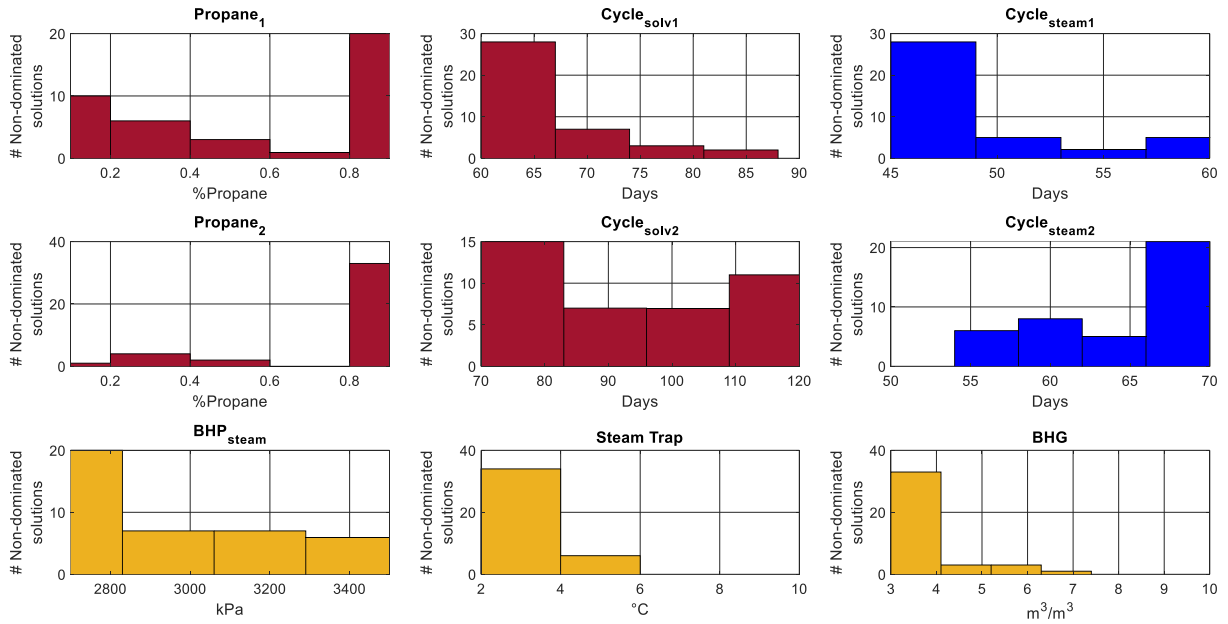

Figure 62. Optimal ranges using PESA-II for the simple heterogeneous model in the magenta quadrant.
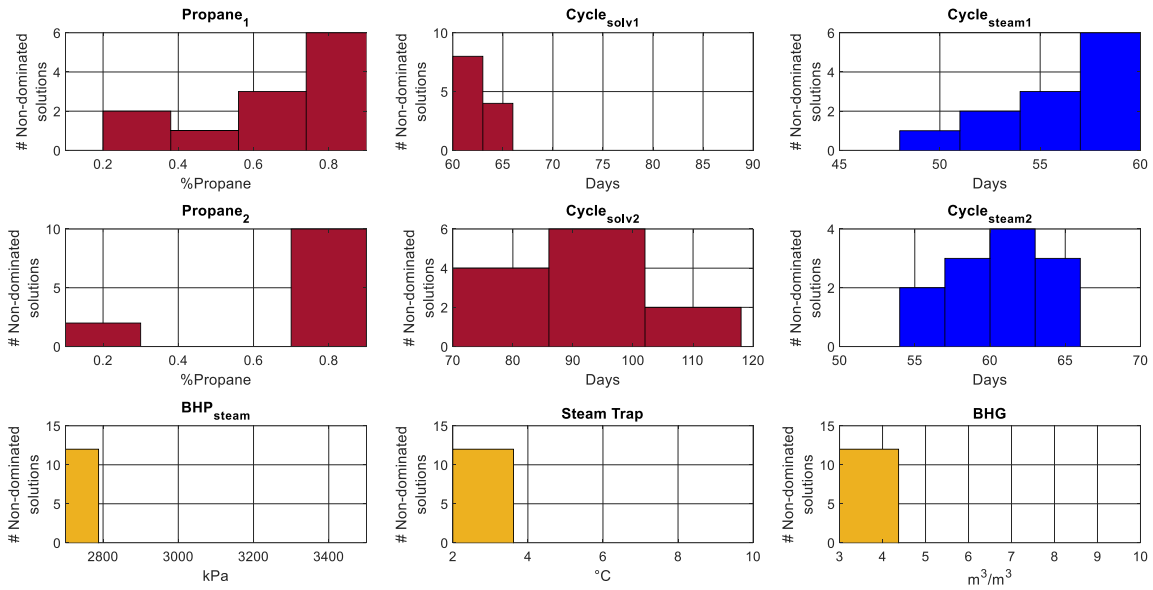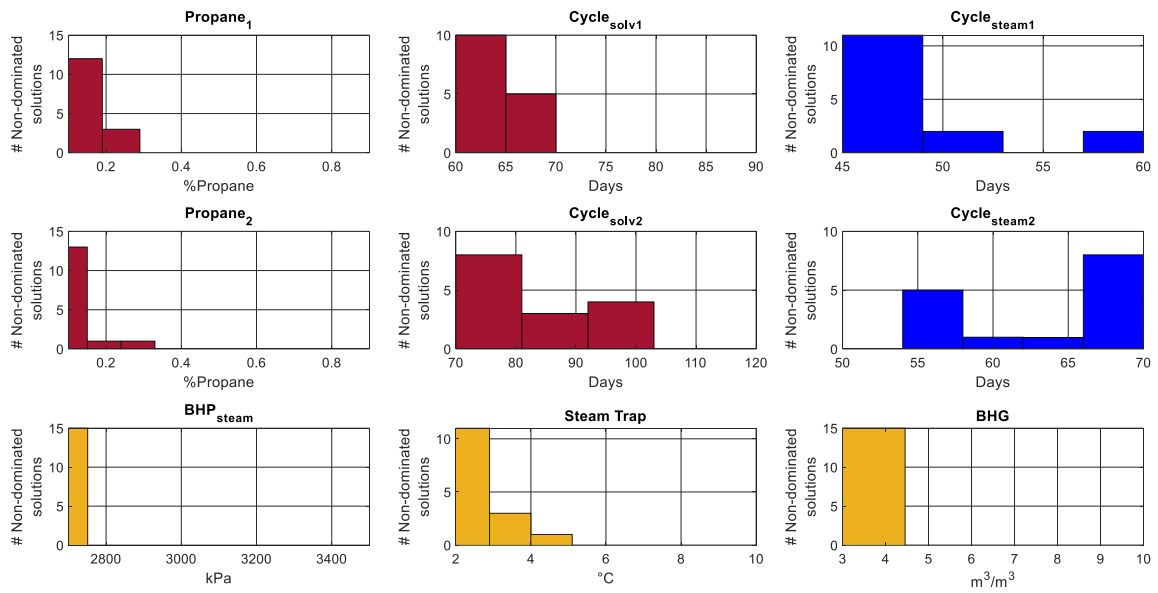
Figure 63. Optimal ranges using PESA-II for the simple heterogeneous model in the red quadrant.
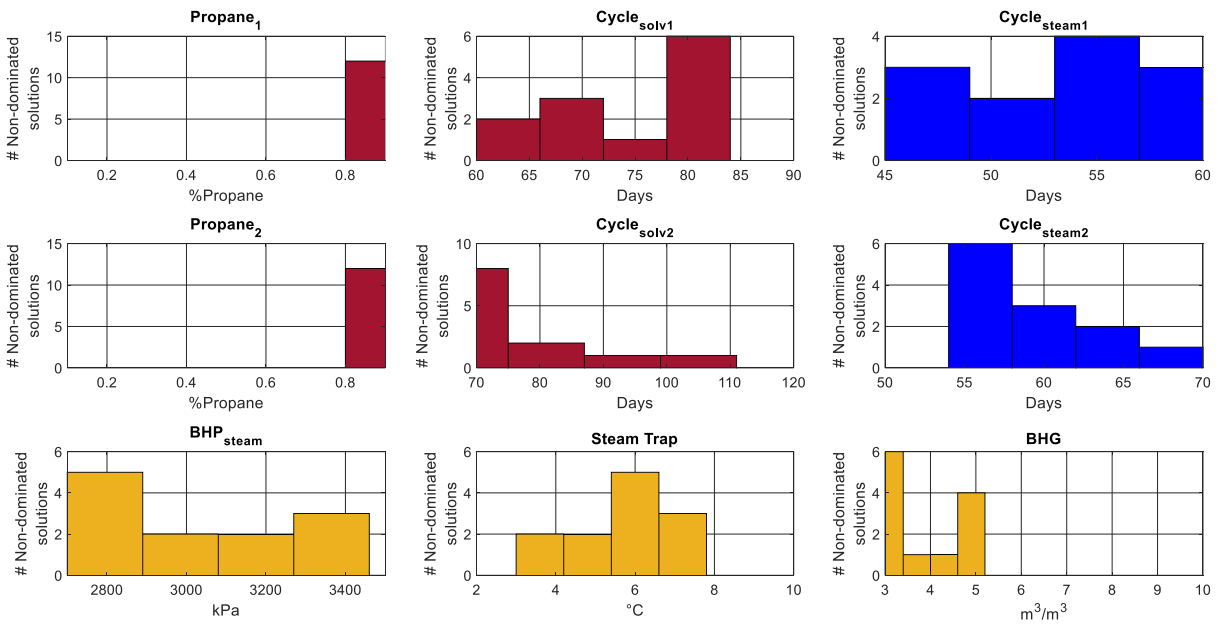
Figure 64. Optimal ranges using PESA-II for the simple heterogeneous model in the green quadrant.
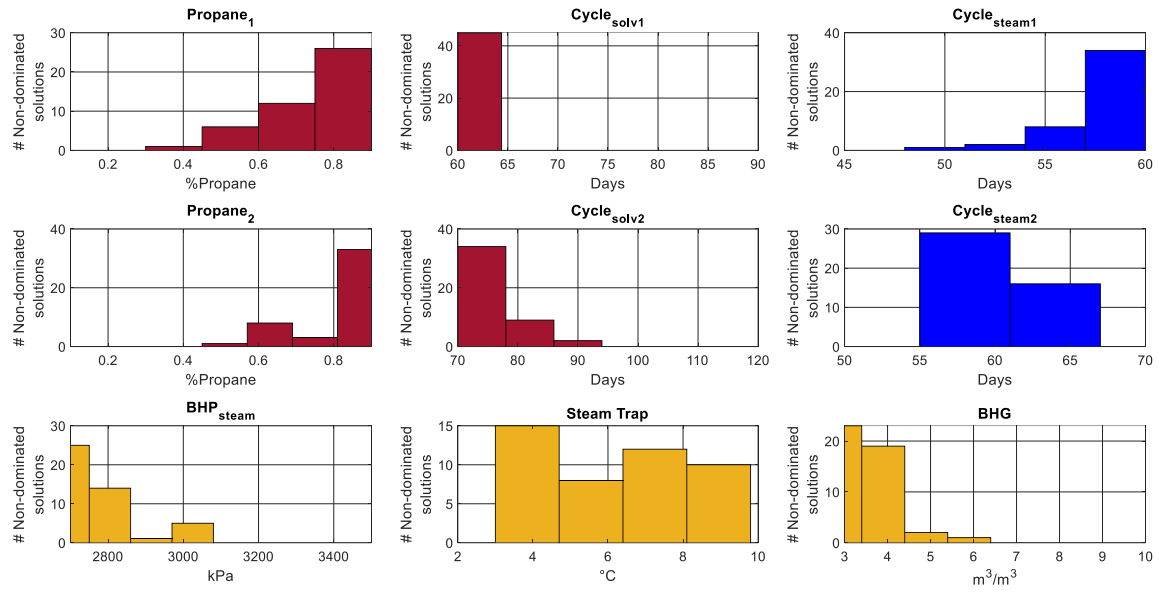
Figure 65. Optimal ranges using PESA-II for the semi-complex heterogeneous model in the blue quadrant.
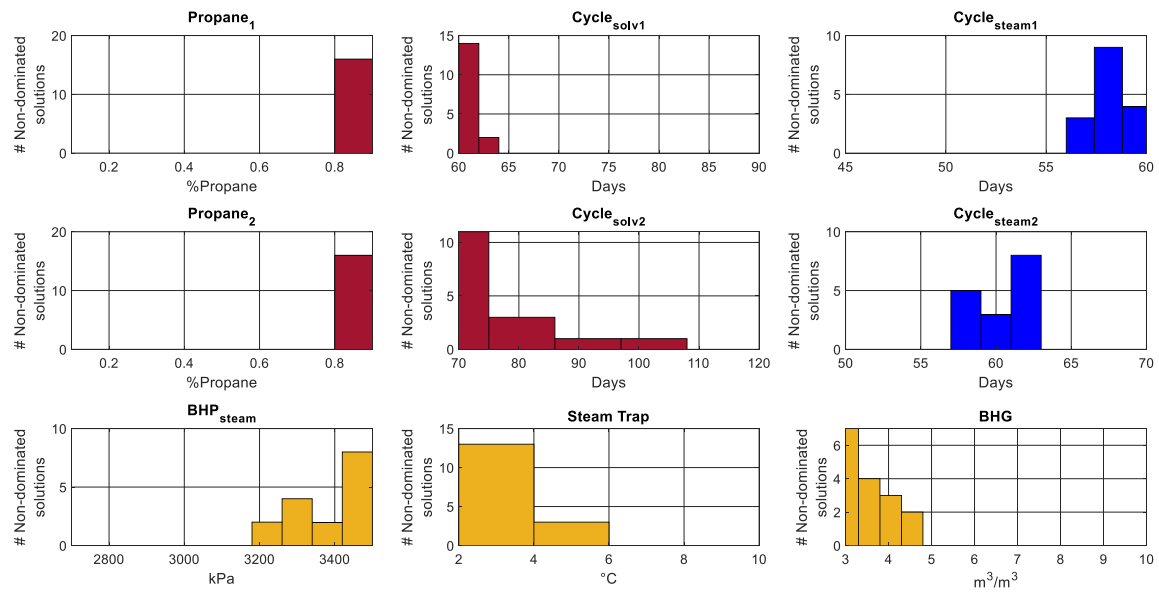
Figure 66. Optimal ranges using PESA-II for the semi-complex heterogeneous model in the magenta quadrant.
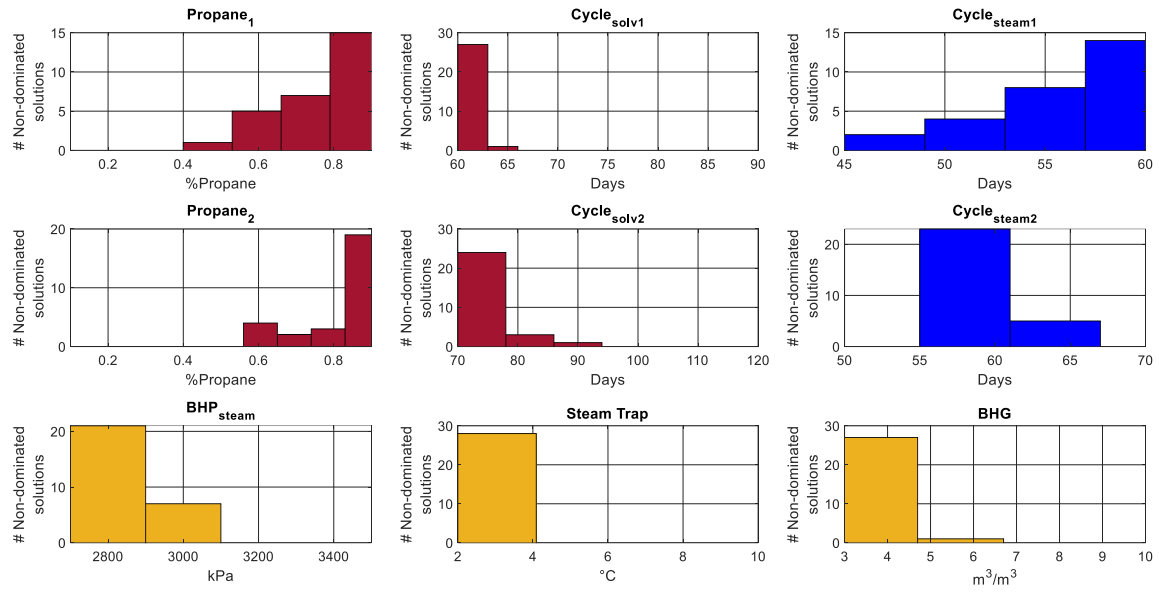
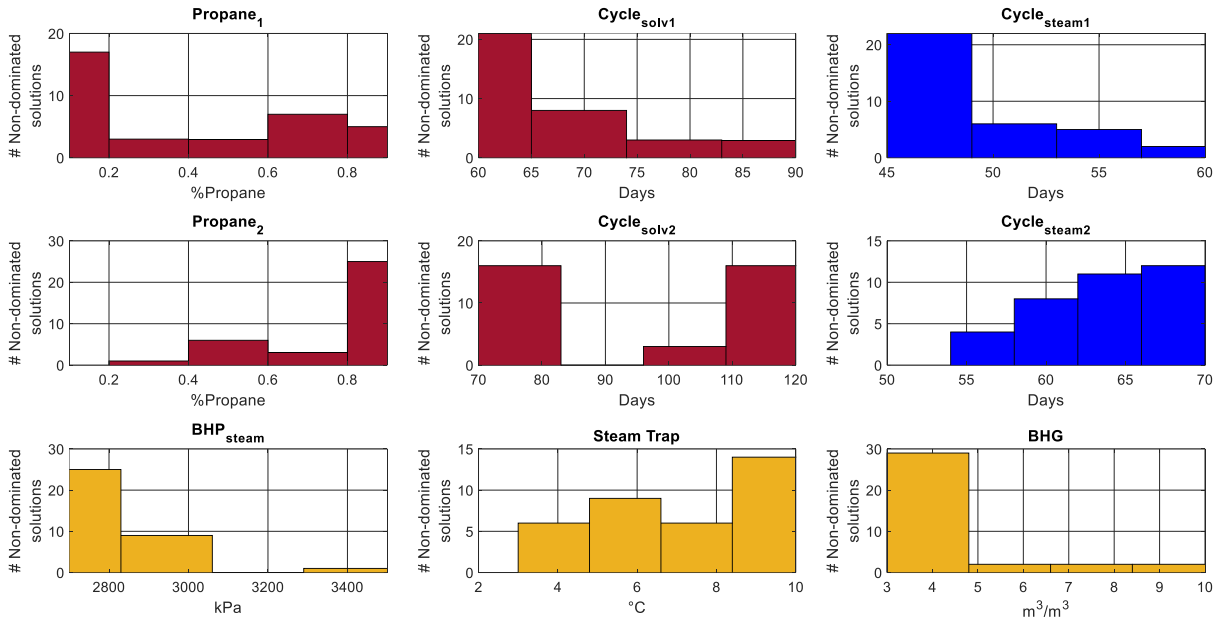**Figure 67. Optimal ranges using PESA-II for the semi-com plex heterogeneous model in the red quadrant.**
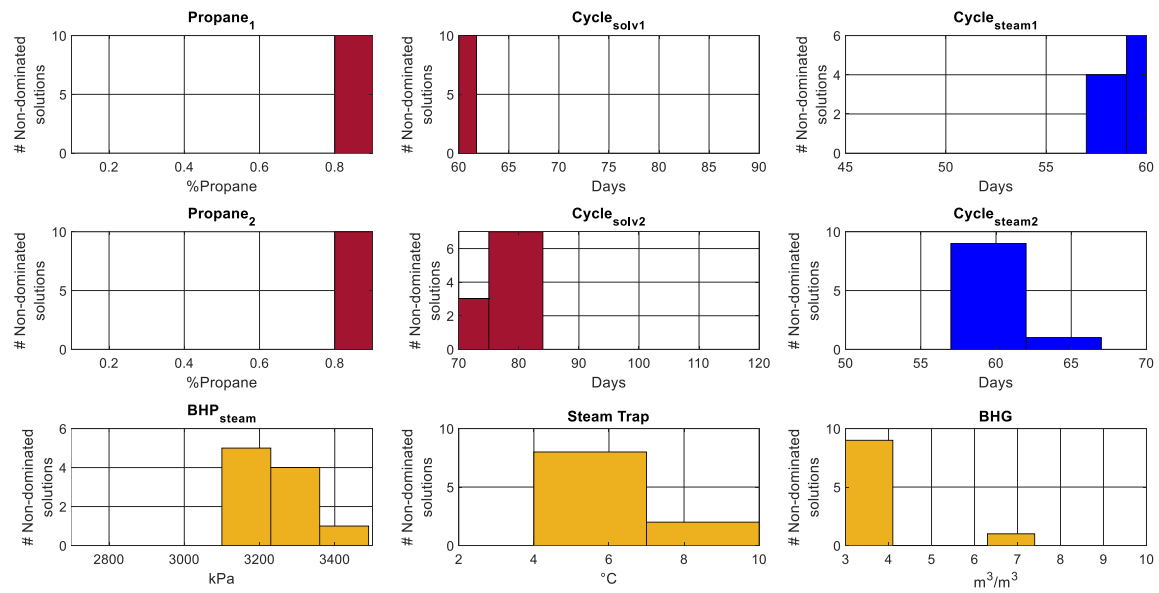
Figure 68. Optimal ranges using PESA-II for the semi-complex heterogeneous model in the green quadrant.
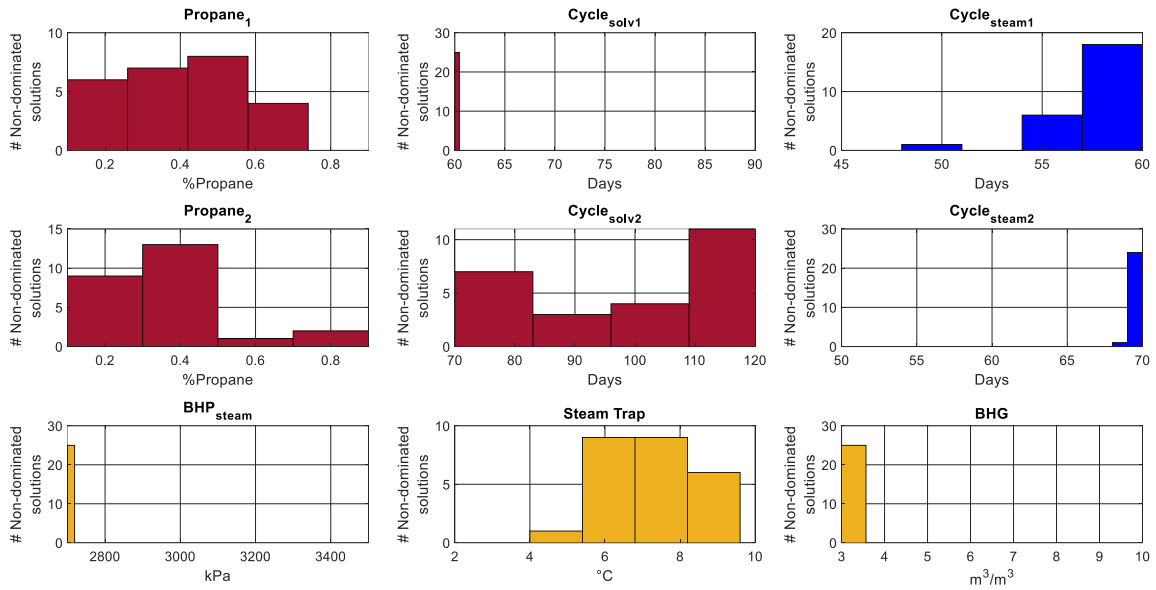
Figure 69. Optimal ranges using PESA-II for the complex heterogeneous model in the blue quadrant.
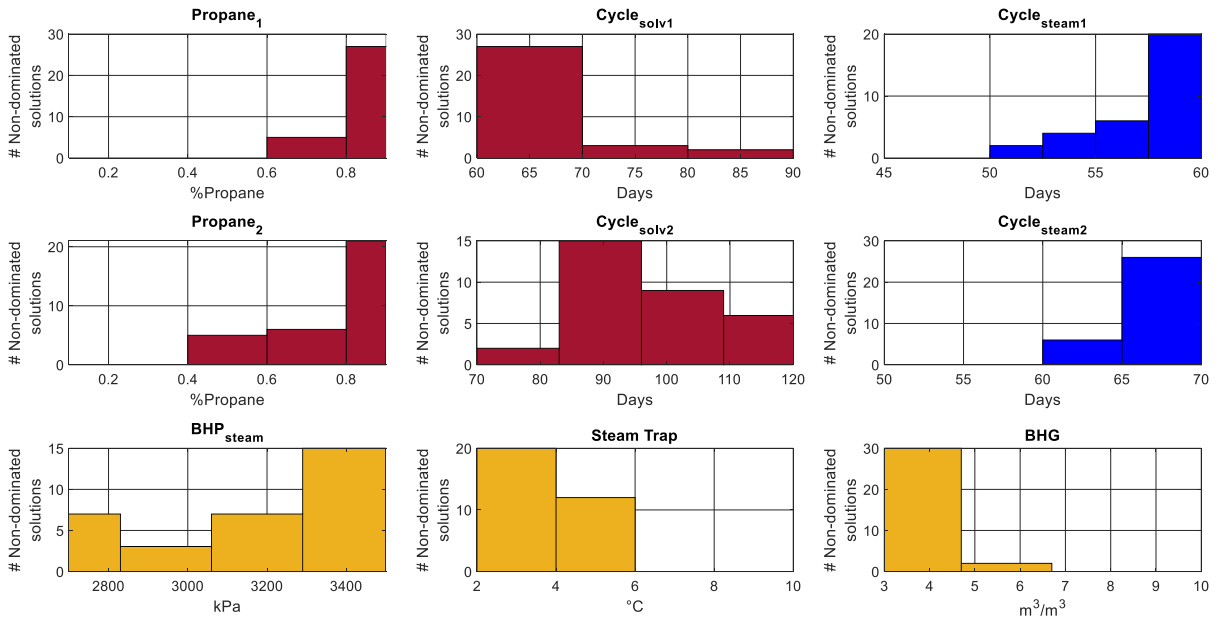
Figure 70. Optimal ranges using PESA-II for the complex heterogeneous model in the magenta quadrant.
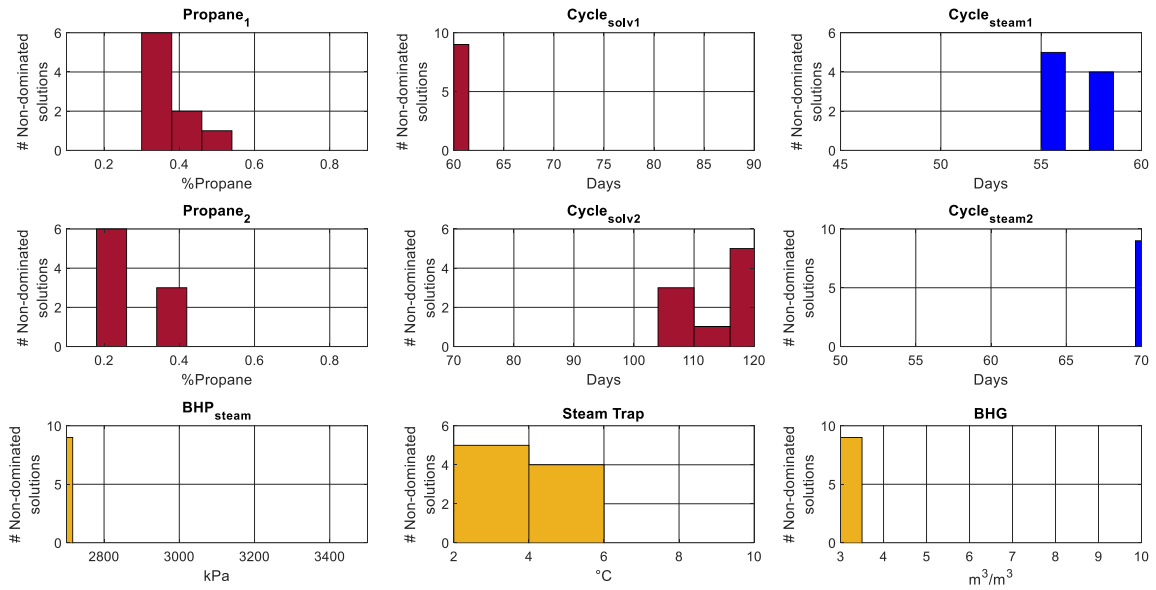
Figure 71. Optimal ranges using PESA-II for the complex heterogeneous model in the red quadrant.
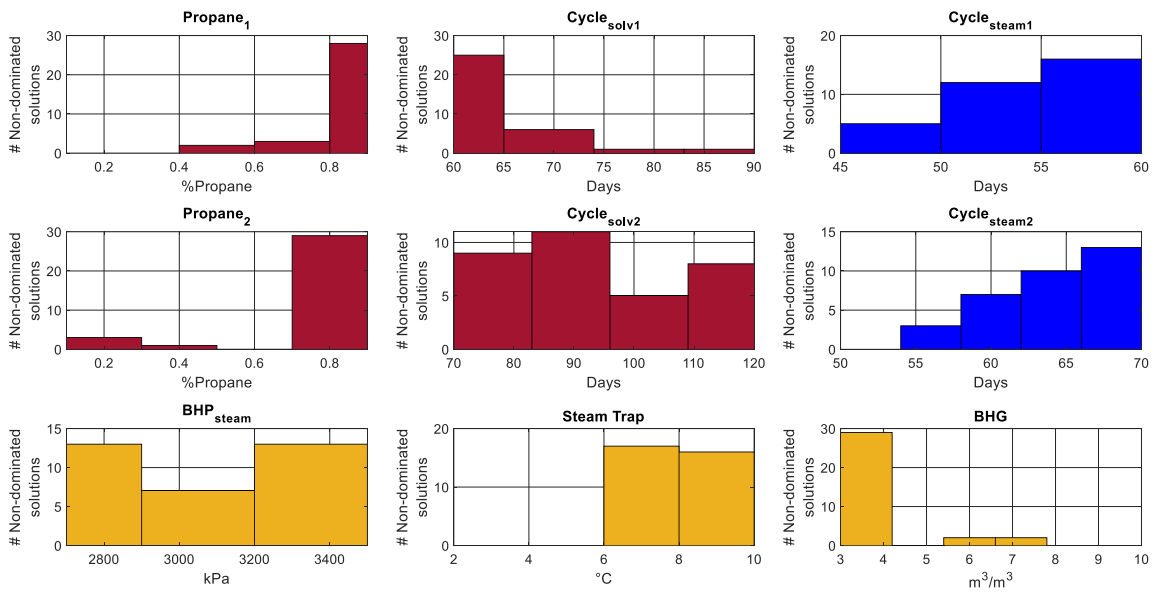
Figure 72. Optimal ranges using PESA-II for the complex heterogeneous model in the green quadrant.
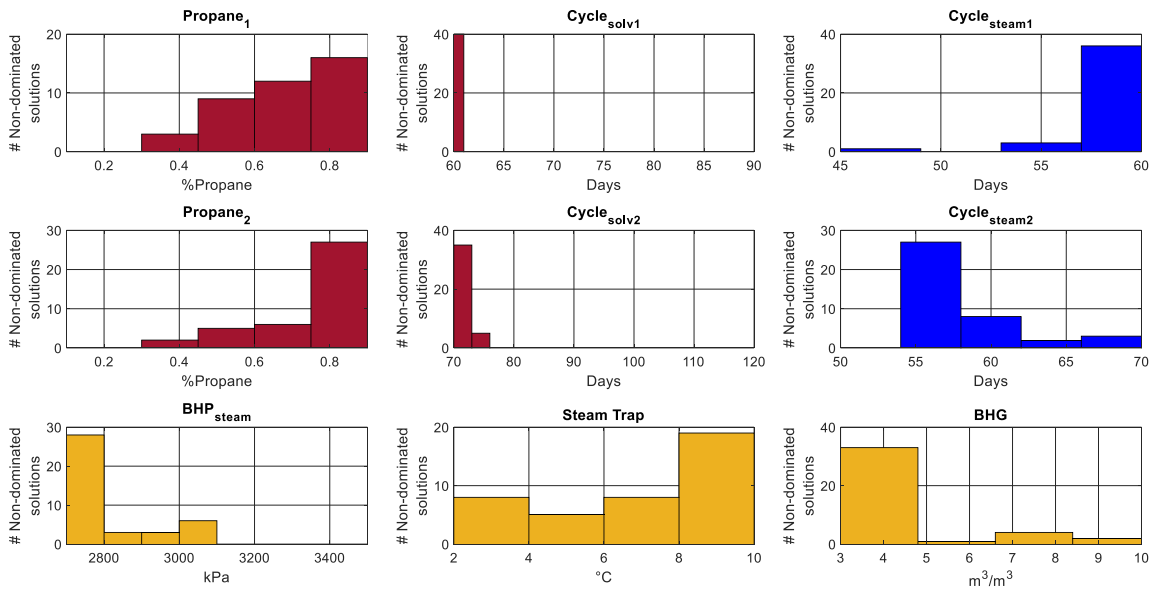
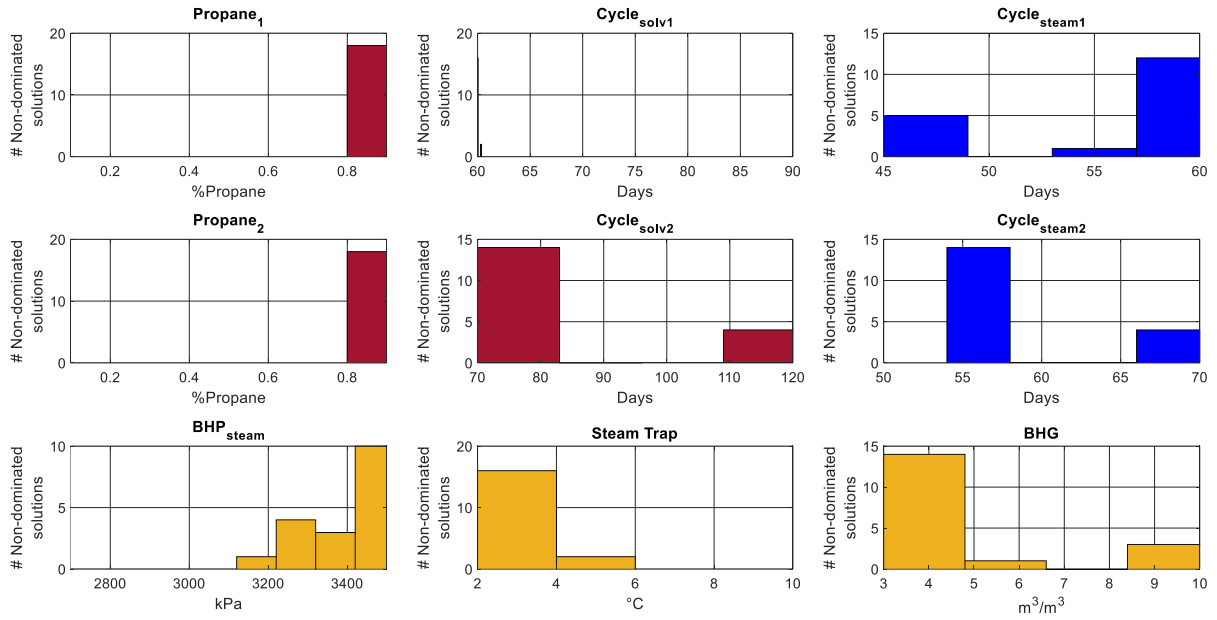**Figure 73. Optimal ranges using MOPSO for the homogeneous model in the blue quadrant.**

Figure 74. Optimal ranges using MOPSO for the homogeneous model in the magenta quadrant.

Figure 75. Optimal ranges using MOPSO for the homogeneous model in the green quadrant.

Figure 76. Optimal ranges using MOPSO for the simple heterogeneous model in the blue quadrant.

123

Figure 77. Optimal ranges using MOPSO for the simple heterogeneous model in the magenta quadrant.
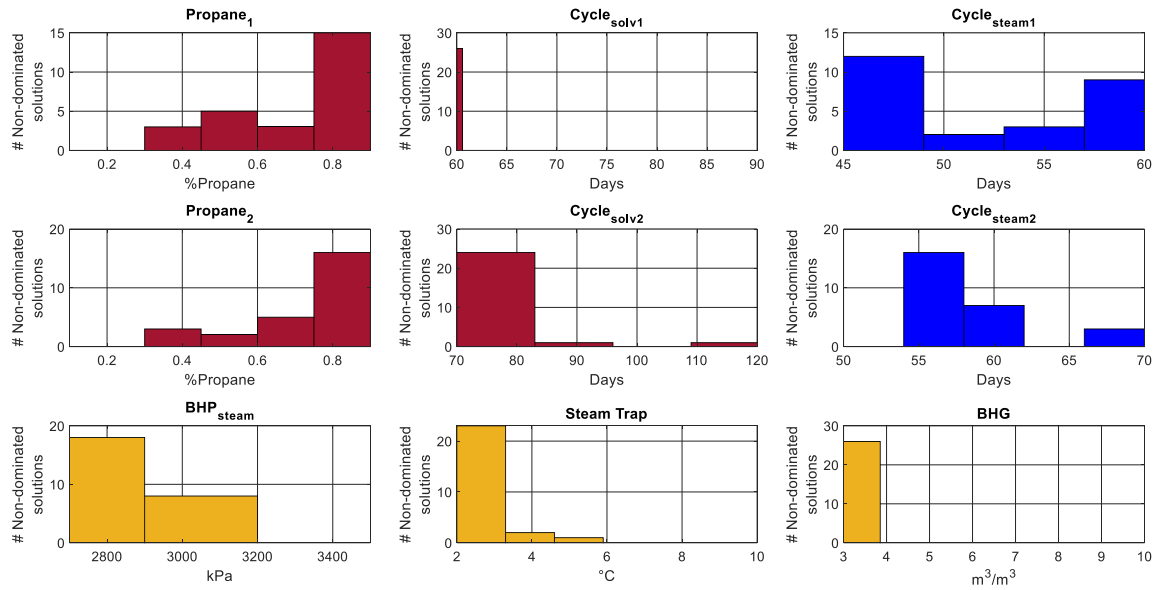

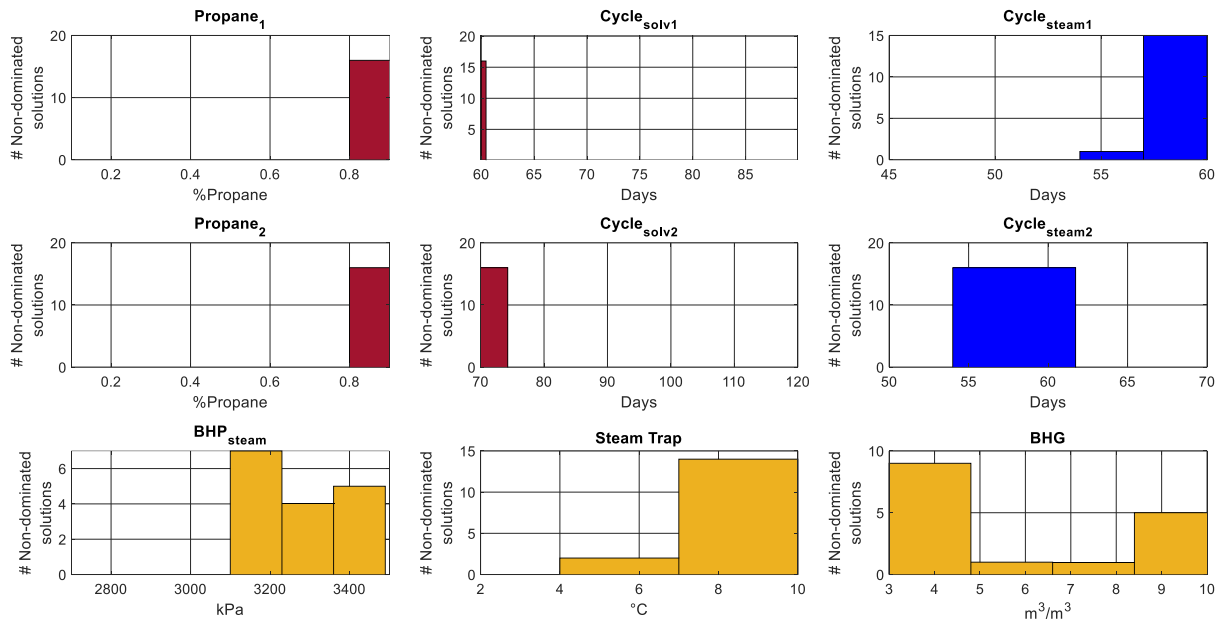**Figure 78. Optimal ranges using MOPSO for the simple heterogeneous model in the red quadrant.**

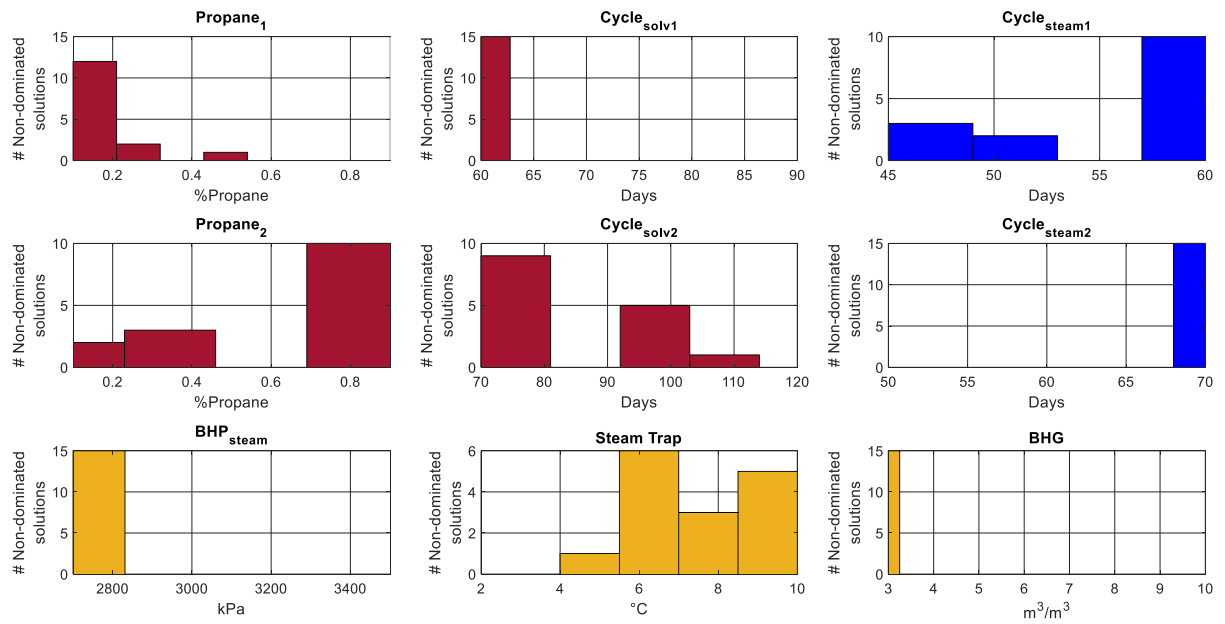**Figure 79. Optimal ranges using MOPSO for the simple heterogeneous model in the green quadrant.**

Figure 80. Optimal ranges using MOPSO for the semi-complex heterogeneous model in the blue quadrant.

125

Figure 81. Optimal ranges using MOPSO for the semi-complex heterogeneous model in the magenta quadrant.

Figure 82. Optimal ranges using MOPSO for the semi-complex heterogeneous model in the red quadrant.

126

Figure 83. Optimal ranges using MOPSO for the semi-complex heterogeneous model in the green quadrant.

Figure 84. Optimal ranges using MOPSO for the complex heterogeneous model in the blue quadrant.
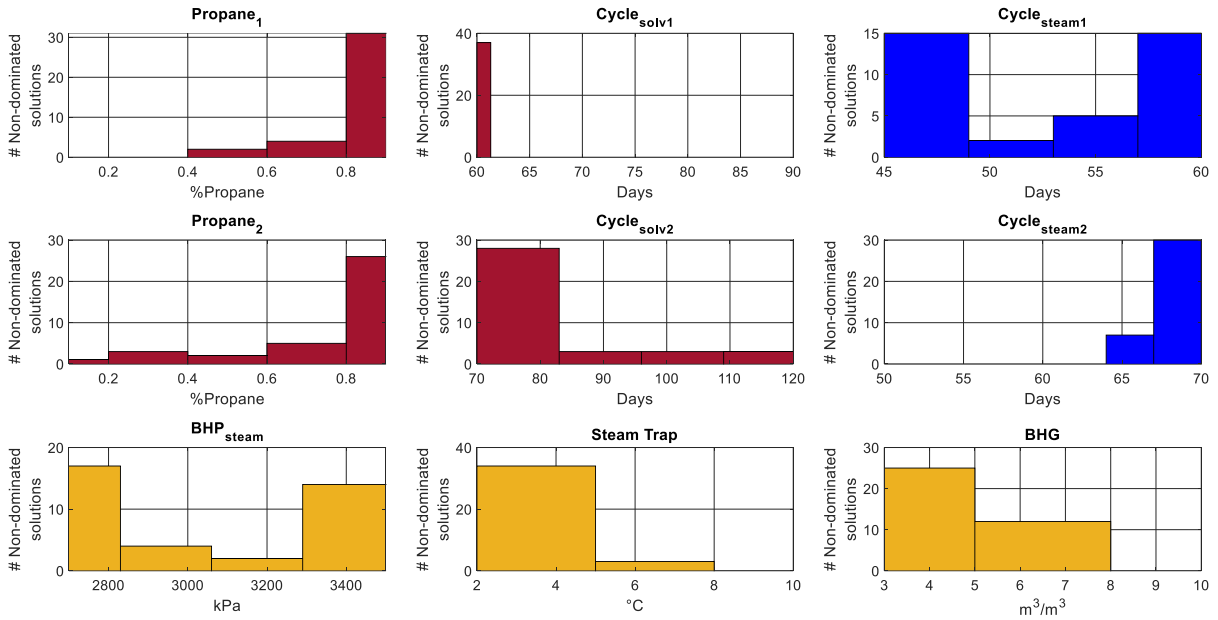
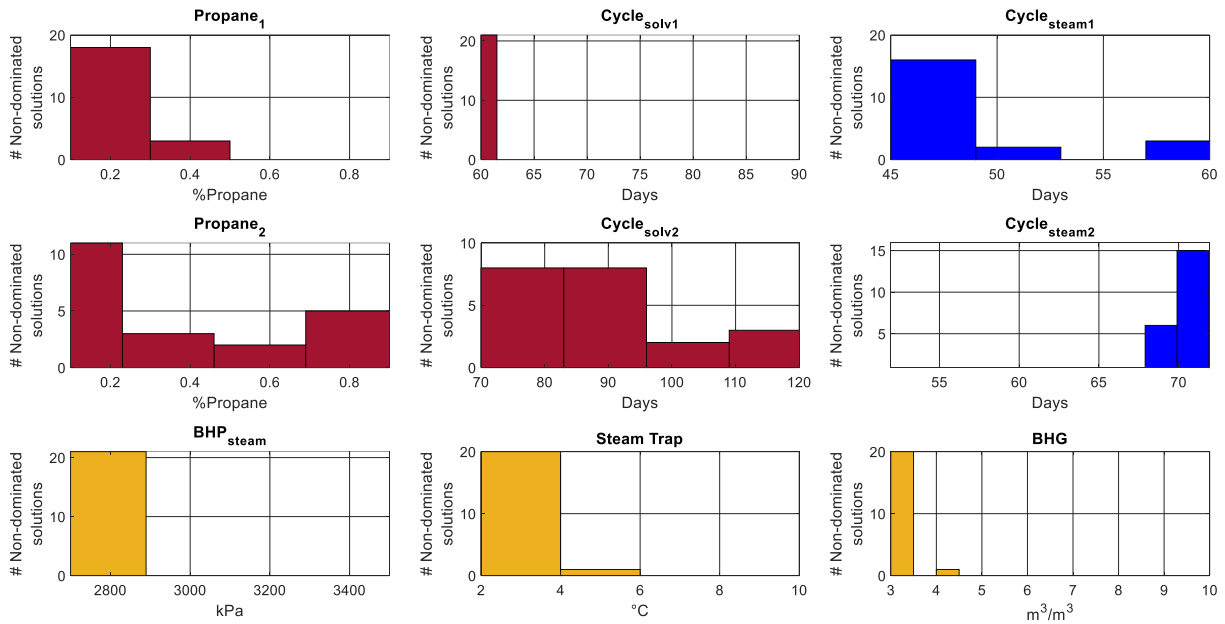**Figure 85. Optimal ranges using MOPSO for the complex heterogeneous model in the magenta quadrant.**

Figure 86. Optimal ranges using MOPSO for the complex heterogeneous model in the red quadrant.
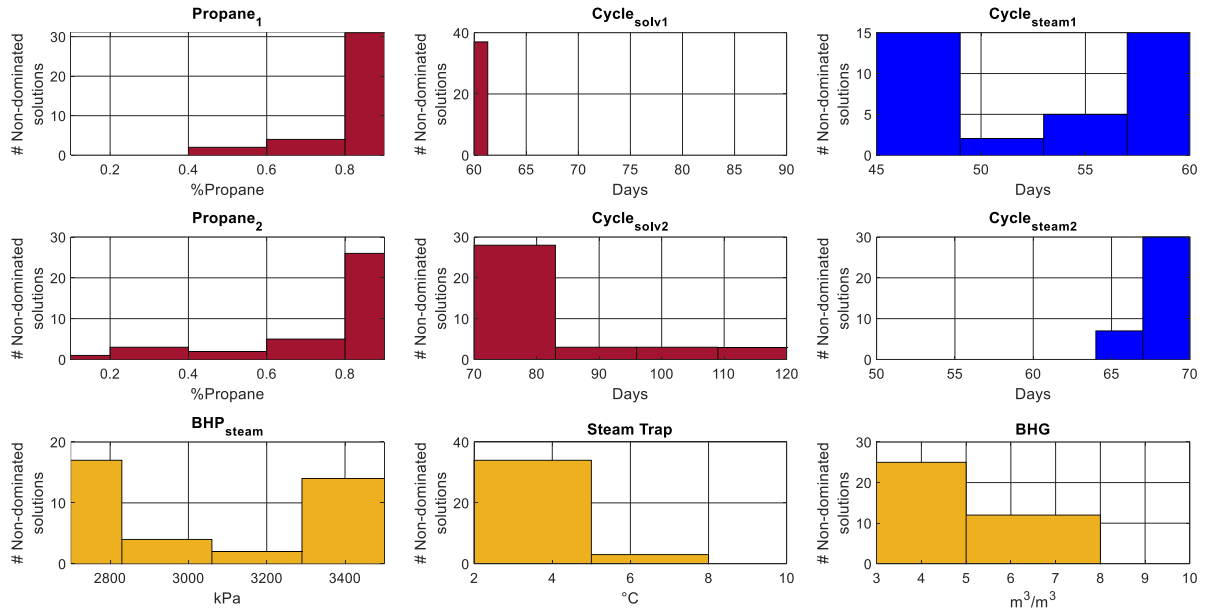
Figure 87. Optimal ranges using MOPSO for the complex heterogeneous model in the green quadrant.